Surface X-ray Scattering

Alessandro COATI - SixS beamline - Synchrotron SOLEIL

Layout

- Introduction
  - Hard x-rays for surfaces, interfaces and nano-objects
- Surface x-ray Scattering techniques
  - Crystal Truncation Rod (CTR)
  - Surface x-ray diffraction (SXRD)
  - Grazing Incidence Small Angle X-ray Scattering (GISAXS)
- SixS beamline setup
- *In situ* and *operando* scientific applications
  - growth of metallic nanostructures by using vicinal surfaces
  - growth of nanoparticles by atomic layer deposition (ALD)
  - nanoporous formation in alumina
- Conclusions, acknowledgments, references

Introduction

- Definitions (Oxford English Dictionary)

- Interface. A point where two systems, subjects, organizations, etc. meet and interact.

- Surface. The outside part or uppermost layer of something.

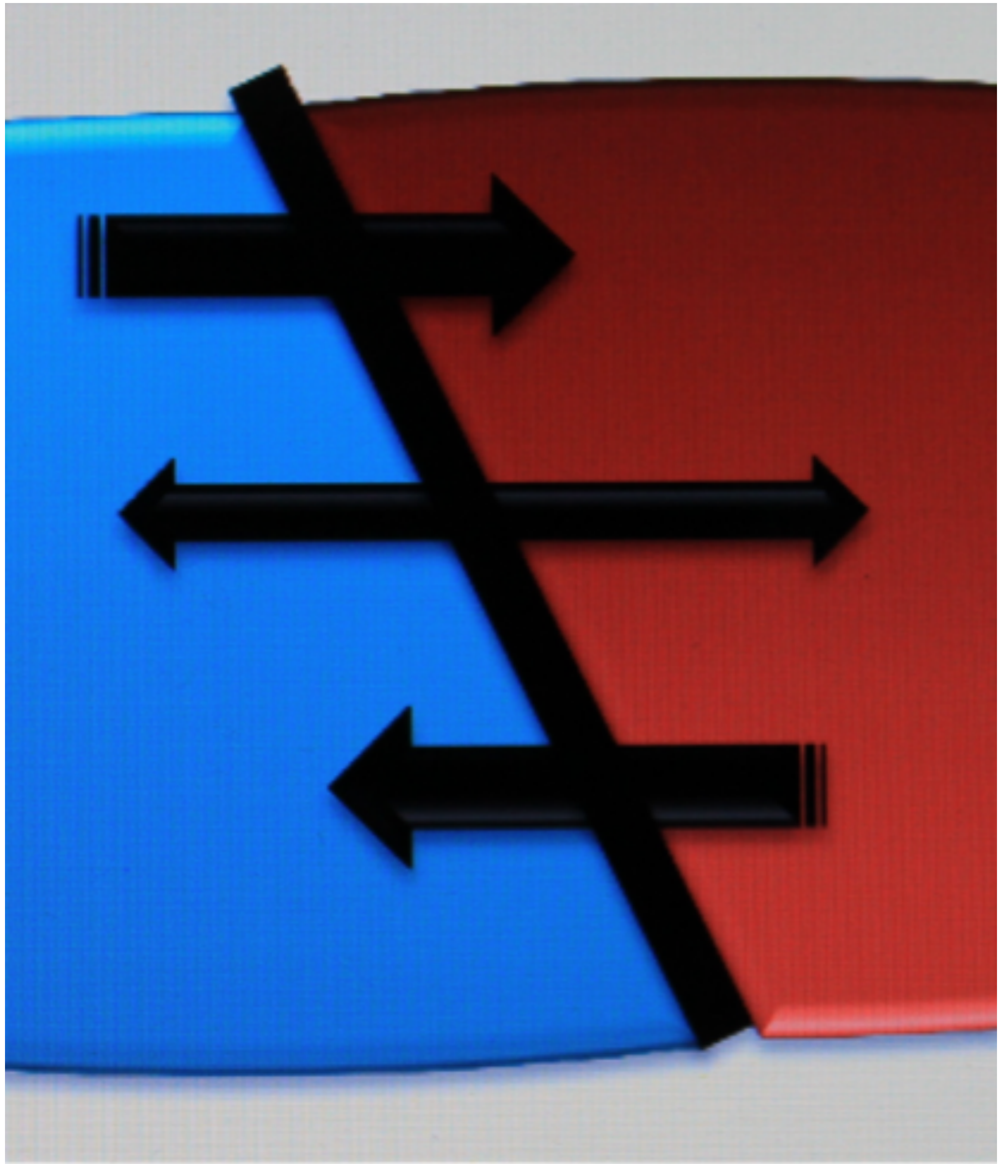

- Surfaces as
  - interface material vs vacuum
  - support of nano-objects

- Physical properties (electronic, catalytic, photonics, magnetic):
  - different from the bulk
  - depending on the interface nature (solid/solid, solid/liquid, solid/gaz, liquid/liquid, liquid/gaz)
  - depend on the atomic structure, the size, the shape and the organisation at the nanometric scale

- X-ray scattering techniques can give information on all these factors

x-ray/matter interactions

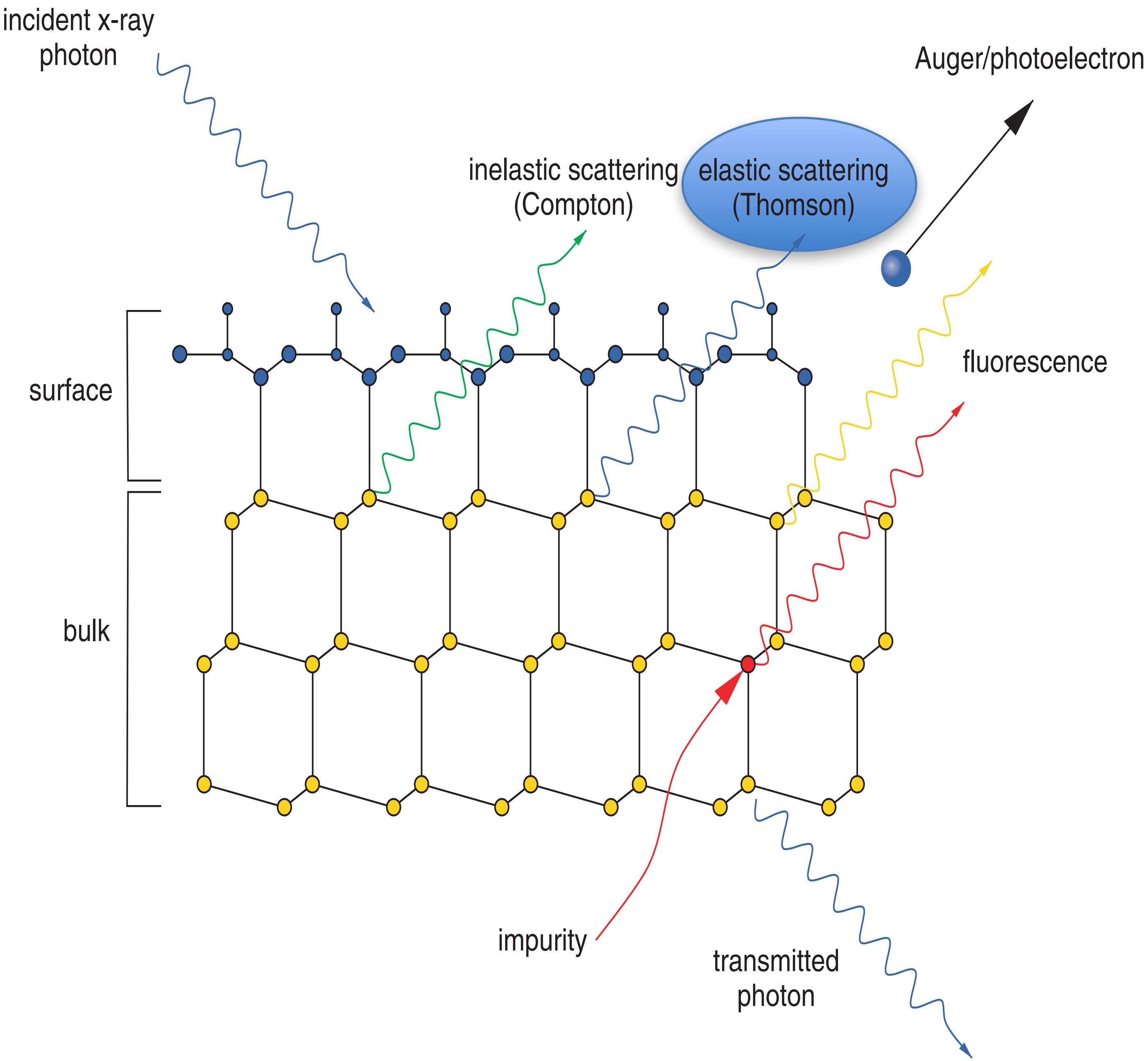

(hard) x-rays for interfaces studies

- atomic scale ($\lambda = 0.1nm$ - interatomic distance)
- non-distructive probe
- avoid sample charging
- *in situ* measurements
- *operando* measurements
- probing statistical information
- allow to study in the same experiment microstructure and functionality of the interface
- surface sensitive, with variable information depth in the pm to μm

surface interface x-ray scattering

- Structure determines functions! > physical properties control

- From models to real life:
  - *In situ* and *operando* experiments at the interfaces in various environments
  - UHV
  - Gaz (pressure gap)
  - Liquid
- From single crystals to (small) nanoparticles (material gap)

- Approaching real conditions by exploiting hard x-ray penetration in materials

surface interface x-ray scattering

Non-destructive techniques, *operando*-compatible

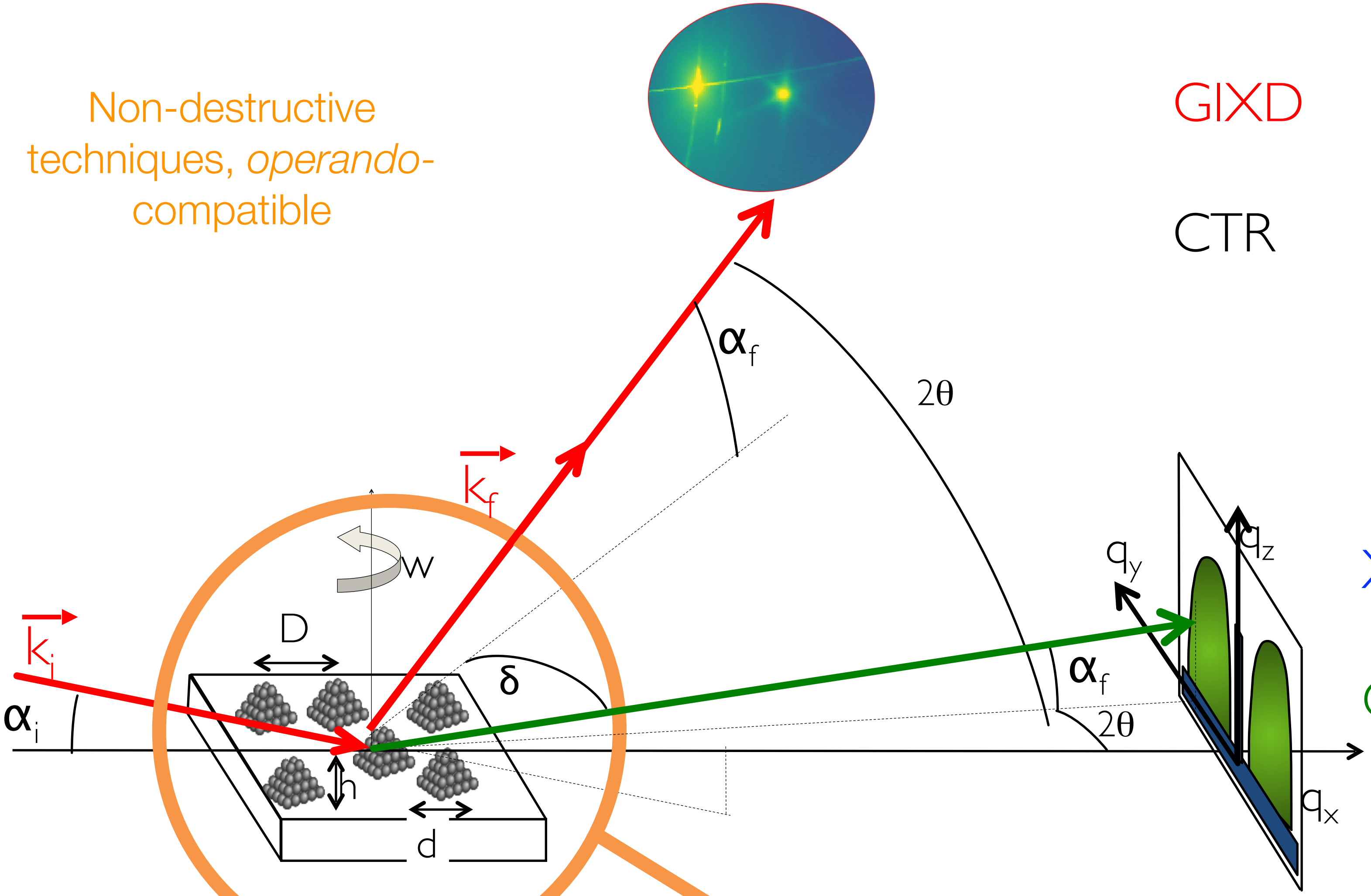

GIXD — Depth-dependent (from nm to μm) structural parameters (lattice parameters, strain, grain size, mosaic distribution)

CTR — Surface / interface structural analysis with pm resolution

Anomalous diffraction
Element specific structural characterization, in combination with the different techniques

XRR — Thickness, density and roughness of layered interfaces

GISAXS — Morphology on nanometer scale

Sample environment:
UHV, MBE, liquid, electrolite, gaz, high T, high p…

surface interface x-ray scattering

Non-destructive techniques, *operando*-compatible

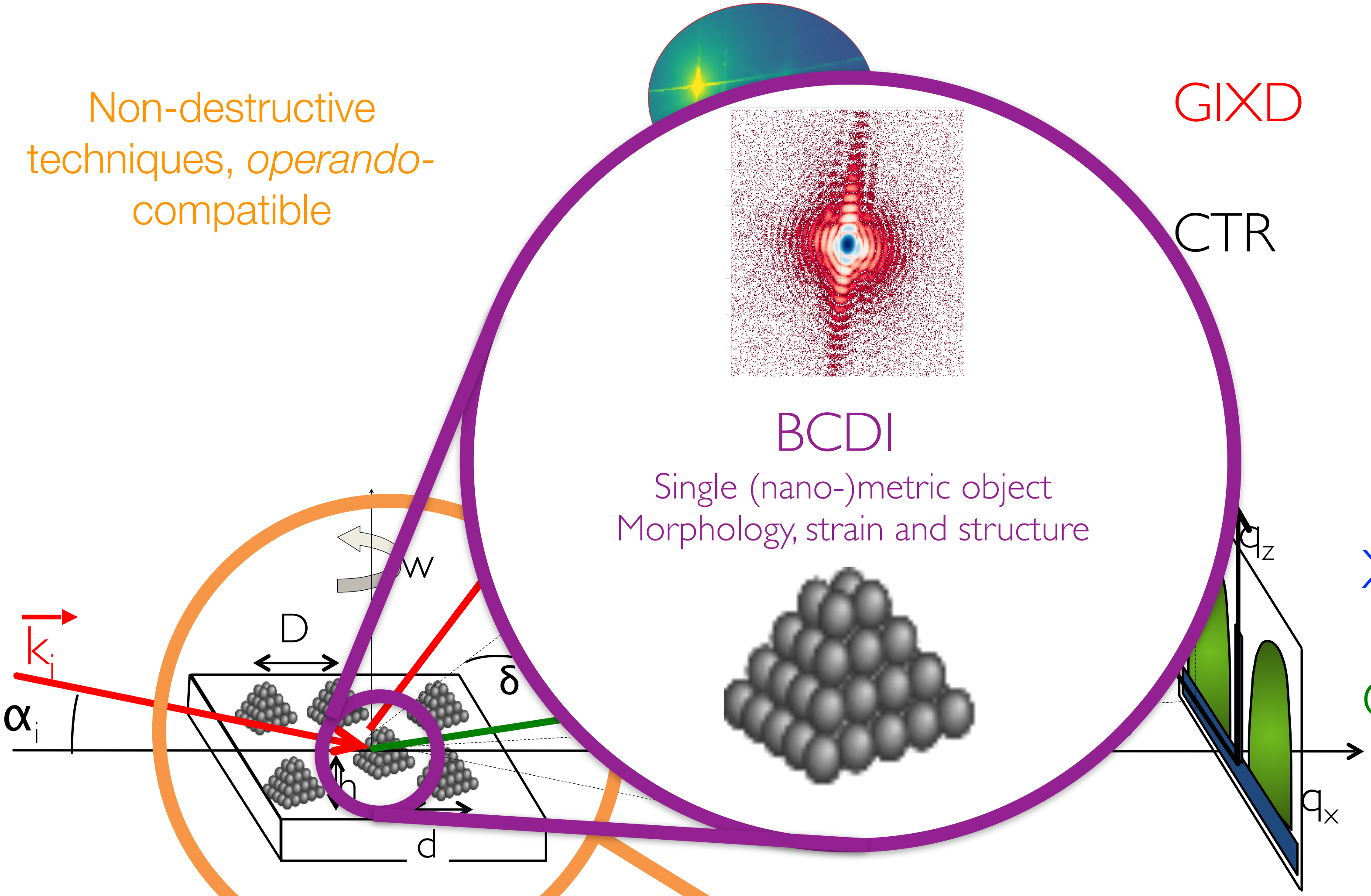

GIXD — Depth-dependent (from nm to µm) structural parameters (lattice parameters, strain, grain size, mosaic distribution)

CTR — Surface / interface structural analysis with pm resolution

Anomalous diffraction
Element specific structural characterization, in combination with the different techniques

XRR — Thickness, density and roughness of layered interfaces

GISAXS — Morphology on nanometer scale

Sample environment:
UHV, MBE, liquid, electrolite, gaz, high T, high p…

Grazing incidence geometry

Total reflection - optics reminder

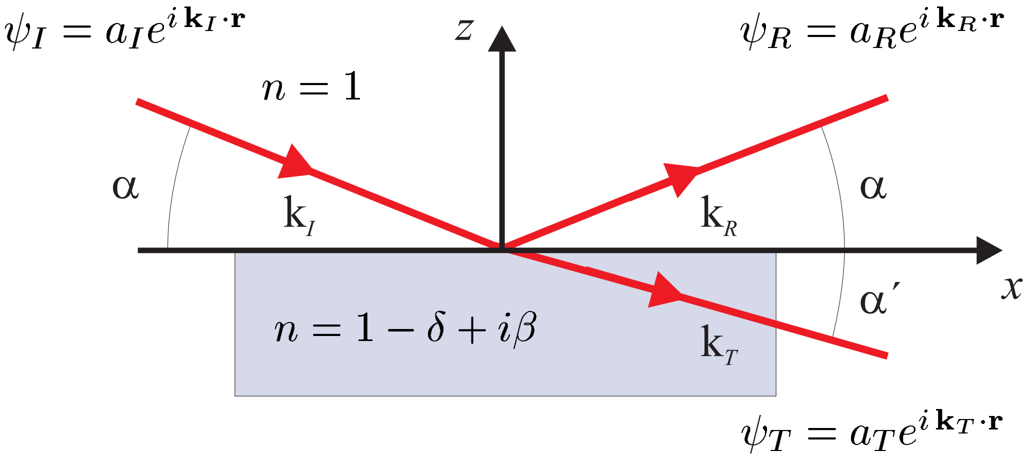

$$\cos(\alpha') = n\cos(\alpha_i)$$

$$\boxed{n = 1 - \delta + i\beta}$$

$$\delta \approx \frac{\lambda}{2\pi}\frac{e^2}{mc^2}\rho_e \approx 10^{-5} \qquad \beta = \frac{\lambda\mu}{4\pi} \approx 10^{-6}$$

$$\cos(\alpha_c) = \mathrm{Re}(n) = 1 - \delta$$

$$\alpha_c \approx \sqrt{2\delta} \approx 10^{-3}\,rad$$

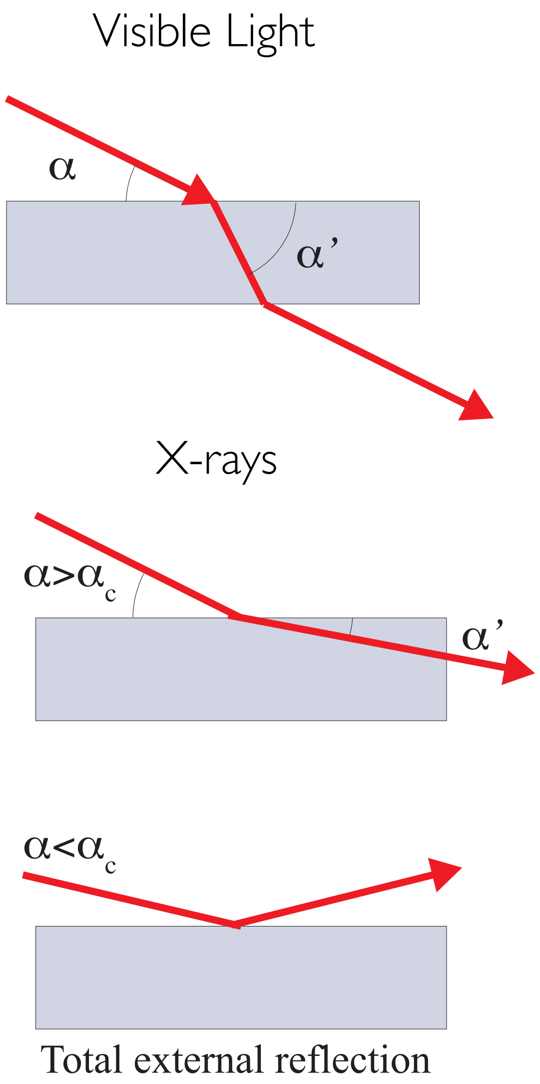

Penetration depth

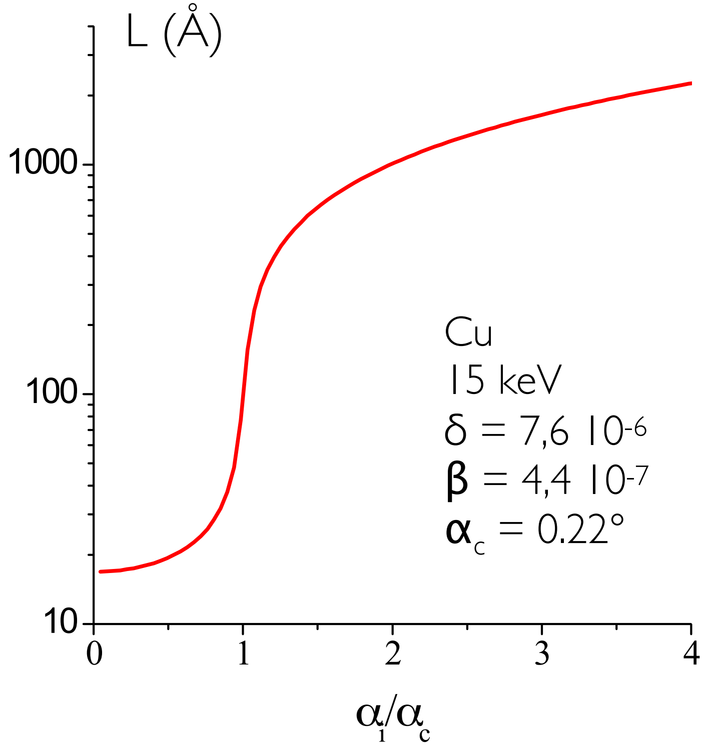

$$L \approx \frac{-\lambda}{4\pi \ \mathrm{Im}\sqrt{\alpha_i^2 - \alpha_c^2 - 2i\beta}}$$

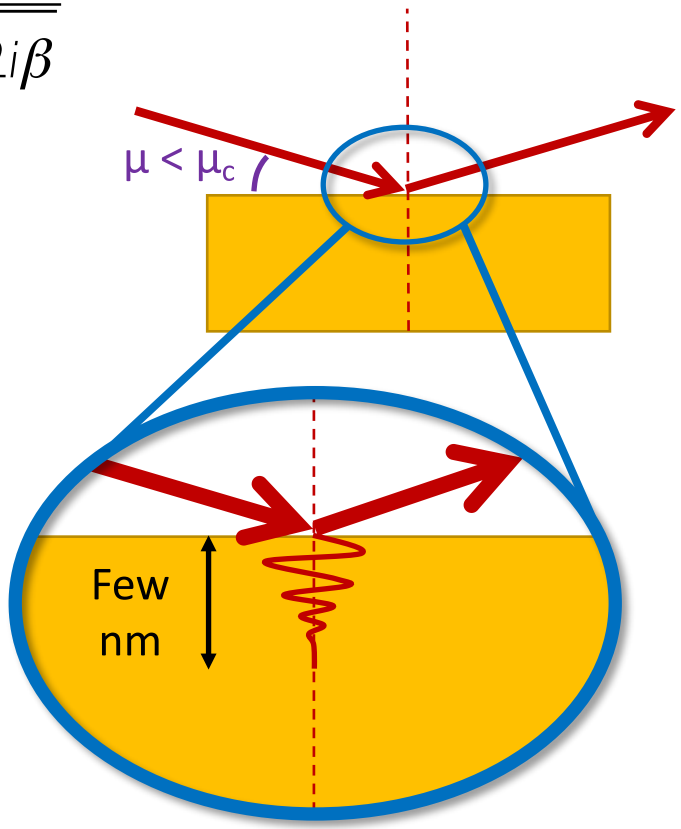

α_i	$0.1\ \alpha_c$	α_c	$2\ \alpha_c$
L (Å)	15	100	1000

Penetration depth

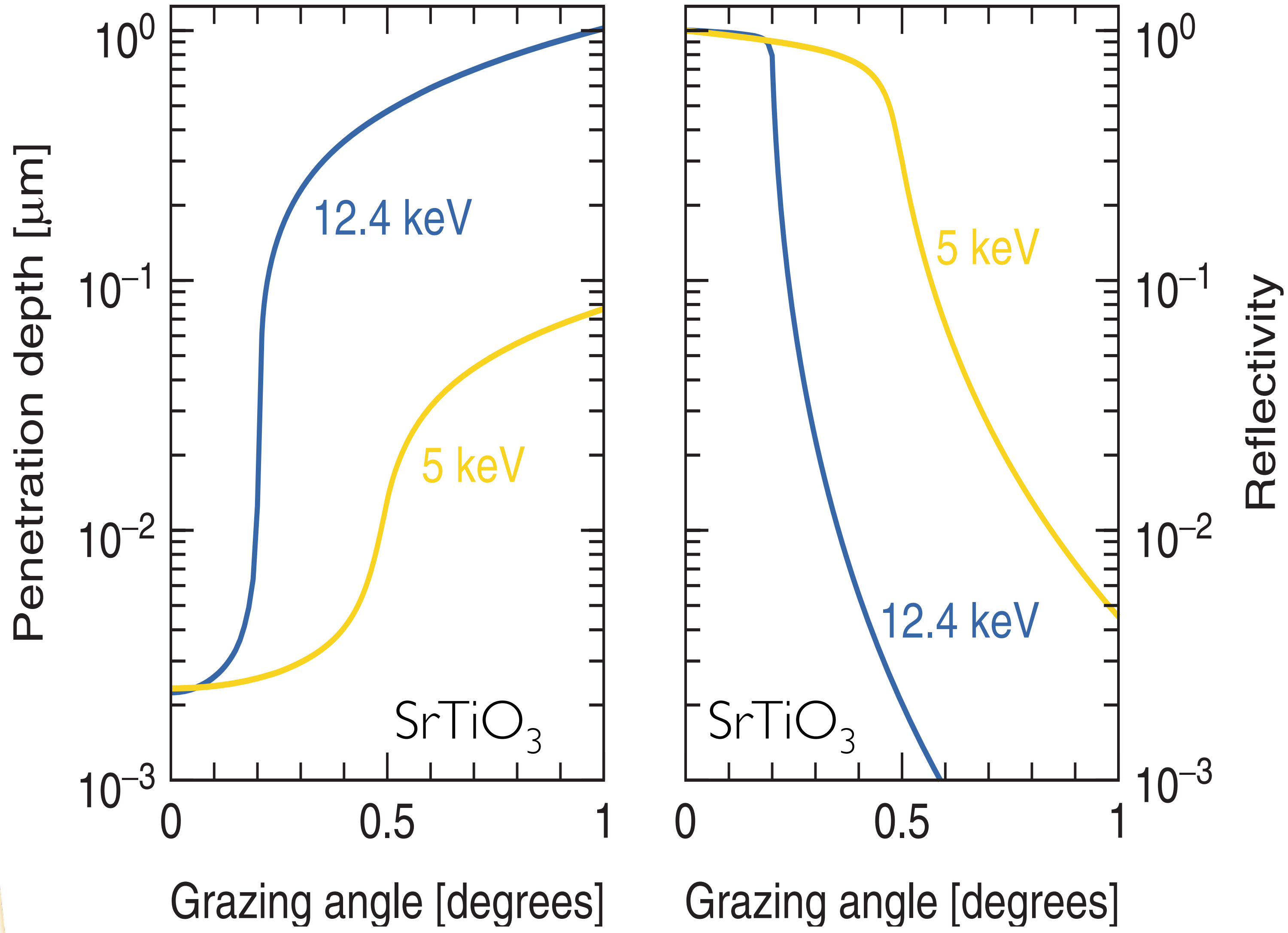

$$L \approx \frac{-\lambda}{4\pi \ \mathrm{Im}\sqrt{\alpha_i^2 - \alpha_c^2 - 2i\beta}}$$

Example: ZnTe/GaAs

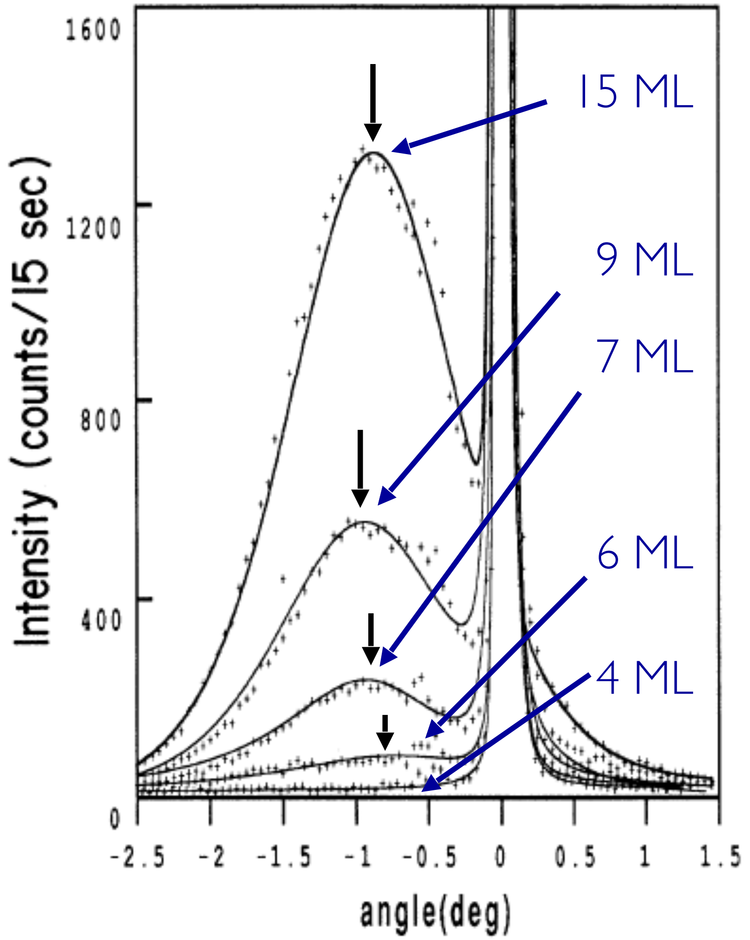

FIG. 1. θ-2θ scans of the (200) reflection from ZnTe/GaAs (001) for heterostructures of increasing thicknesses (4, 6, 7, 9, and 15 ML from bottom to top curve). Profiles are aligned on the substrate Bragg peak.

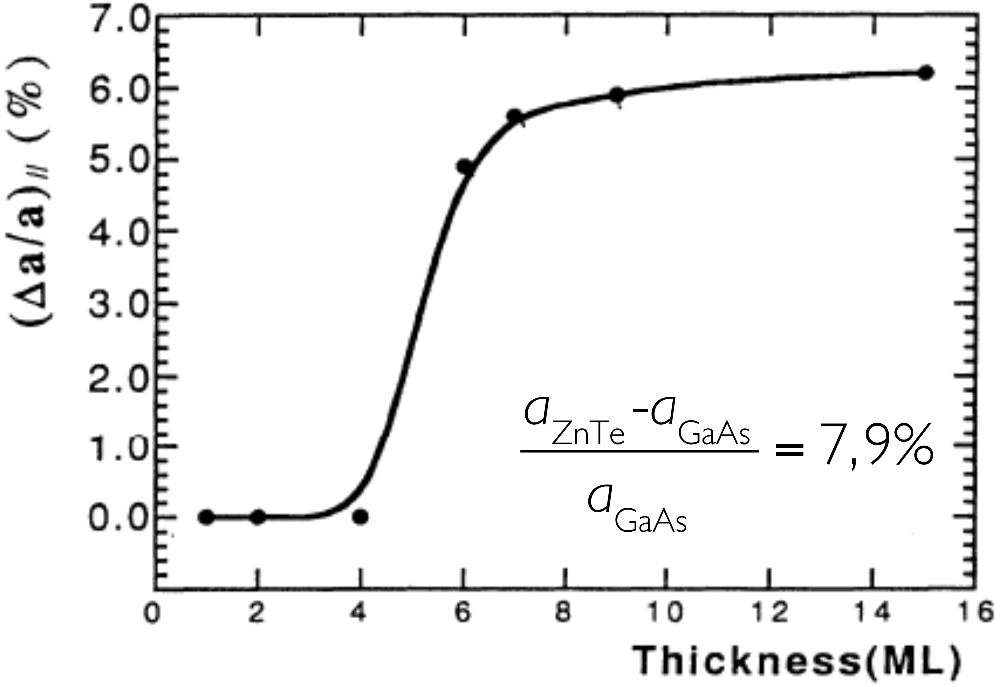

FIG. 2. Variation of $(\Delta a/a)_{||}$ with the film thickness.

V. H. Etgens et al. Phys. Rev. B47, 10607 (1993)

Example: ZnTe/GaAs

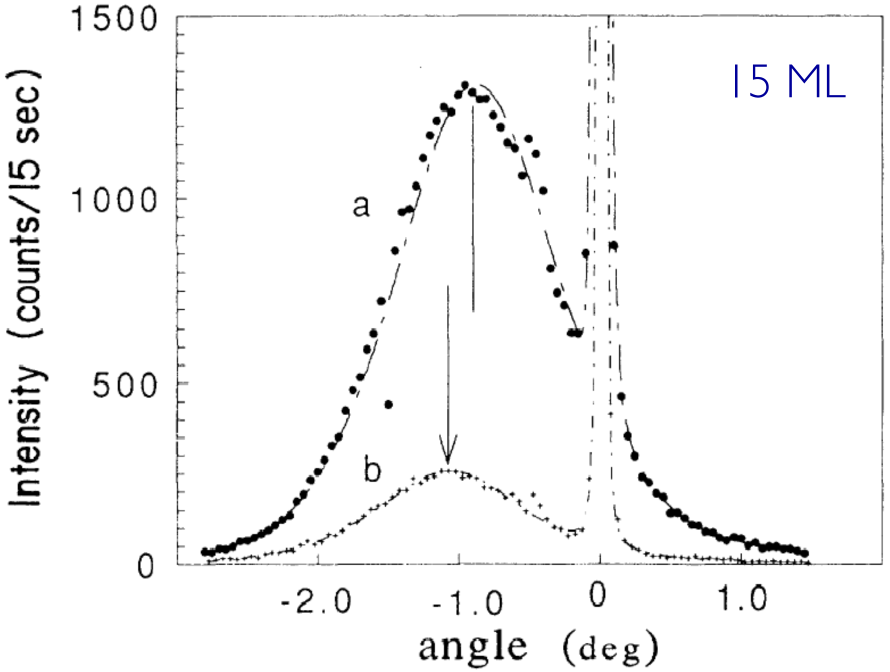

FIG. 6. Radial scans of the 15-ML ZnTe/GaAs at different inside angles. (curve a) $\alpha = \alpha_c$; (curve b) $\alpha = 0.3\alpha_c$.

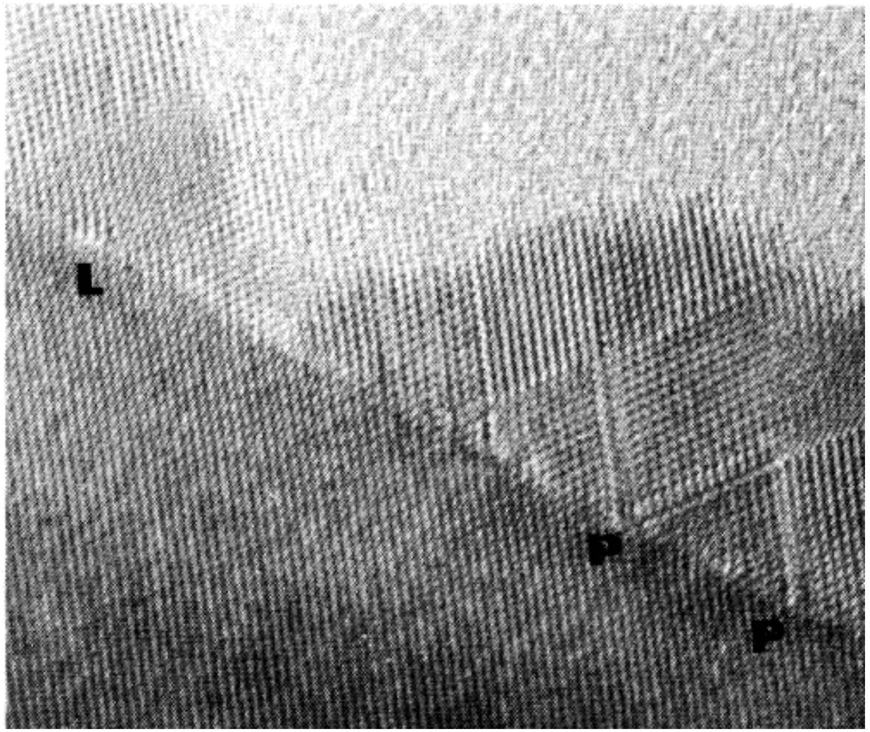

V. H. Etgens et al. Phys. Rev. B47, 10607 (1993)

Data collection geometry

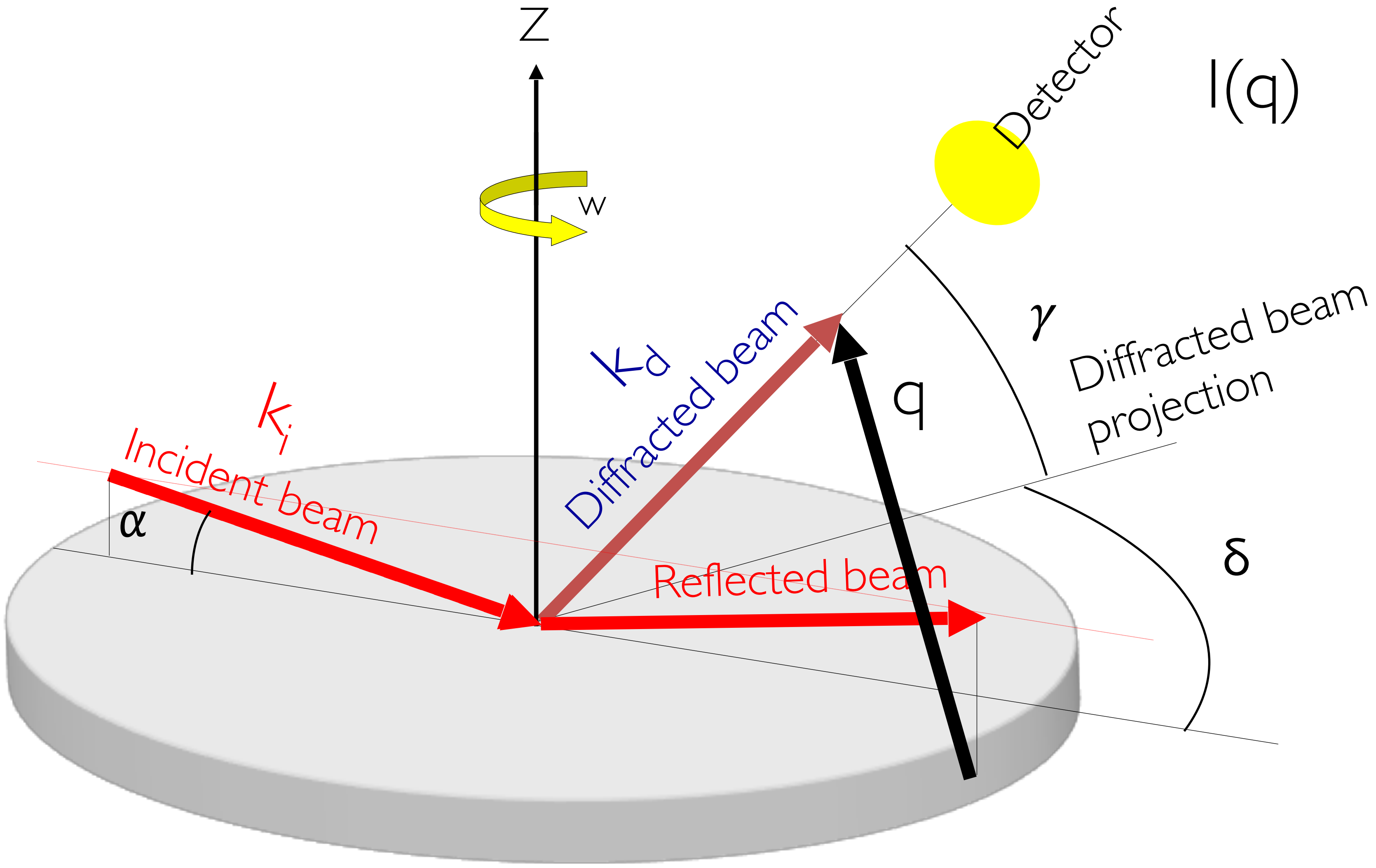

Scattering Vector : $q = k_d - k_i$

Crystal Truncation Rod (CTR)

Scattering intensity from a crystal

$$I(\mathbf{q}) = |A(\mathbf{q})|^2 \propto \left| \int_\infty d^3r\, \rho(\mathbf{r}) \exp(i\mathbf{q}\cdot\mathbf{r}) \right|^2$$

Kinematic approximation

Decomposition : crystal description

Atom $f_{atome}(\mathbf{q}) = \int d^3r \;\; \rho_{atome}(\mathbf{r}) \;\; e^{-i\mathbf{q}.\mathbf{r}}$ Atomic scattering factor

Unit Cell $F_n(\mathbf{q}) = \sum_j f_j \;\; e^{-i\mathbf{q}.\mathbf{r}_j} = TF[unit\ cell]$ Structure Factor

Cristal $A(\mathbf{q}) = \sum_n \sigma(\mathrm{R}_n)\; F_n(\mathbf{q}) \;\; e^{-i\mathbf{q}.\mathrm{R}_n}$

Lattice vector : R_n

Crystal shape : $\sigma(\mathbf{r})$

Perfectly ordered structure : $F_n(\mathbf{q}) = F(\mathbf{q})$

The intensity scattered by the crystal is :

$$\boxed{I(\mathbf{q}) = |F(\mathbf{q})|^2 \left[|\Sigma(\mathbf{q})|^2 \otimes \sum_{G_{hkl}} \delta(\mathbf{q} - G_{hkl}) \right]}$$

where $\Sigma(\mathbf{q}) = TF[\sigma(\mathbf{r})]$

Atomic structure

Finite size effects

periodicity

the atomic form factor is a complex quantity $f(q)=f^0(q)+f'+i\,f''$
the terms f' et f'' are only dependent on the X-ray energy and represent the dispersion and absorption corrections, they take significant values in a close vicinity of absorption edges of the considered atom (anomalous effect)

Scattering intensity from a semi-infinite crystal

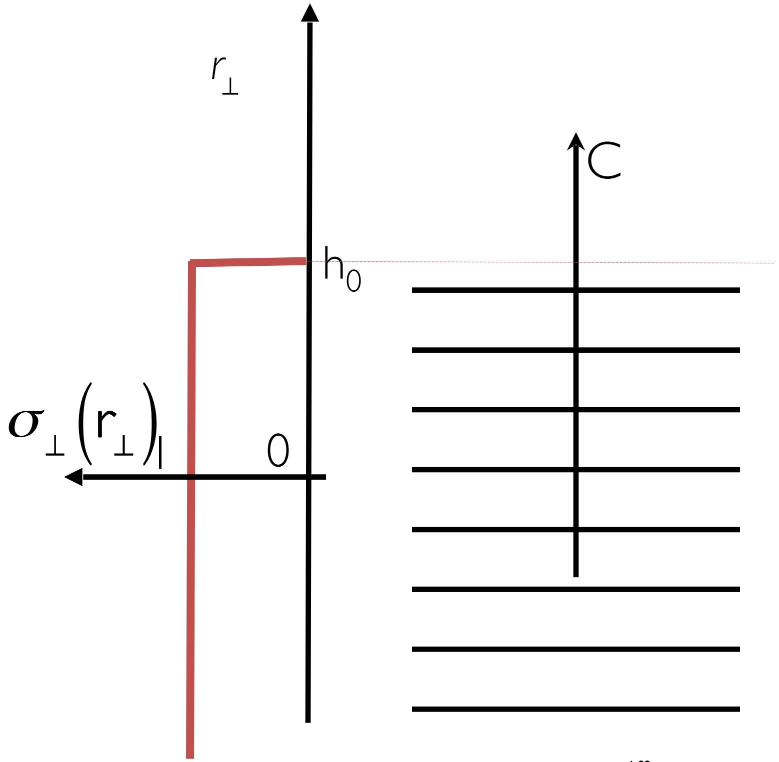

$$\sigma(r) = \sigma_{//}(r_{//})\ \sigma_\perp(r_\perp)$$

where $\sigma_{//}(r_{//}) = 1$

$$\sigma_\perp(r_\perp) = 1 \quad \text{pour } r_\perp < h_0$$
$$\sigma_\perp(r_\perp) = 0 \quad \text{pour } r_\perp > h_0$$

Fourier transform of $\sigma(r)$:

$$\Sigma(q) = \frac{e^{-iq_\perp . h_0}}{-iq_\perp}\ \delta(q_{//}) \Rightarrow \left|\Sigma(q)\right|^2 = \frac{1}{q_\perp^2}\ \delta(q_{//})$$

$$\sum_{n=-\infty}^{+\infty} \frac{1}{(q_\perp - n\, c^*)^2} = \left(\frac{\pi}{c^* \sin(\pi L)}\right)^2$$

$$\boxed{I(q) = \frac{|F(q)|^2}{s^2}\left(\frac{1}{2\sin(\pi l)}\right)^2 \left[\sum_{G_{//}} \delta(q_{//} - G_{//})\right]}$$

→ Crystal Truncation Rods (CTR):
issued from Bragg peak & perpendicular to the surface

Cristal Truncation Rod (CTR)

$$I(\mathrm{q}) = \frac{|F(\mathrm{q})|^2}{s^2}\left(\frac{1}{2\sin(\pi l)}\right)^2\left[\sum_{G_{//}}\delta(\mathrm{q}_{//}-\mathrm{G}_{//})\right]$$

Real space

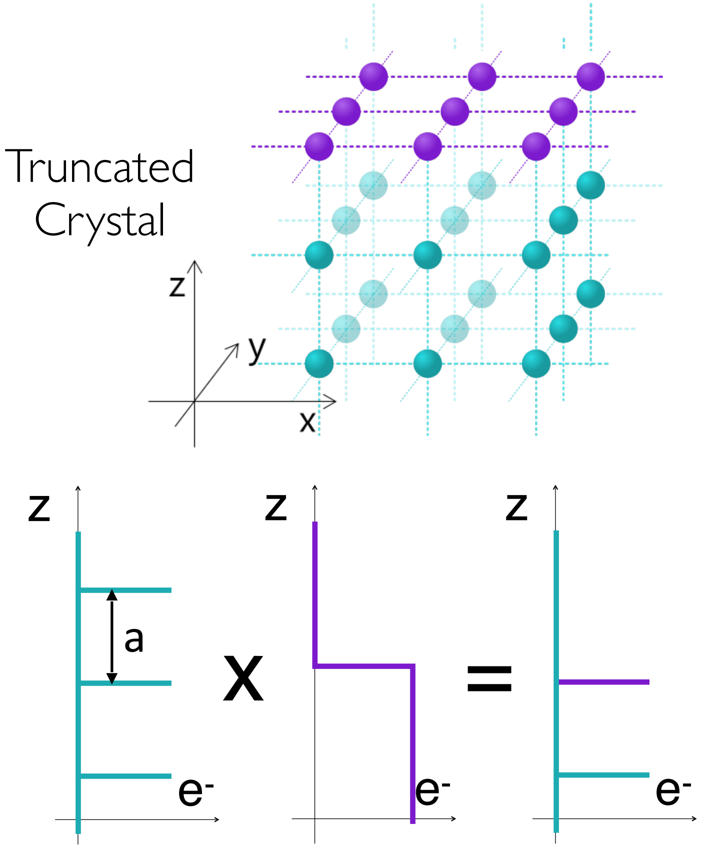

Reciprocal space

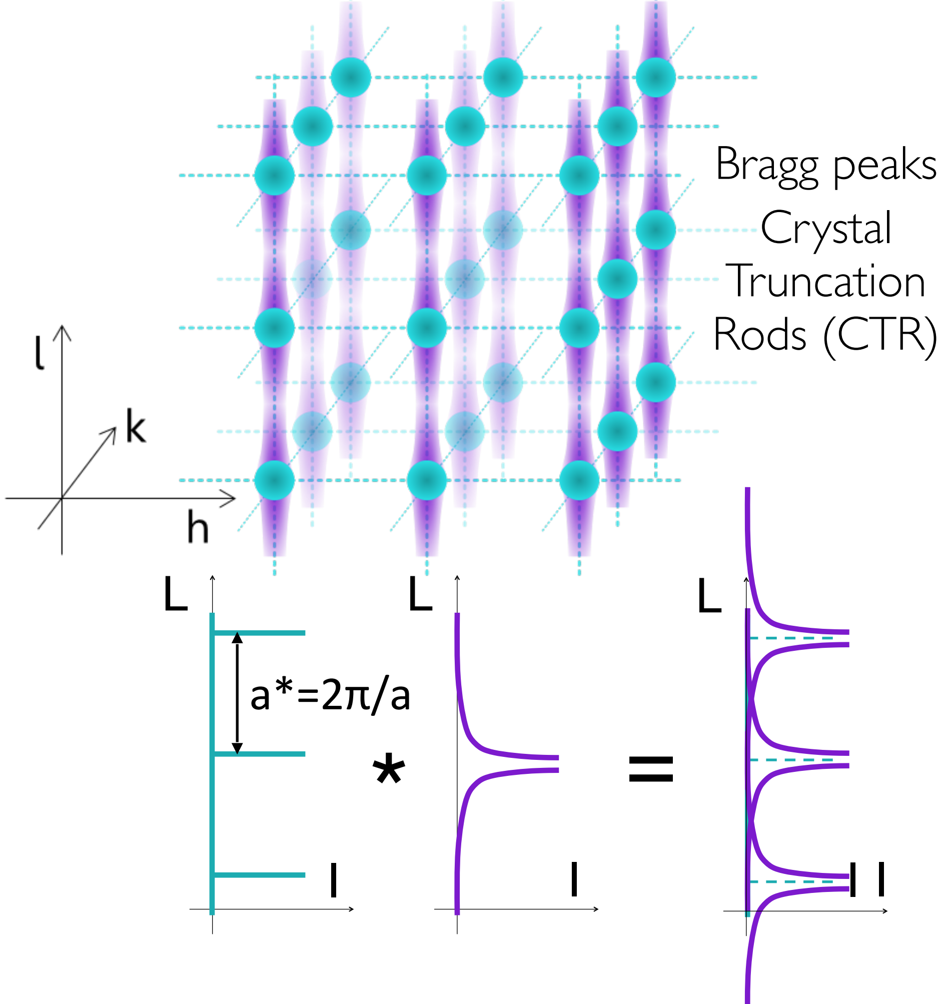

Cristal Truncation Rod (CTR)

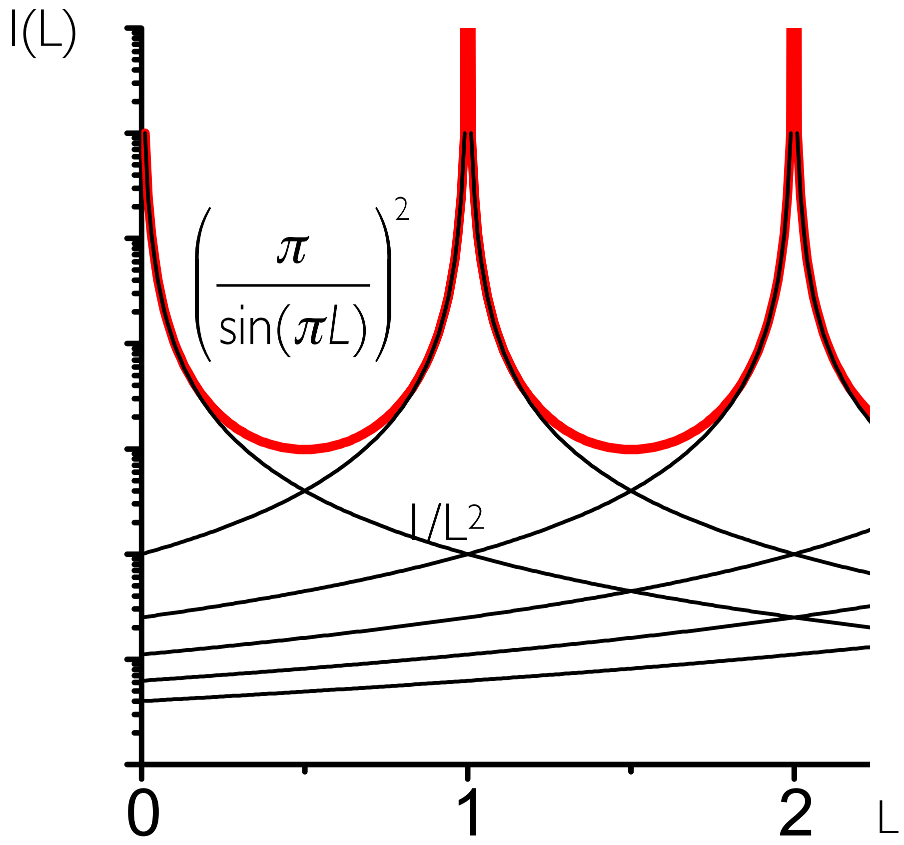

$$\sum_{n=-\infty}^{+\infty} \frac{I}{\left(q_\perp - n\, c^*\right)^2} = \left(\frac{\pi}{c^* \sin(\pi L)}\right)^2 \qquad q_\perp = L c^*$$

Surface roughness

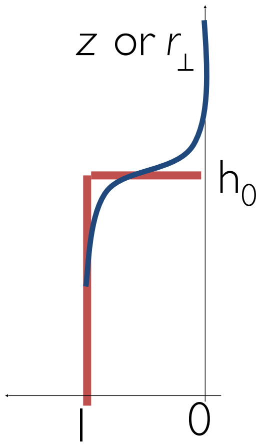

$$\sigma_\perp^{surf}(r_\perp) = 1 \quad \text{for } r_\perp < h_0$$
$$\sigma_\perp^{surf}(r_\perp) = 0 \quad \text{for } r_\perp > h_0$$

$$\sigma_\perp^{surf.\,rgh.}(r_\perp) = \sigma_\perp^{surf}(r_\perp) \otimes g(r_\perp)$$

$$\Rightarrow \quad \left|\Sigma^{surf.rgh.}(q_\perp)\right|^2 = \frac{1}{q_\perp^2}\left|TF\left[g(r_\perp)\right]\right|^2$$

The Intensity decays more rapidly from the reciprocal node than for a flat surface
Roughness models:

i. a simple two level model (E.Vlieg)
ii. an exponential decay (I. Robinson)
iii. a gaussian distribution of successive layers occupancy (P. Guenard)

CTR from a rough surface

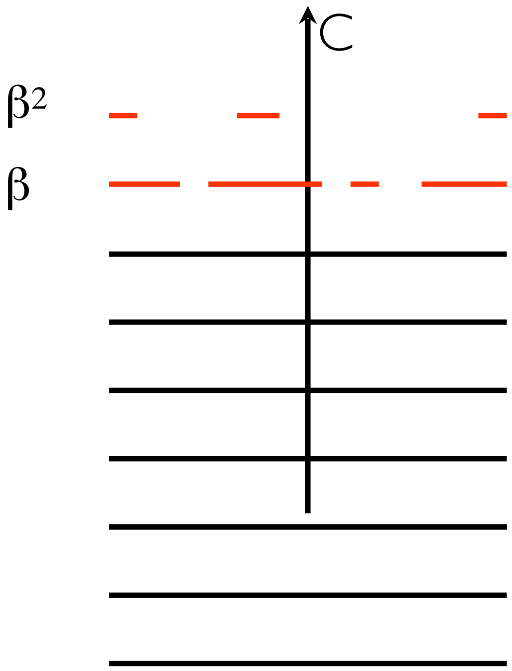

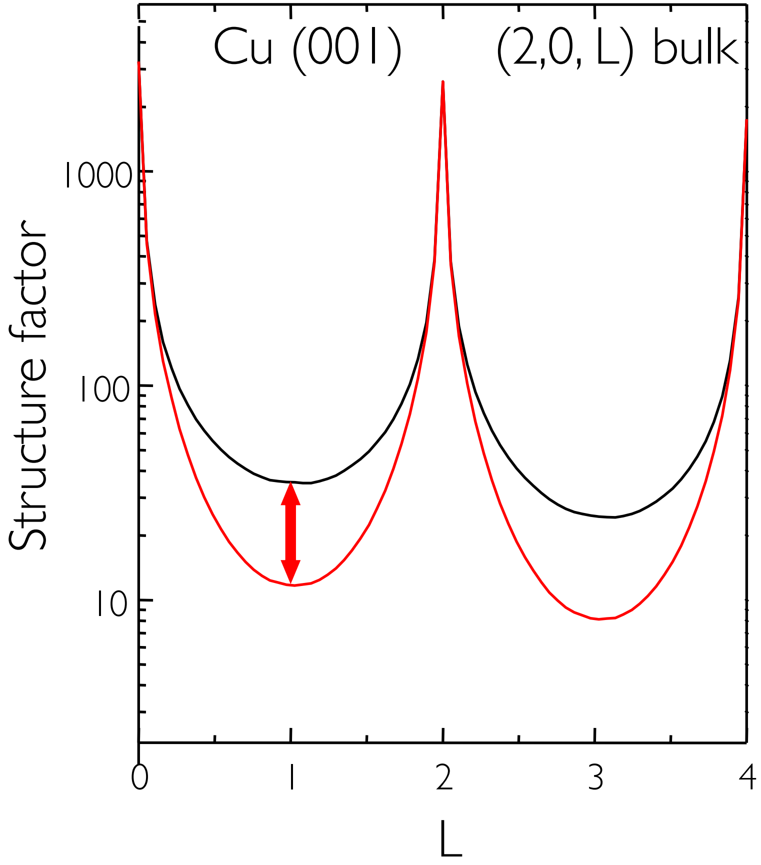

Optimal sensitivity in « anti-bragg » position, used to monitor layer by layer growth through pseudo-periodic oscillations

CTR from a relaxed surface

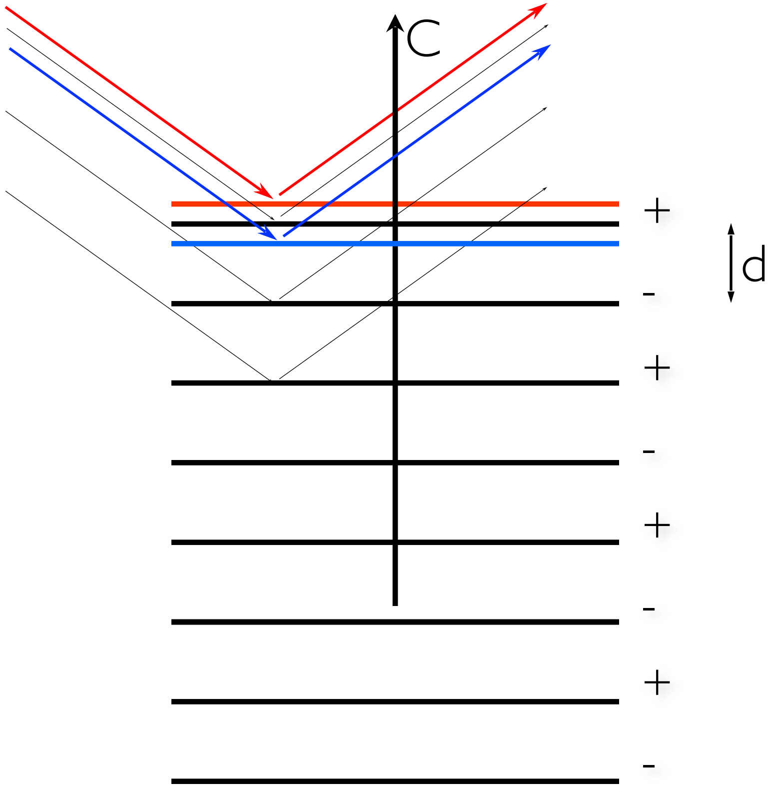

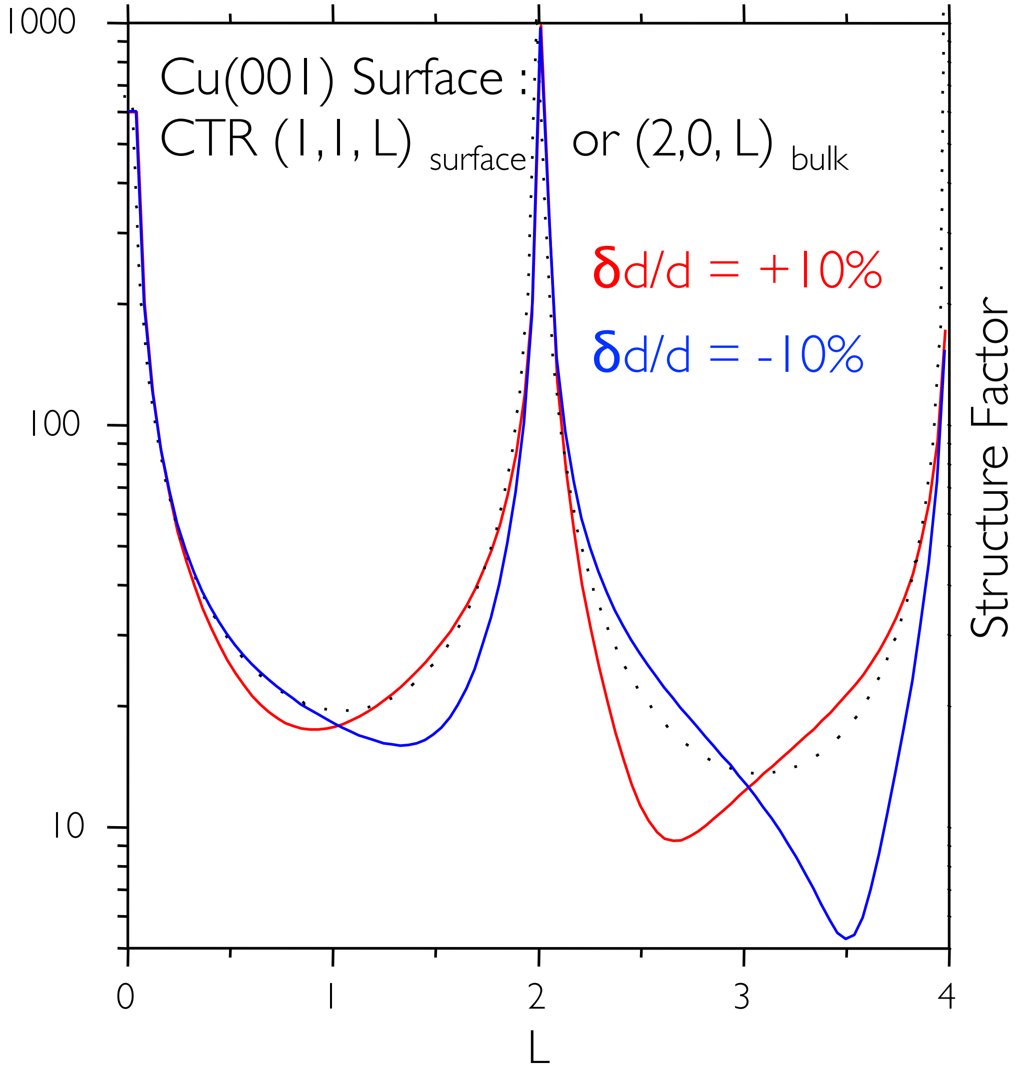

CTR : Cu (001) et N/Cu(001)

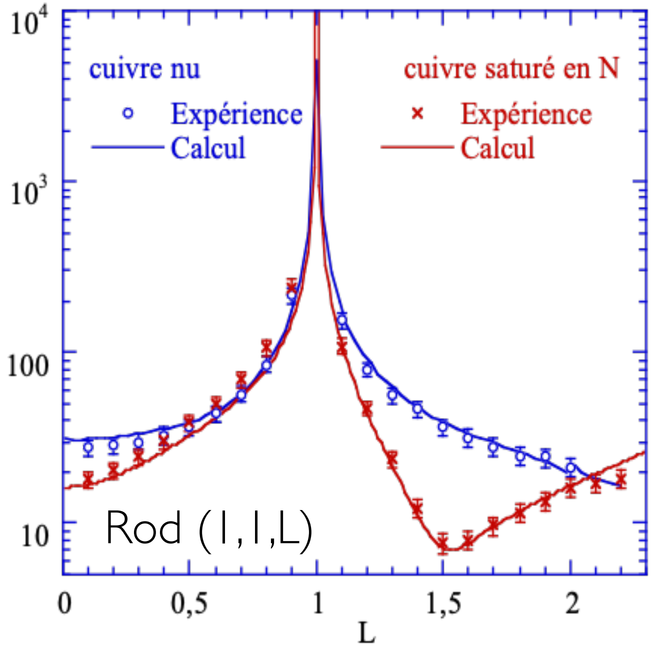

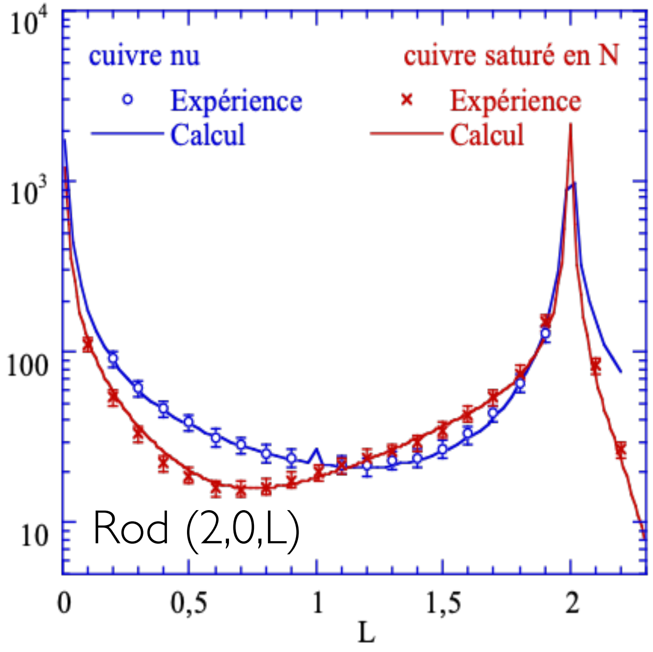

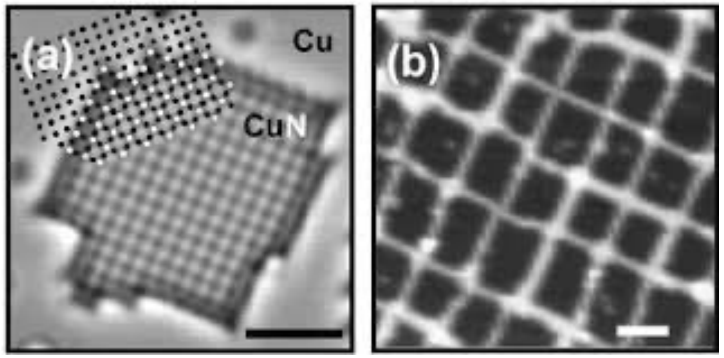

Light element (N)
but it is possible to see the relaxations induced on the Cu(001) substrate

	bare Cu	saturated Cu (q =1)
Relaxation d_{12}	-3,16%	+13,54%
Relaxation d_{23}	-0,54%	+1,46%

B. Croset et al., Phys. Rev. Lett. 88,056103 (2002)

CTR and interfaces

SiNi$_2$/Si(111) interface

NiSi$_2$ Structure and thickness known

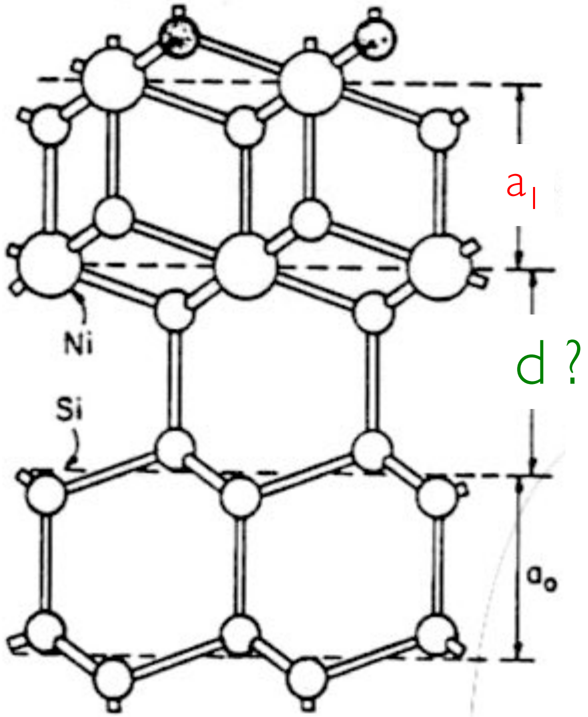

Si(111) structure known

around Si(111) Bragg peak

$$F_{Total} = F_{si} + \exp(2\pi l d)\, F_{NiSi_2}$$

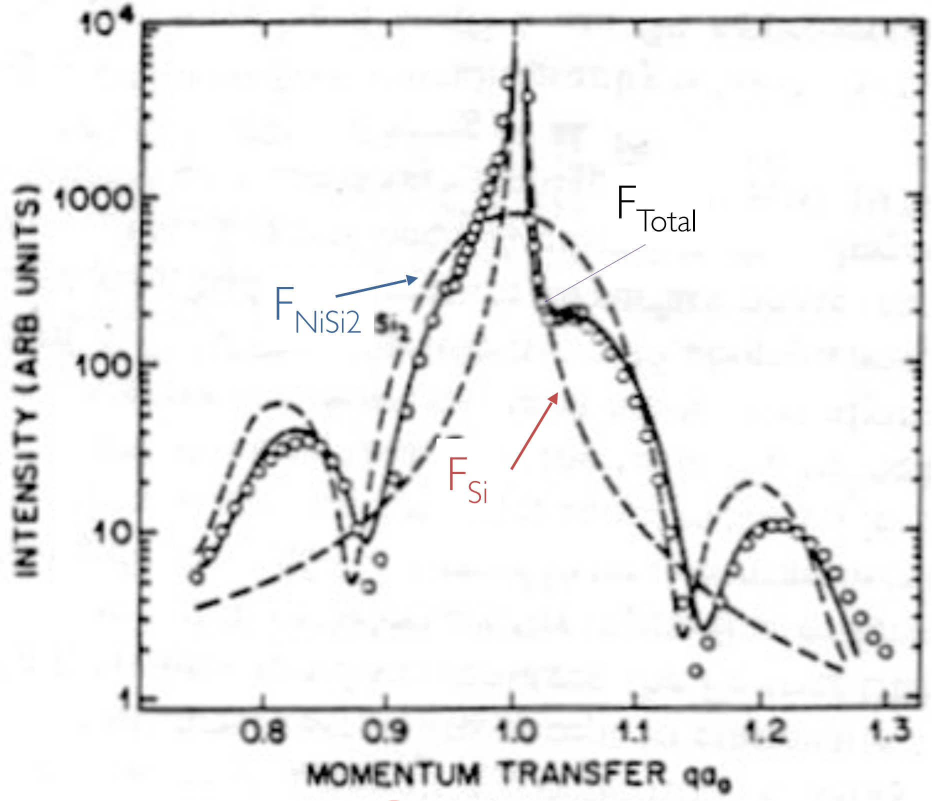

Adjustment → $\dfrac{d}{a_o} = 1.10 \pm 0.02$, $\dfrac{a_l}{a_o} = 0.996 \pm 0.003$

I. K. Robinson et al., Phys. Rev. B 38, 3632(R)

Surface x-ray Diffraction

2D crystal

$$\sigma(r) = \sigma_{//}(r_{//})\ \sigma_{\perp}(r_{\perp}) \quad \text{where} \quad \sigma_{//}(r_{//}) = 1$$
$$\sigma_{\perp}(r_{\perp}) = \delta(r_{\perp})$$

Fourier transform of $\sigma(r)$:

$$\Sigma(q) = const\ \delta(q_{//}) \Rightarrow \left|\Sigma(q)\right|^2 = const^2\ \delta(q_{//})$$

Real space

$$\boxed{I(q) = \frac{\left|F(q)\right|^2}{s^2} const^2 \left[\sum_{G_{//}} \delta(q_{//} - G_{//})\right]}$$

Reciprocal space

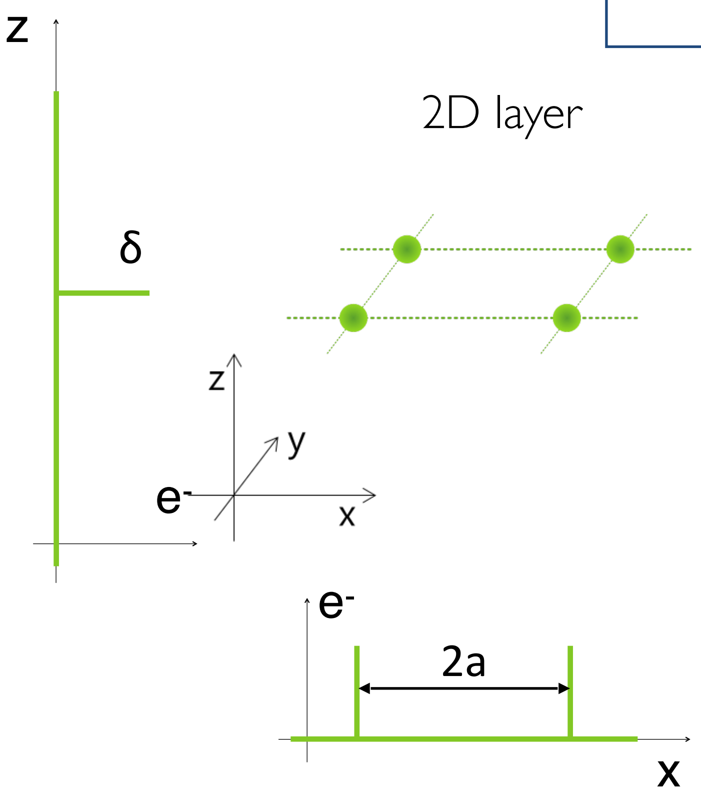

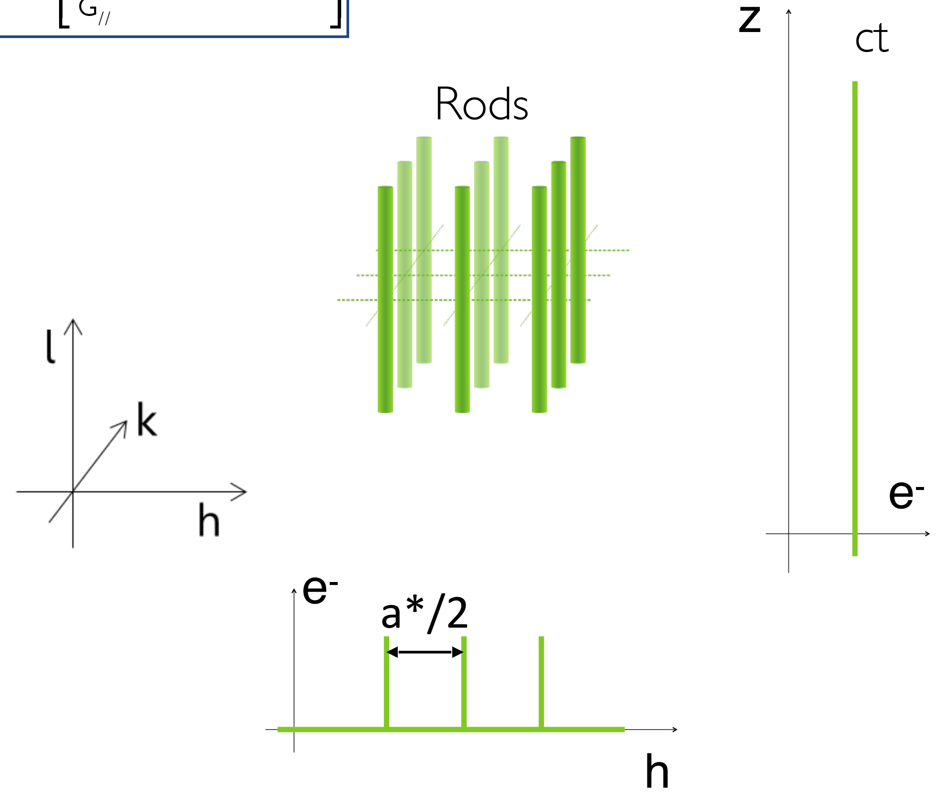

2D crystal - spheres

$$I(\mathrm{q}) = \frac{|F(\mathrm{q})|^2}{s^2} const^2 \left[\sum_{\mathrm{G}_{//}} \delta(\mathrm{q}_{//} - \mathrm{G}_{//}) \right]$$

2D layer
of spheres

Real space

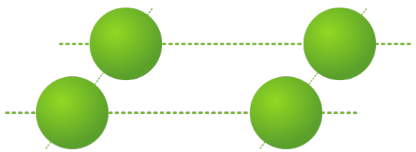

Reciprocal space

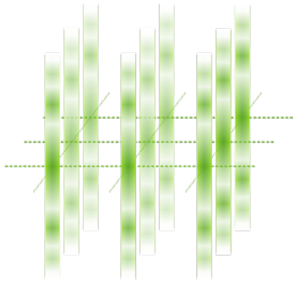

Modulated
intensity

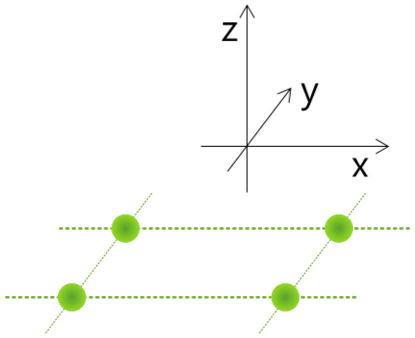

*

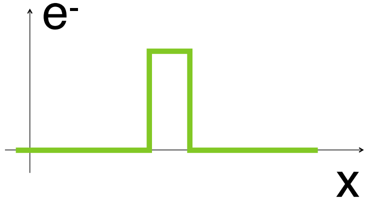

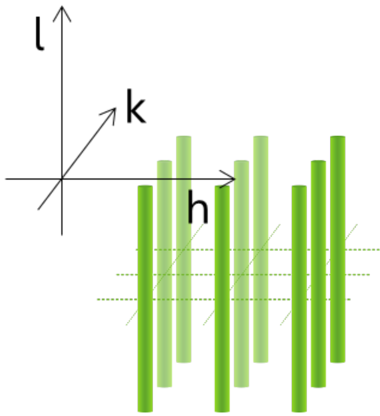

X

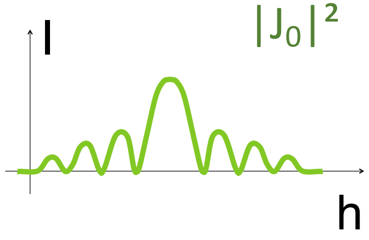

Surface x-ray Diffraction

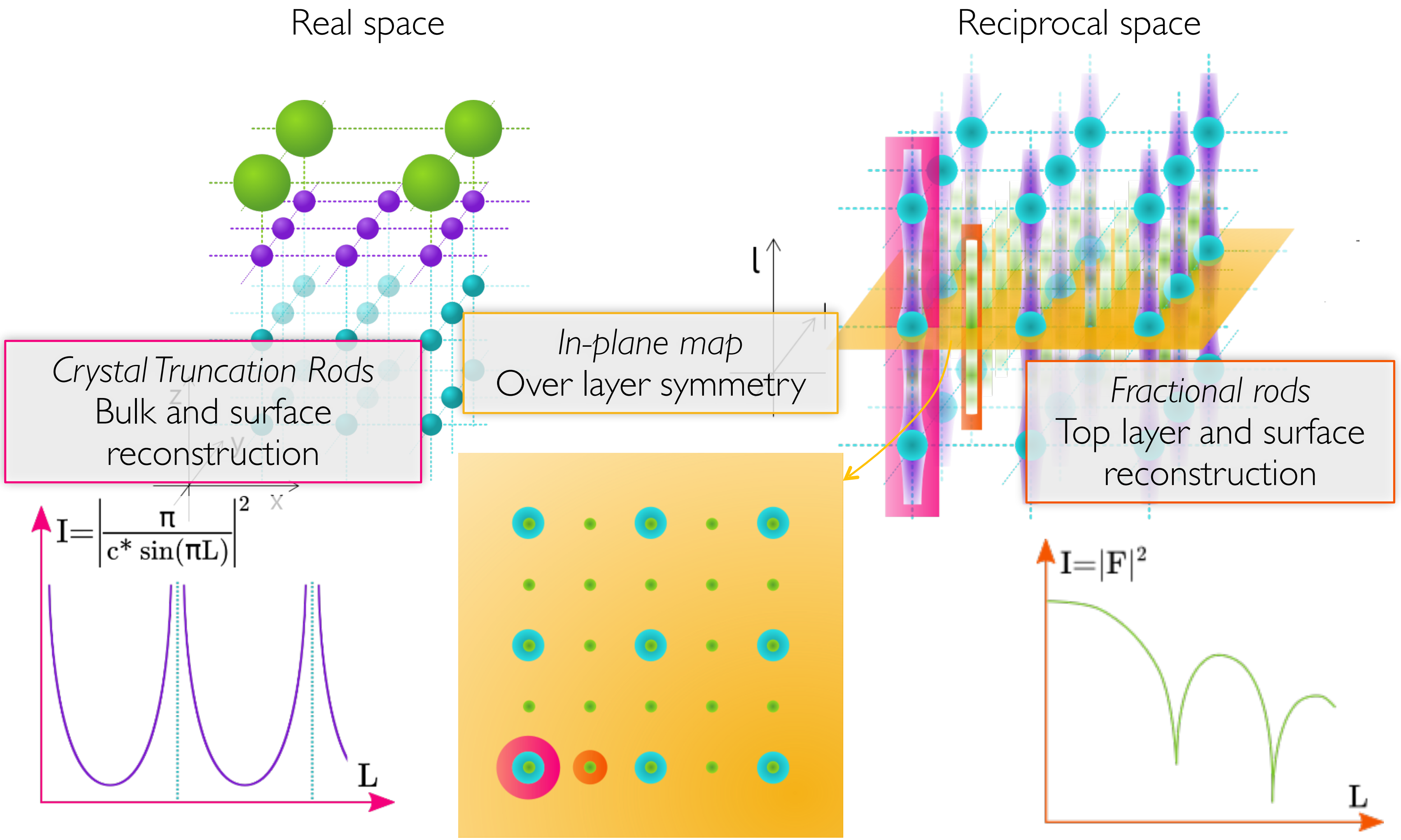

Surface crystallography

Ex: (110) cut in the
3 cubic lattices

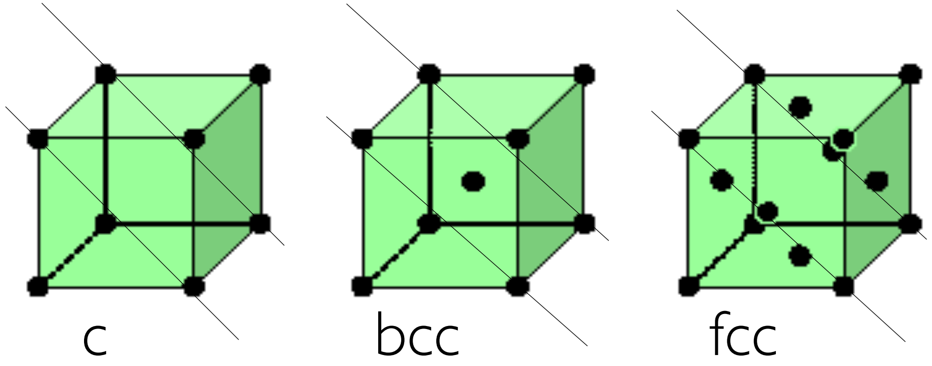

Basis vectors a_s b_s
of the 1x1 surface cells

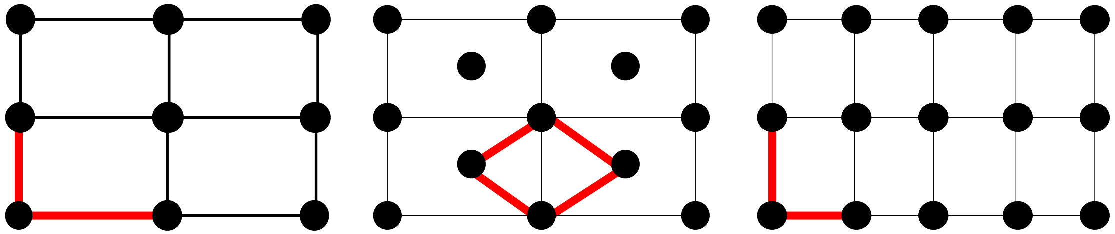

Basis vectors of a 2x2 unit cell on a
reconstructed (110) surface of an fcc lattice

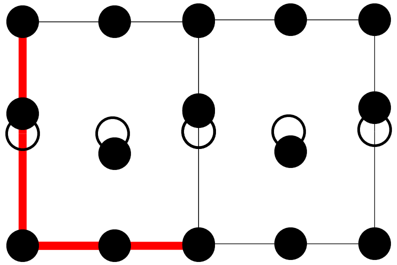

More generally mxn reconstruction

Graphene growth

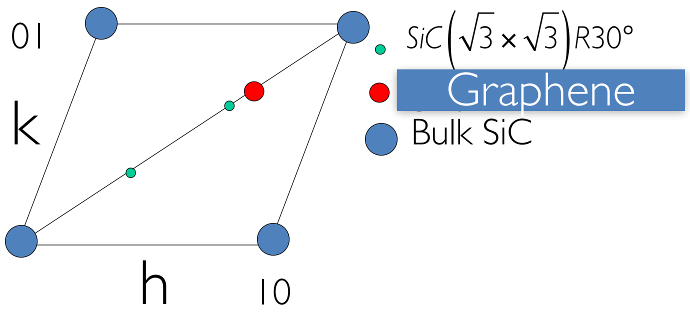

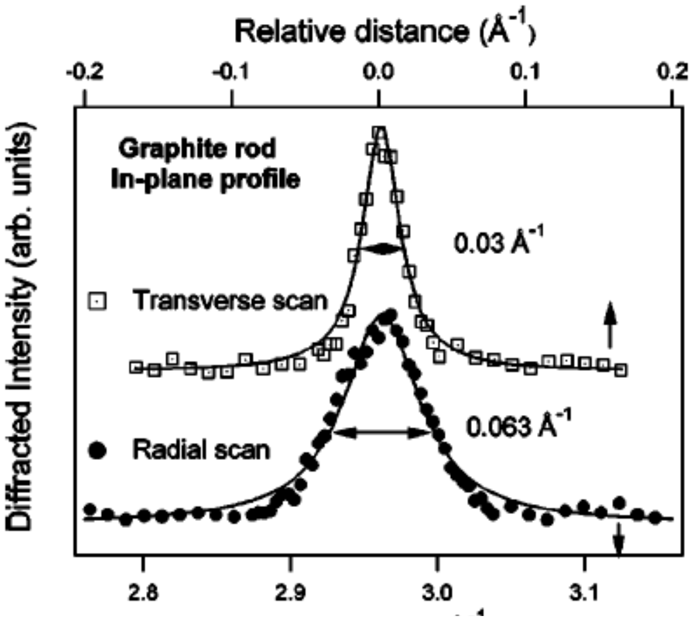

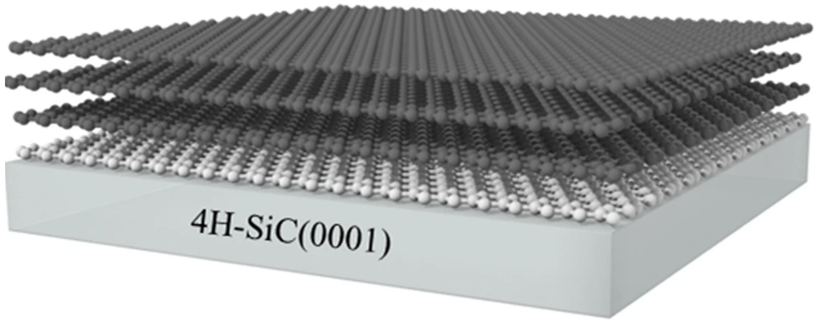

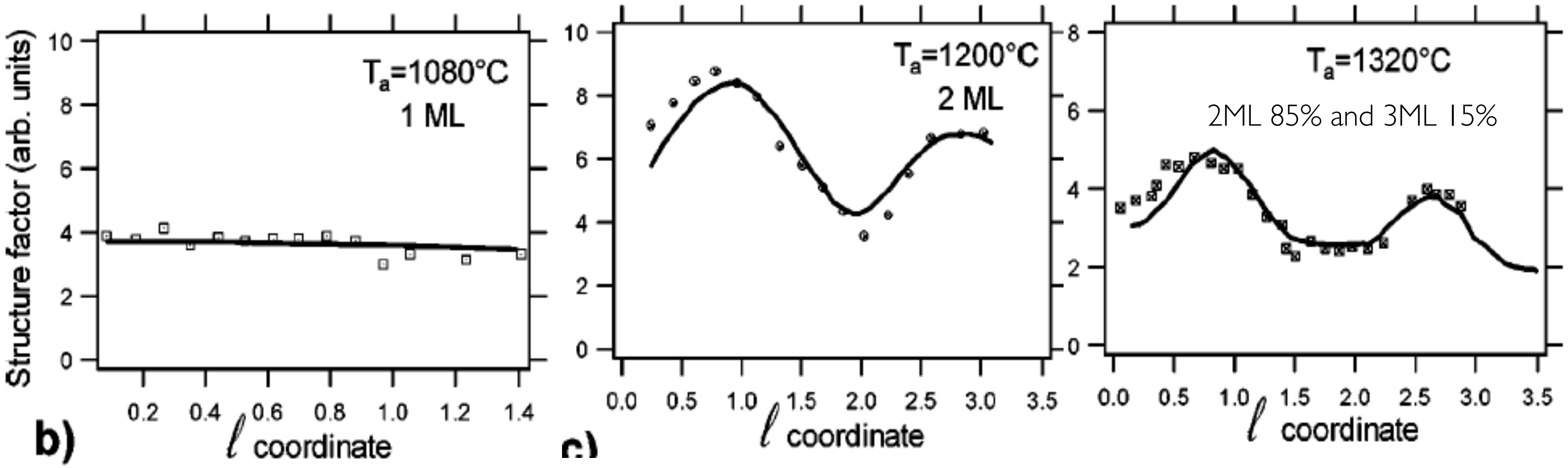

Charrier et al. J. Appl. Phys. 92, 2479(2002)

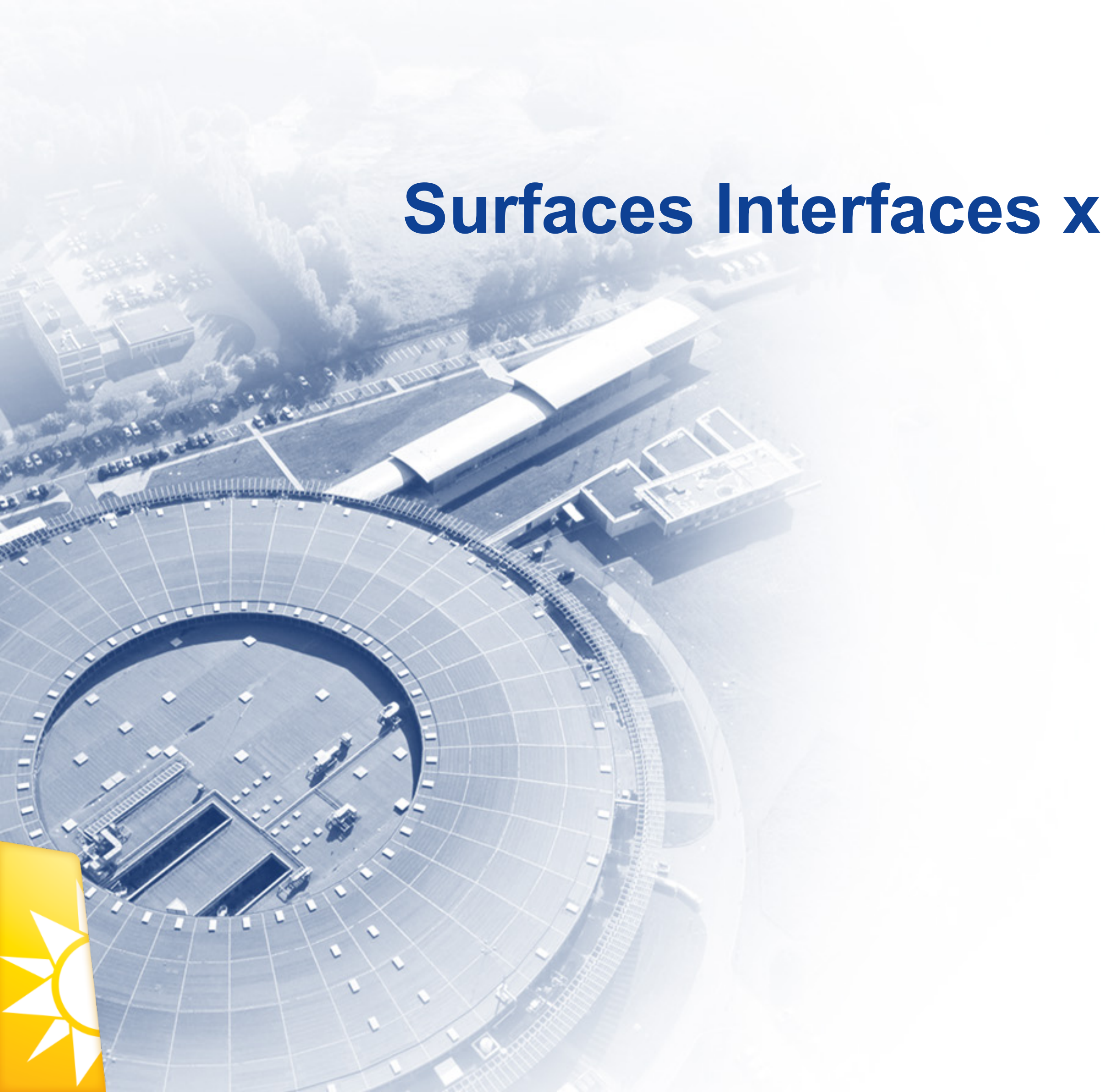

Surfaces Interfaces x-ray Scattering (SixS) beamline

@ Synchrotron SOLEIL

This is Us (SixS team 2024)

Alessandro COATI

Yves GARREAU

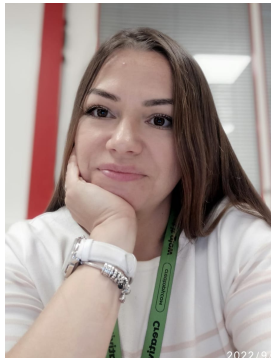

Alina VLAD

Michèle SAUVAGE

Benjamin VOISIN

Andrea RESTA

SixS beamline overview

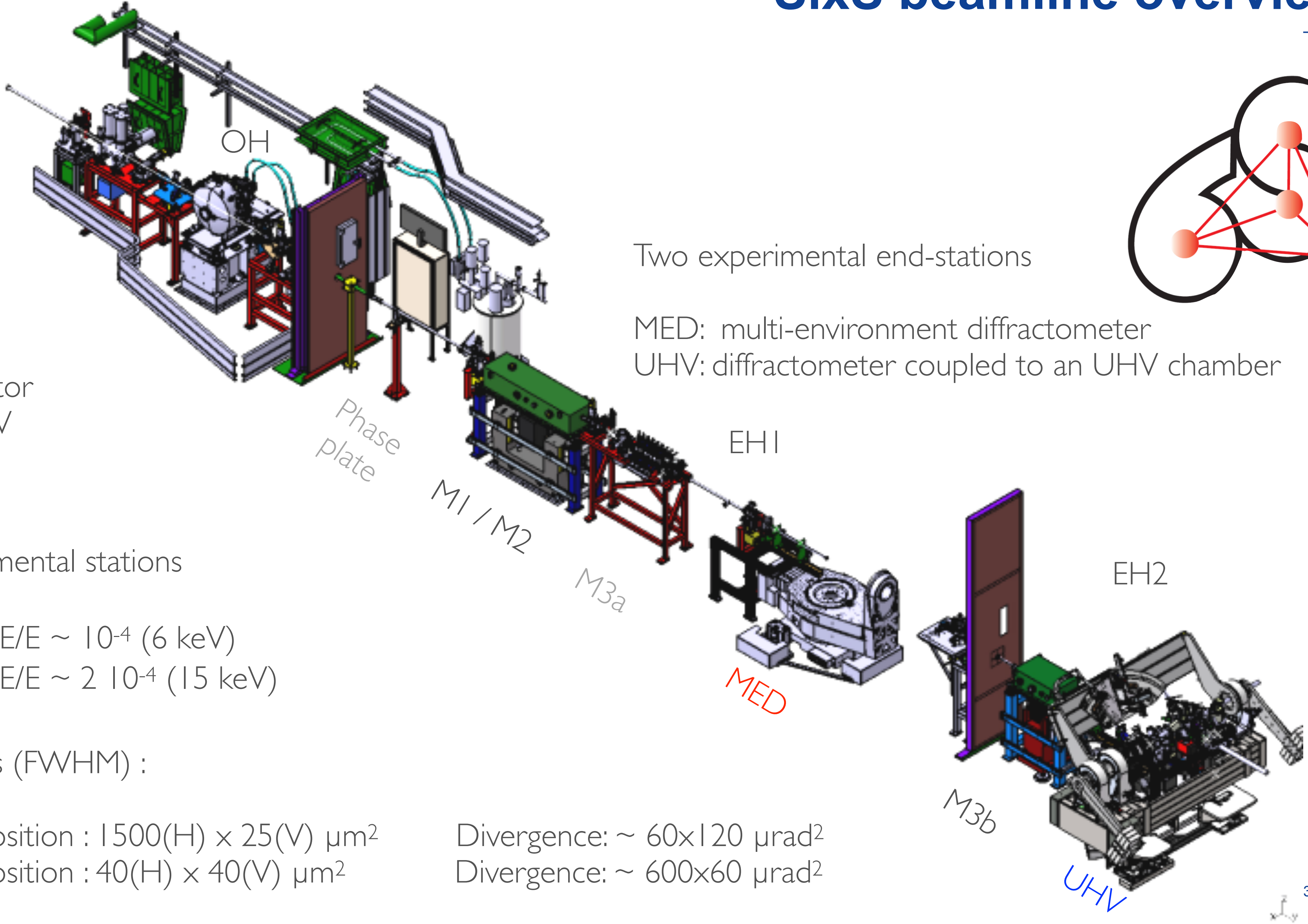

Two experimental end-stations

MED: multi-environment diffractometer
UHV: diffractometer coupled to an UHV chamber

U20 undulator
Si(111) monochromator
Energy range 5-20 keV

Flux on both experimental stations

$4\ 10^{13}$ ph/s with $\Delta E/E \sim 10^{-4}$ (6 keV)
$3\ 10^{12}$ ph/s with $\Delta E/E \sim 2\ 10^{-4}$ (15 keV)

Beam sizes (FWHM) :

at MED position : 1500(H) x 25(V) µm² Divergence: ~ 60x120 µrad²
at UHV position : 40(H) x 40(V) µm² Divergence: ~ 600x60 µrad²

SOLEIL - SixS beamline - UHV end-station

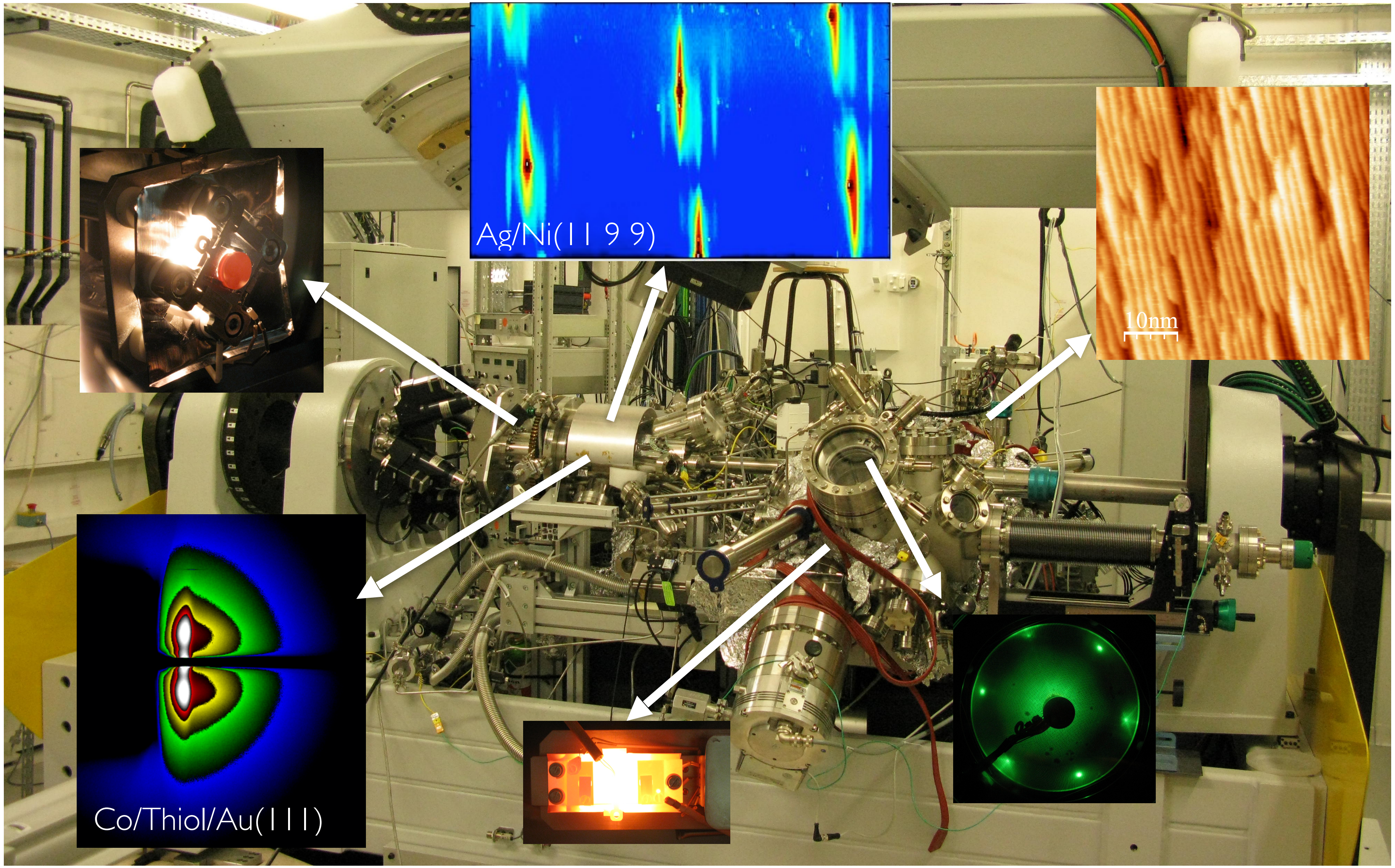

SOLEIL - SixS beamline - MED end-station

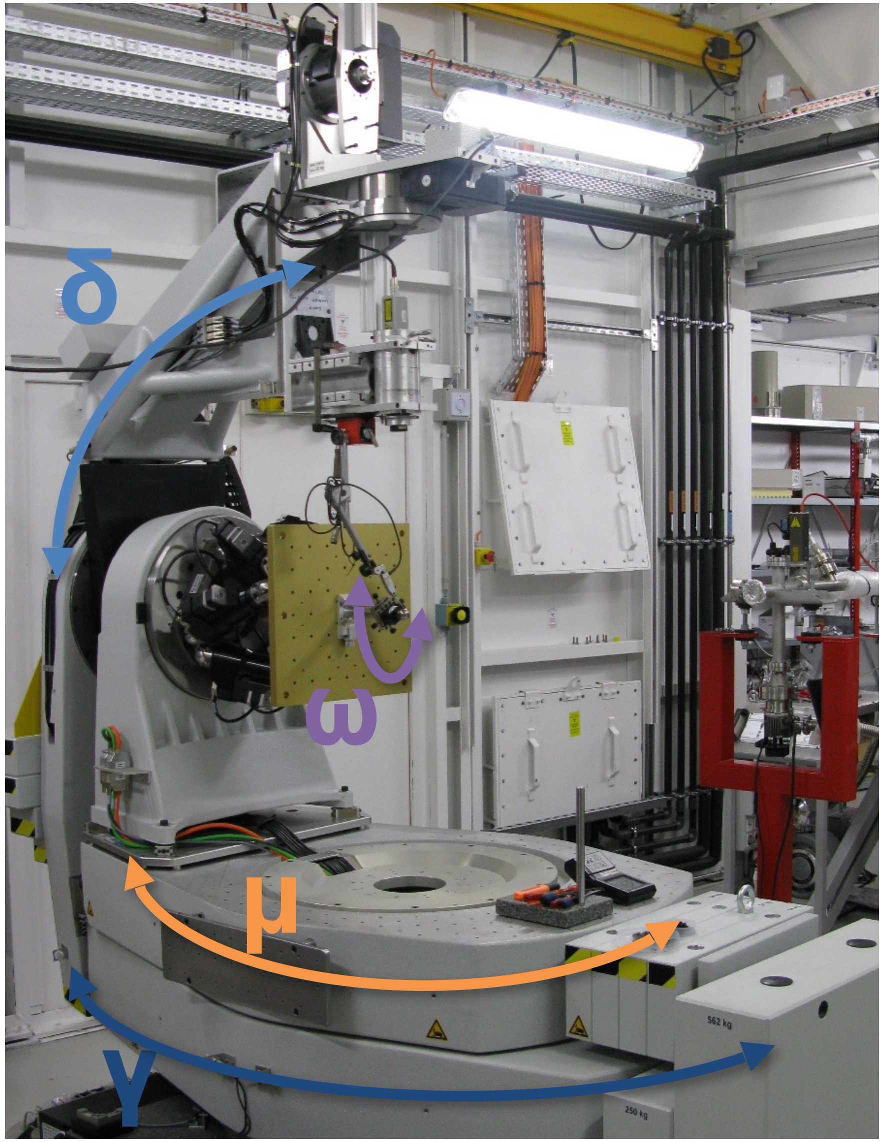

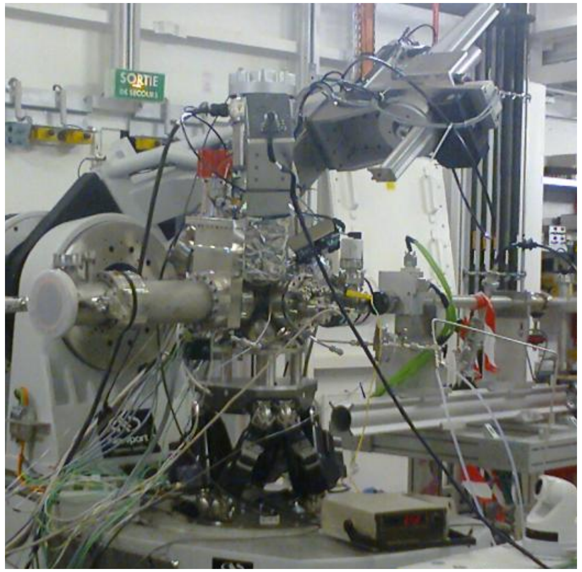

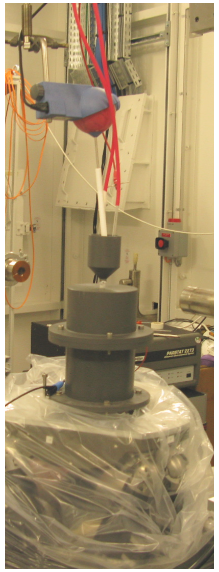

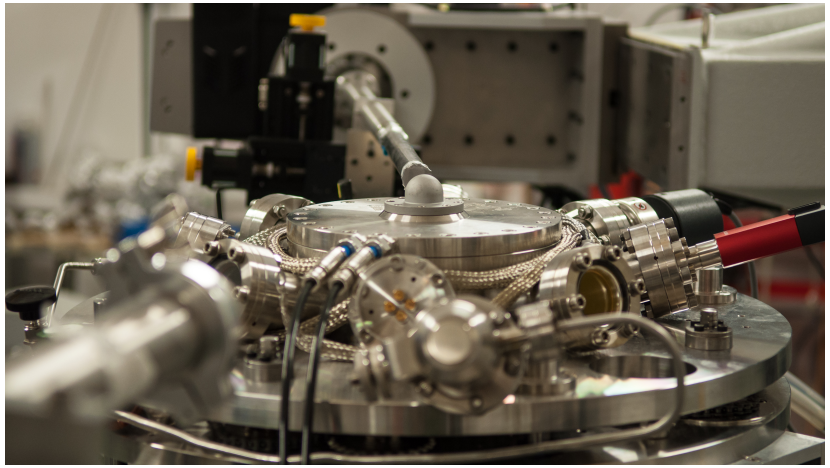

Fast Surface Diffraction

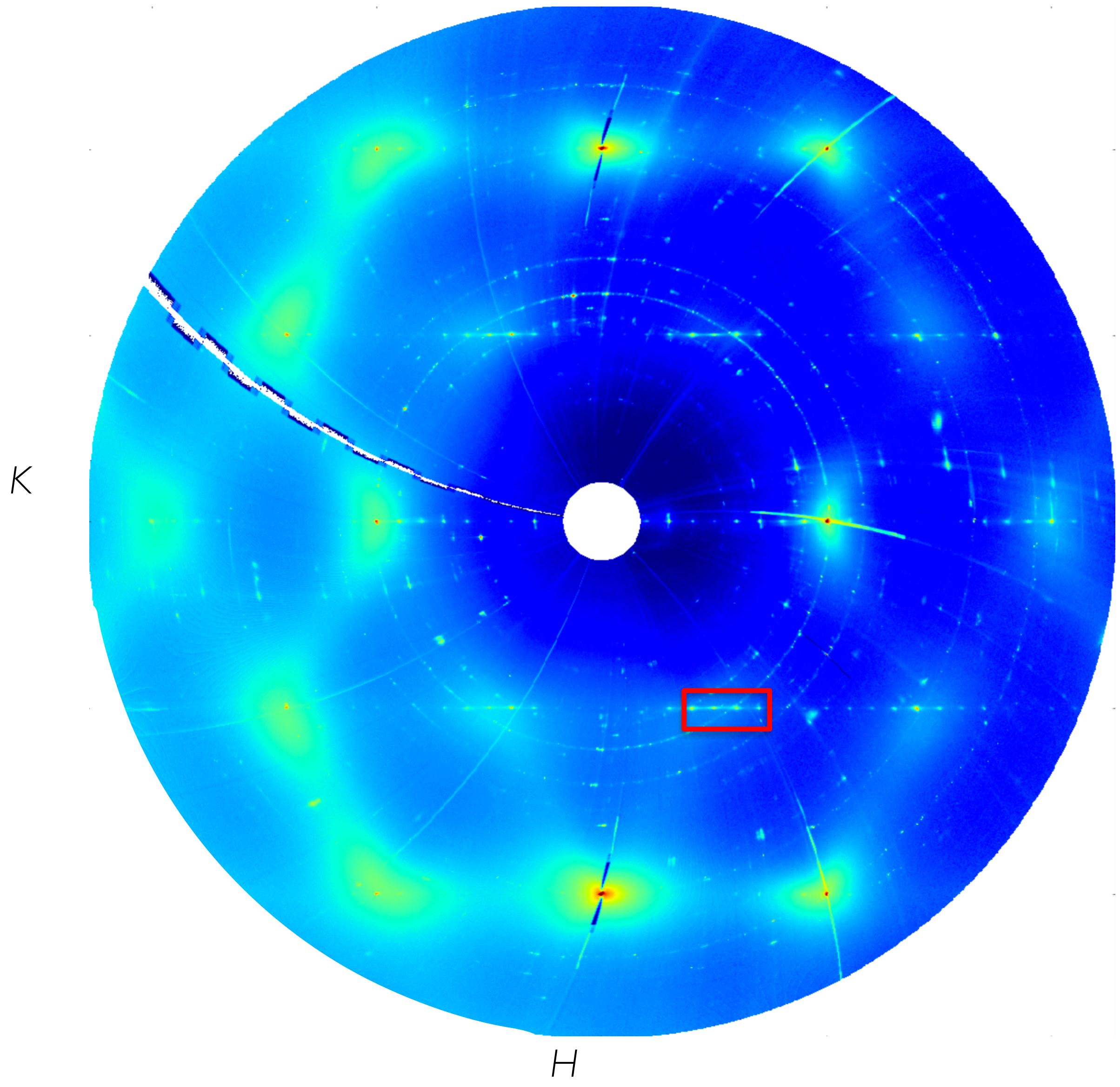

Pentacene/Cu322
(M. Sauvage, K. Muller, A. Kara, et al.)
In-plane (*hk*) – map
1h, 36000 images

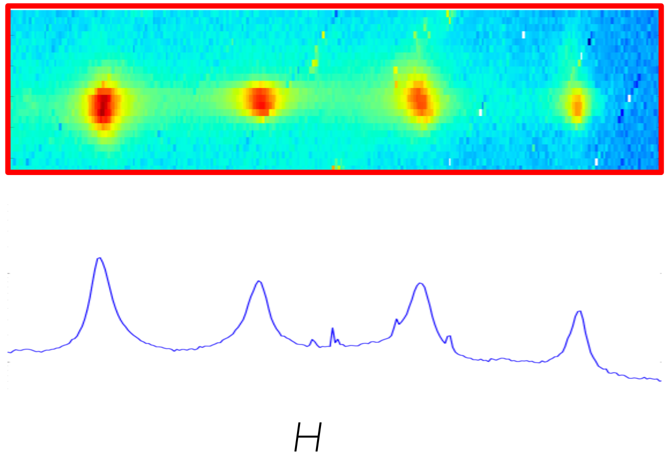

Surface structure
Surface periodicity

CTR in flyscan

- Less than 1 min
- Projection in the (*h l*) plane
- Beam Attenuators correction

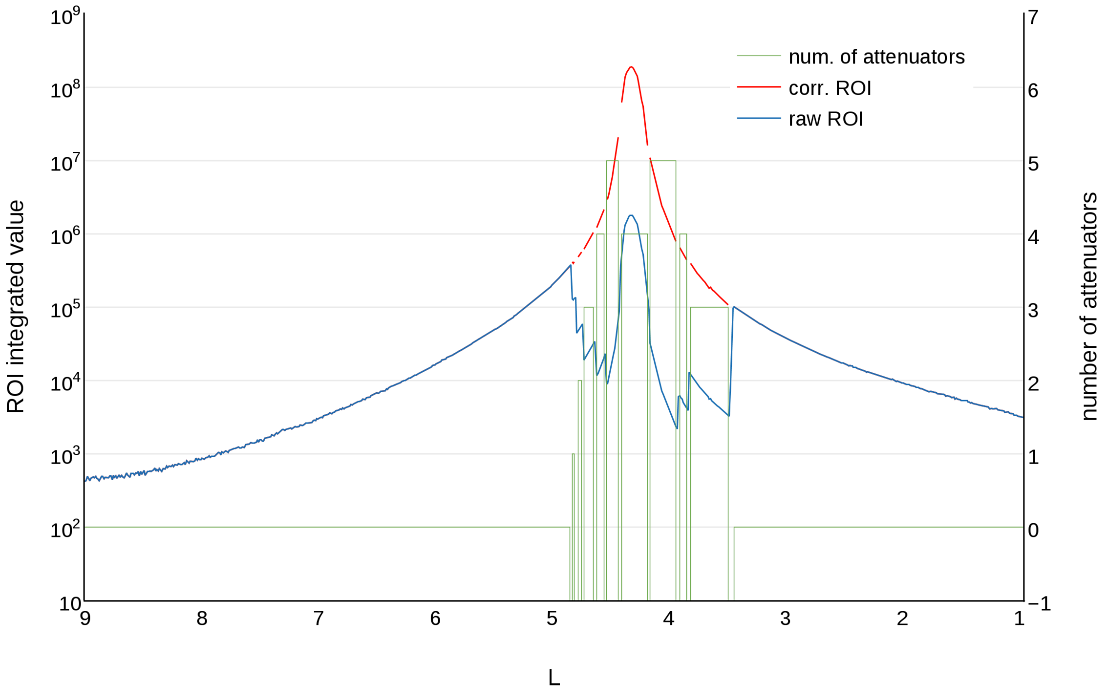

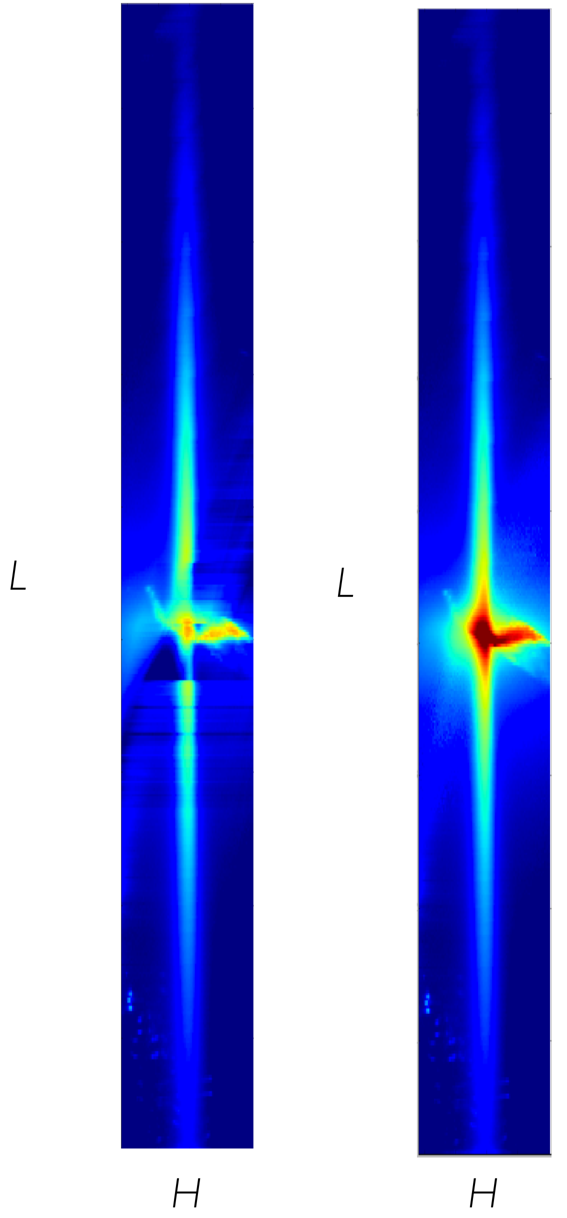

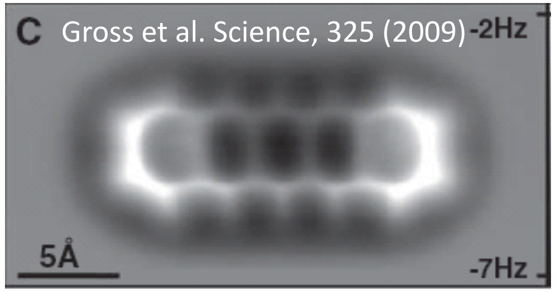

Average phenyl ring width : 2.42Å

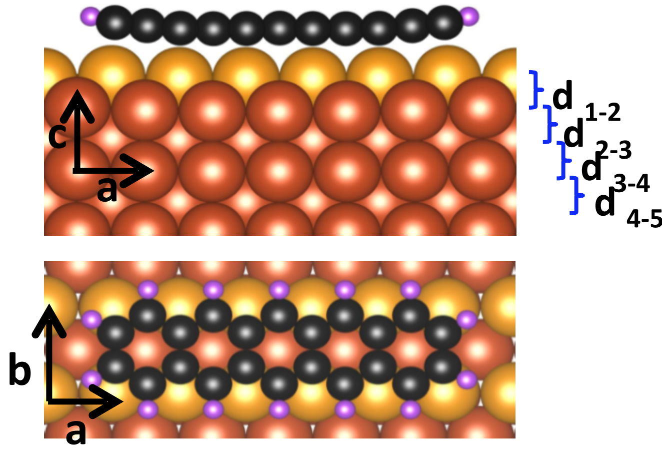

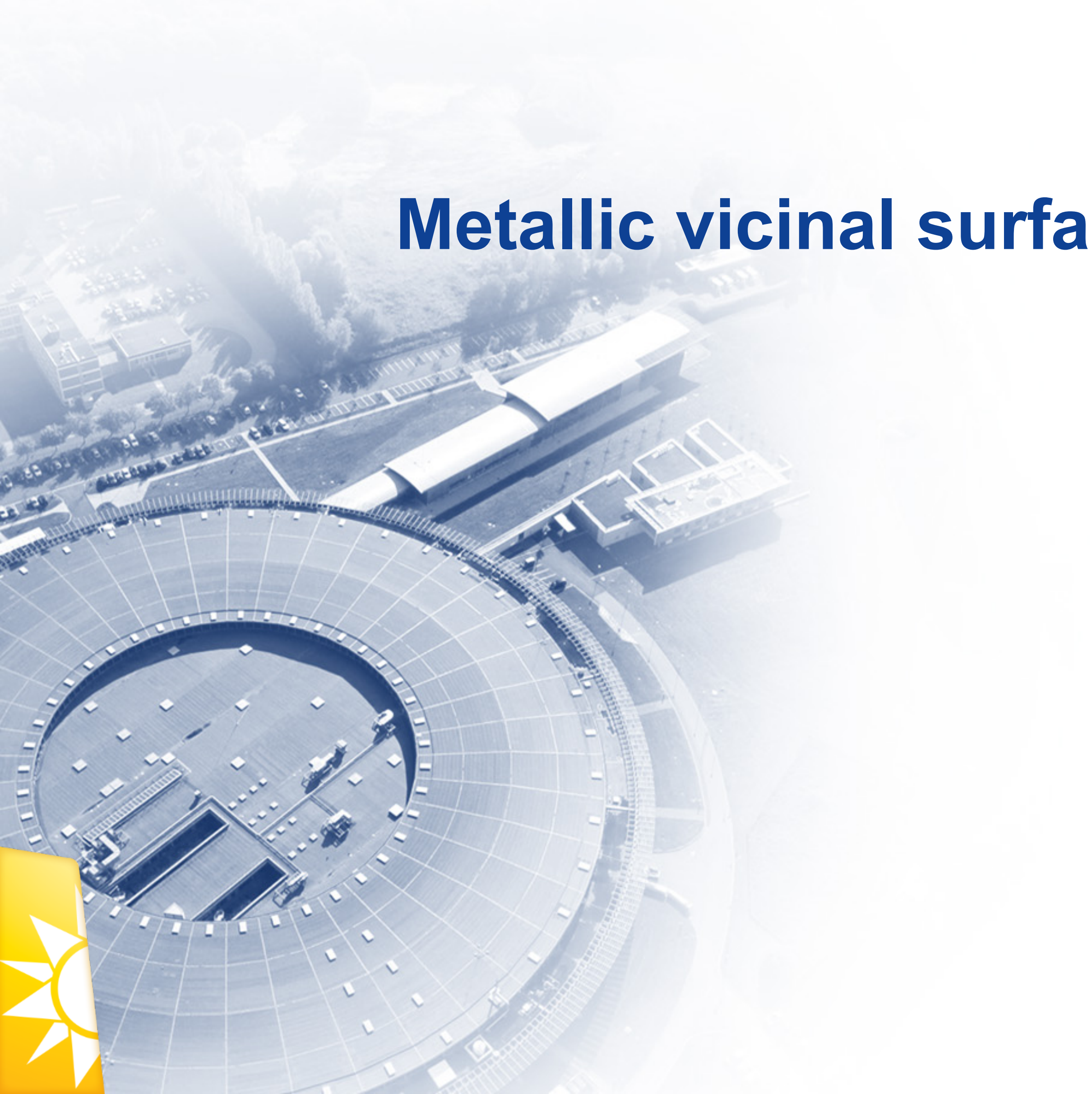

Metallic vicinal surfaces for nanostrucures growth

An *in situ* study

Vicinal Surface

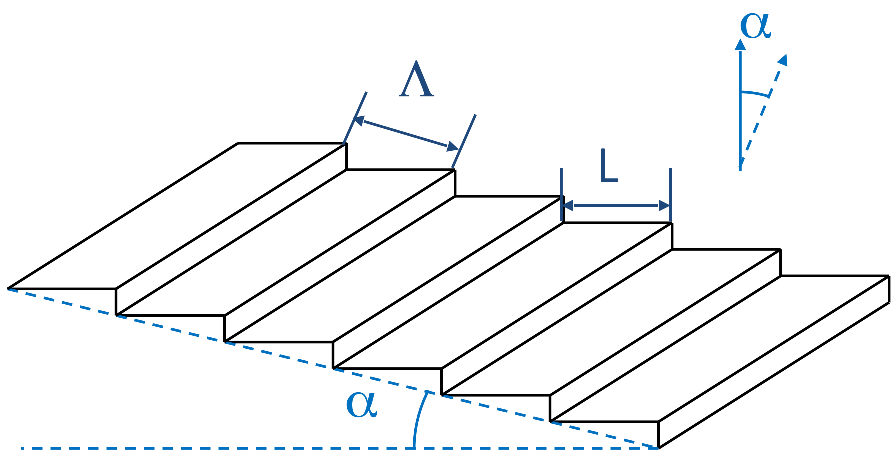

Cu(433) (100x100) nm

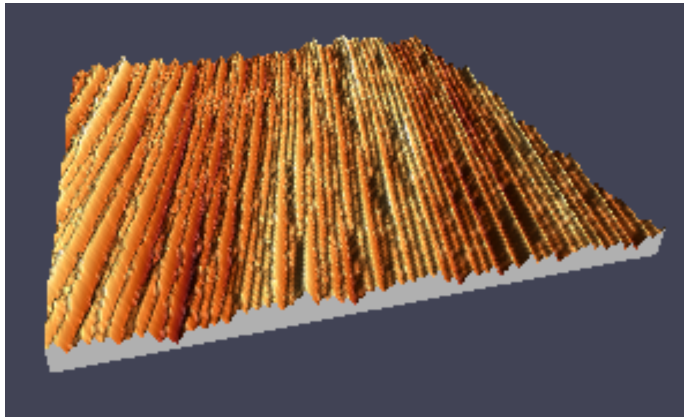

Self Organisation: Ag / Cu (433)

0.3 ML Ag/Cu(433) (200x200) nm

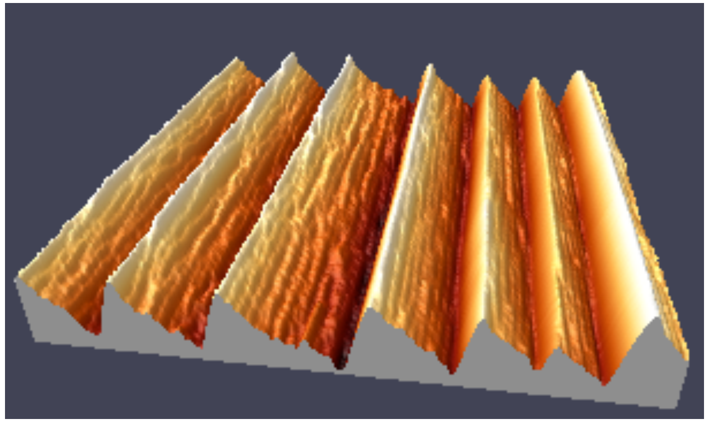

Cu (433) (100x100) nm

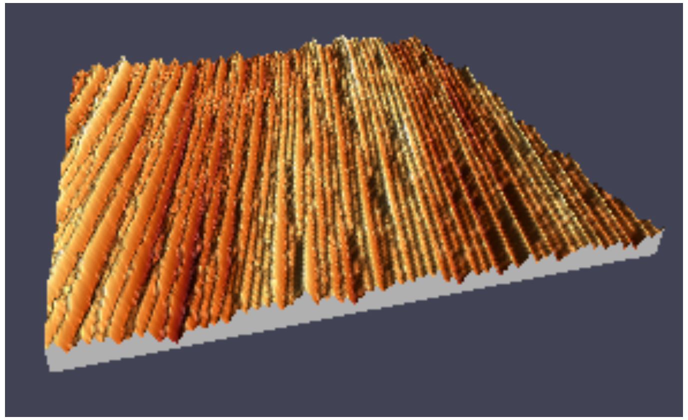

0.6 ML Ag/Cu(433) (200x200) nm

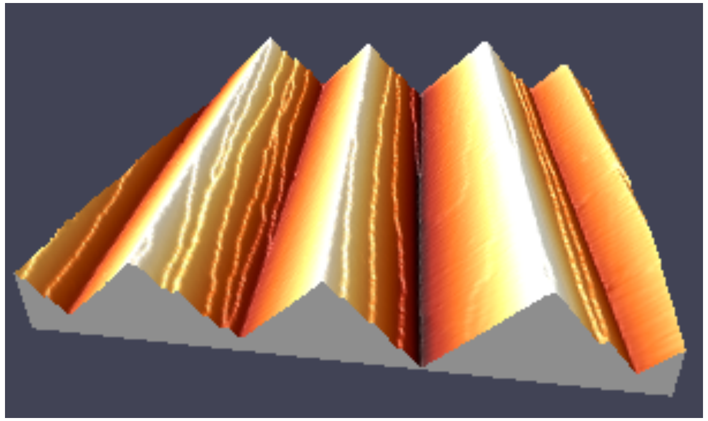

Self Organisation: Ag/Ni

Ag/Ni(11 9 9)

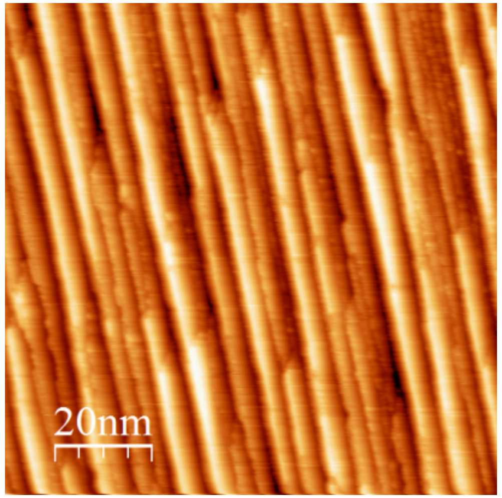

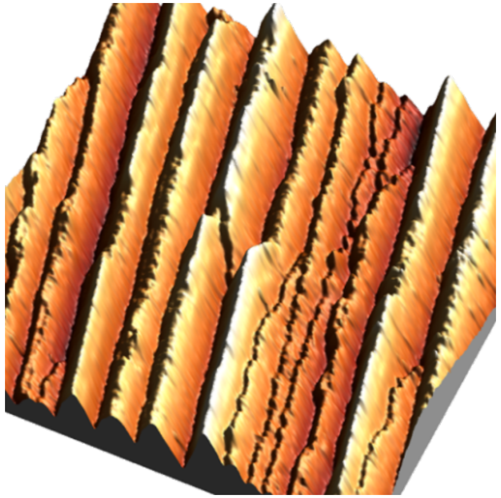

1D Organisation

Ag/Ni(27 17 19)

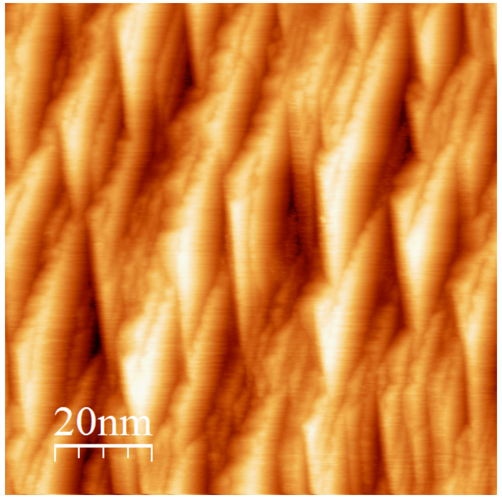

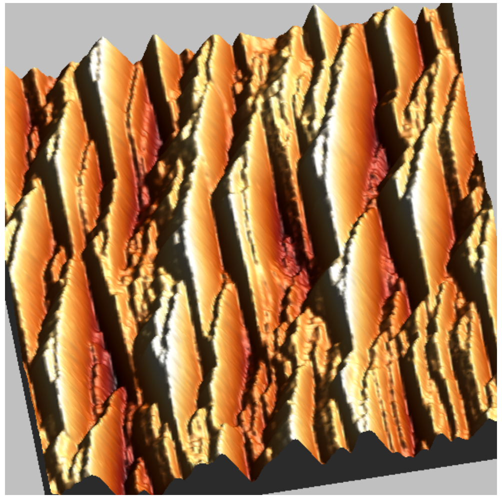

2D Organisation

Self Organisation: Co/Au

Co/Au(788)

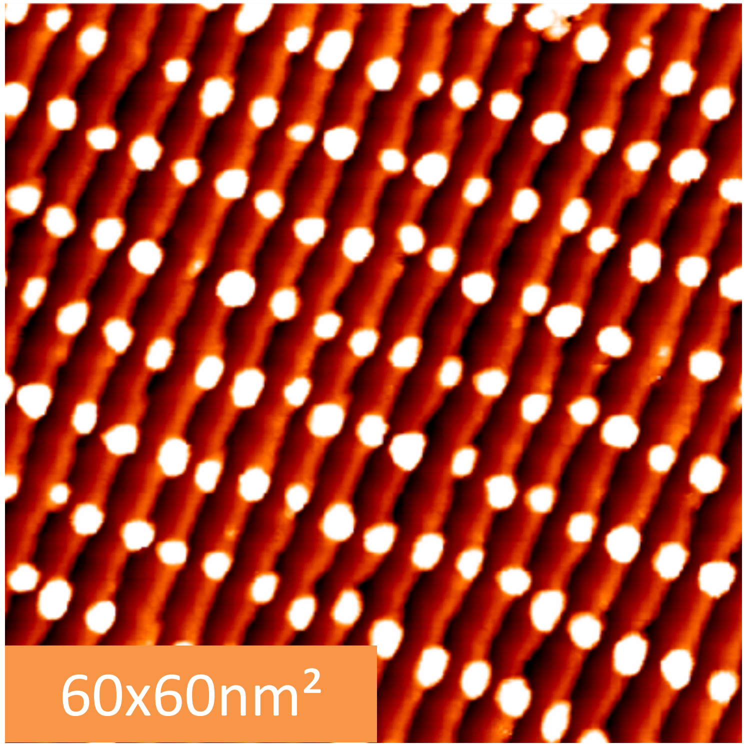

Vicinal Surfaces (111) fcc

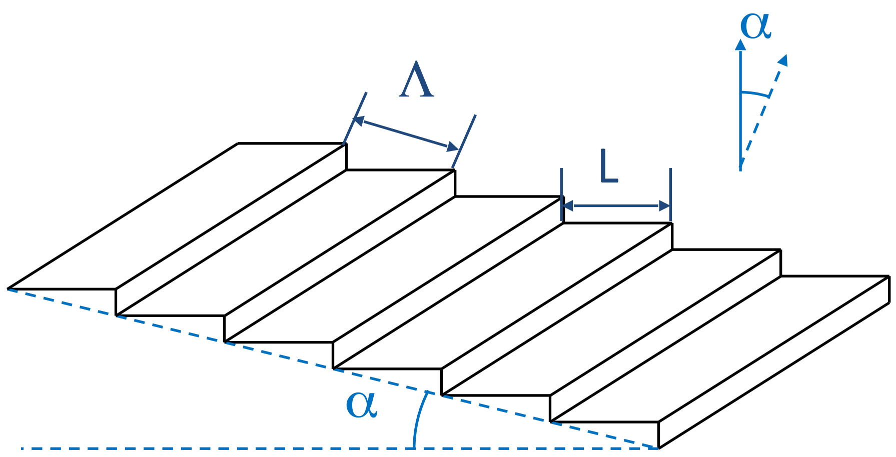

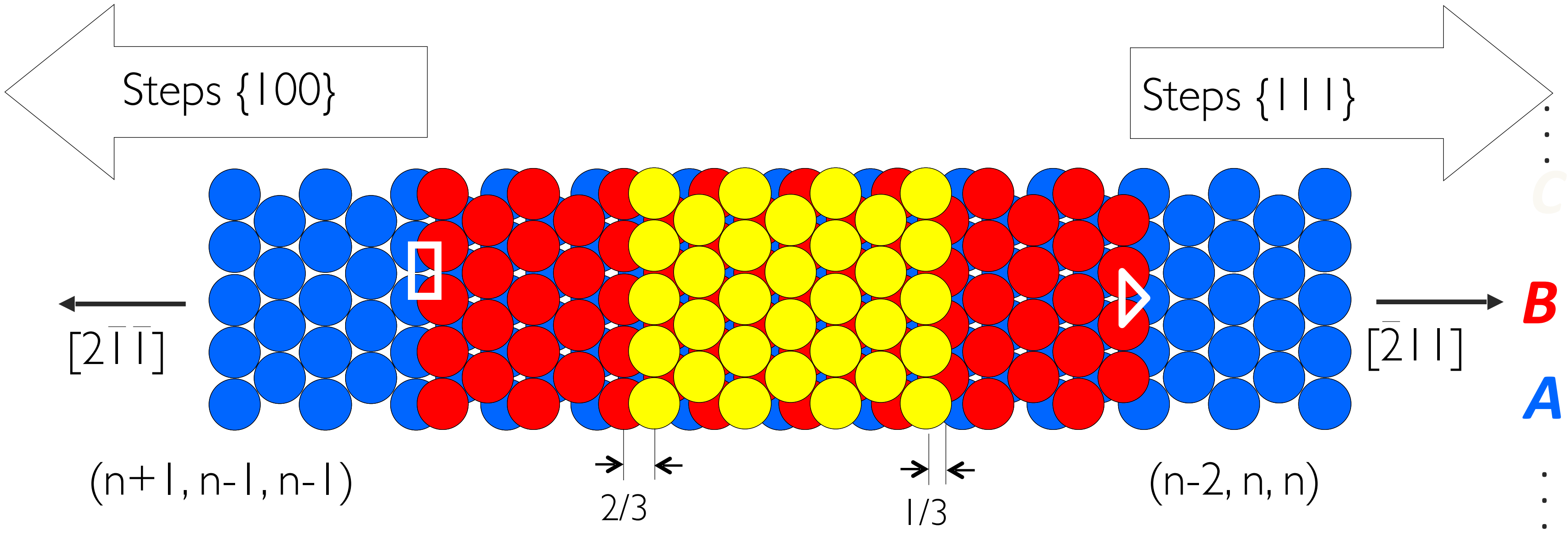

Vicinal Surfaces (111) fcc

	Angle (°)	Lines	Λ (nm)
Cu(211)	(-)19.5	2+2/3	0.626
Au(322)	(-)11.4	4+2/3	1.17
Ni(1199)	(-) 5.57	9+2/3	2.096

	Angle (°)	Lines	Λ (nm)
Au(233)	10.0	5+1/3	1.33
Ag(133)	22.0	2+1/3	0.629
Ag(799)	6.46	8+1/3	2.095

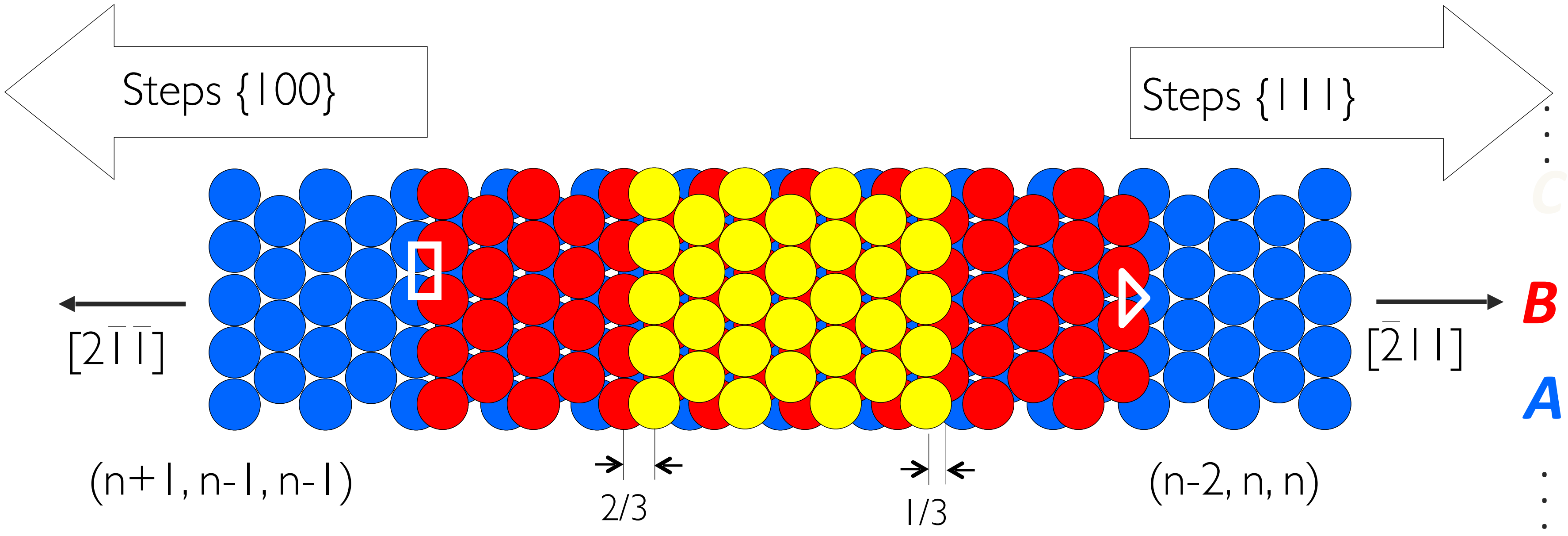

“Model Systems”: Ag/Cu, Ag/Ni

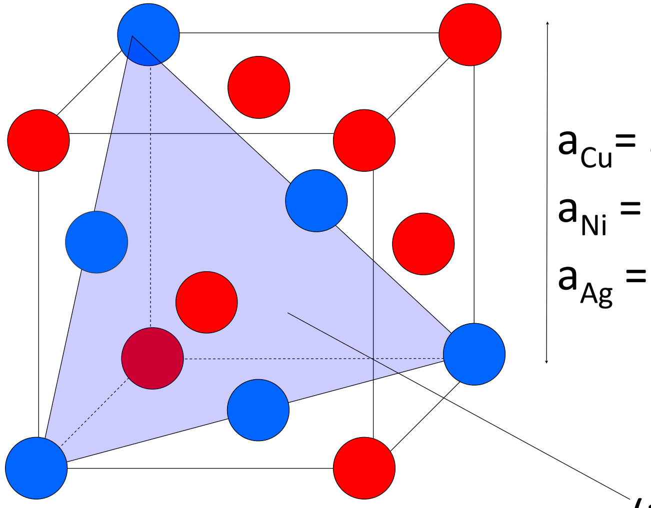

a_{Cu}= 3.61 Å
a_{Ni} = 3.52 Å
a_{Ag} = 4.09 Å

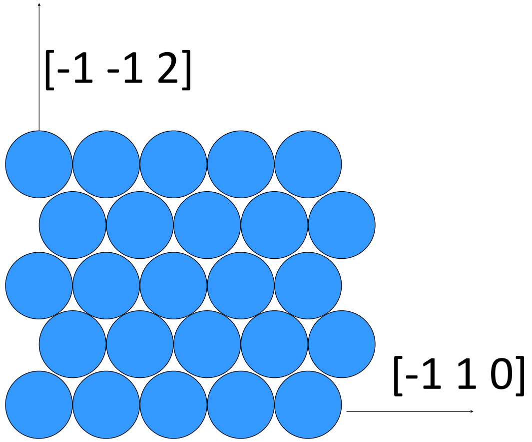

- fcc structure
- Immiscibles
- atomic radii $r_{Ag}/r_{Cu}=1{,}13$ $r_{Ag}/r_{Ni}=1{,}15$
- cohesion energies : $E_{NCu}=-3{,}50$ eV $E_{cNi}=-4{,}44$ eV $E_{cAg}=-2{,}96$ eV

Ag segregates on Ni or Cu
Abrupt Interfaces

Adsorbate induced faceting : X-ray measurements

Cu(433) Vicinal Surface (100x100) nm²

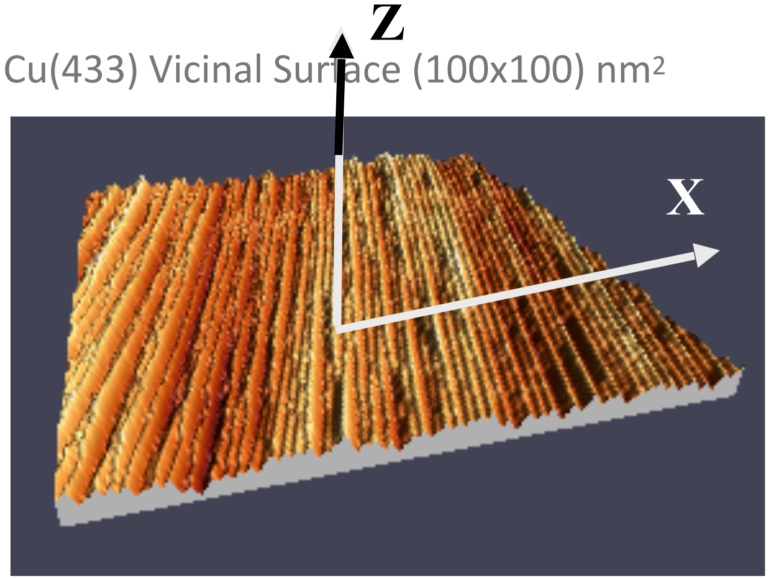

clean Cu(433)

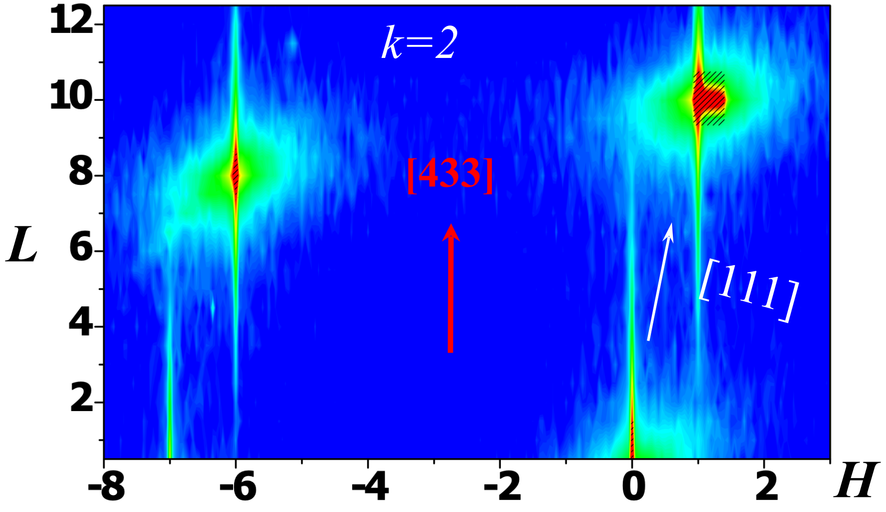

~1/3 ML Ag/Cu(433) (200x200) nm²

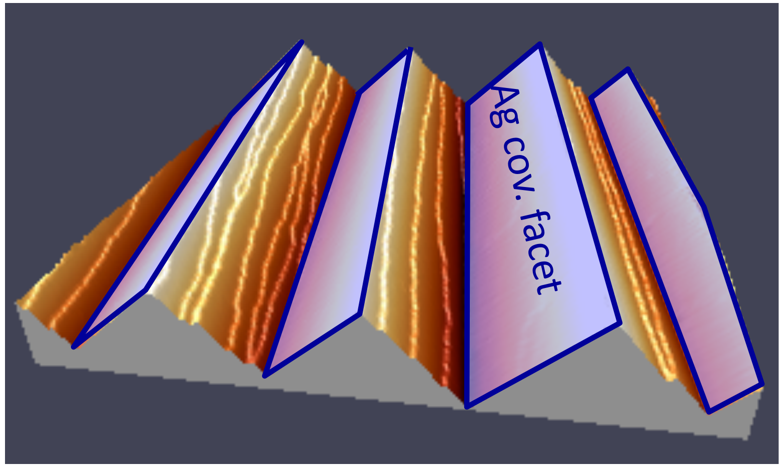

After Ag deposition and annealing

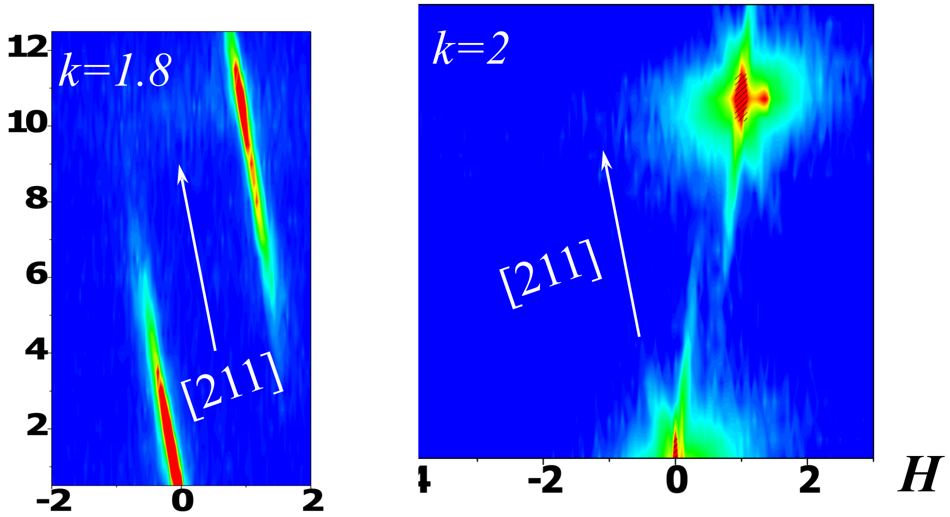

Adsorbate induced faceting : X-ray measurements

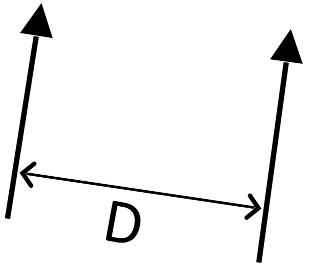

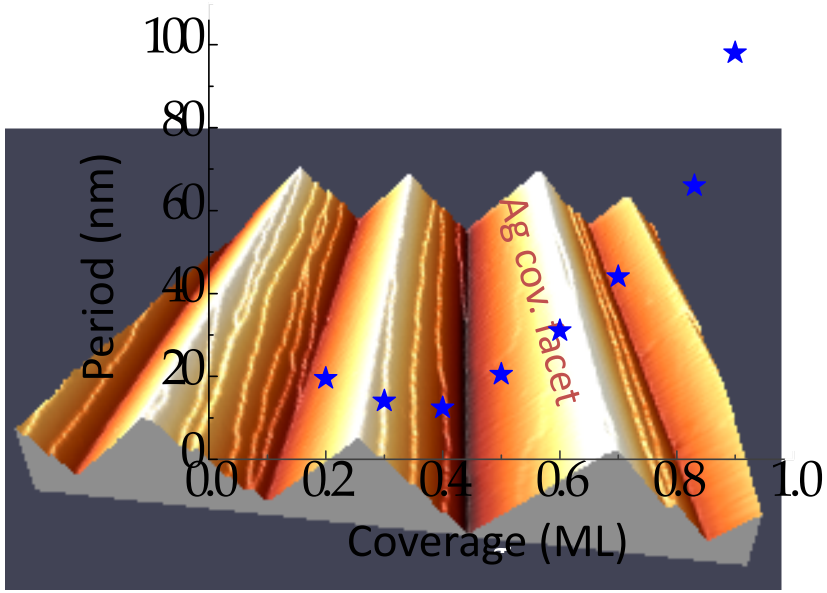

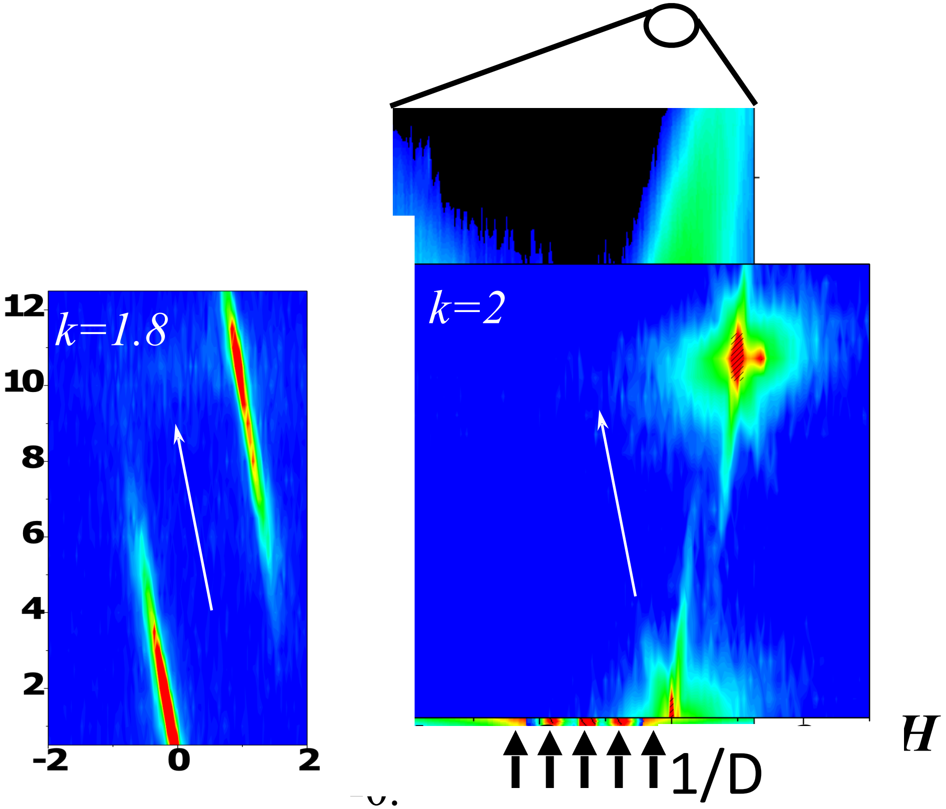

Cu(211)

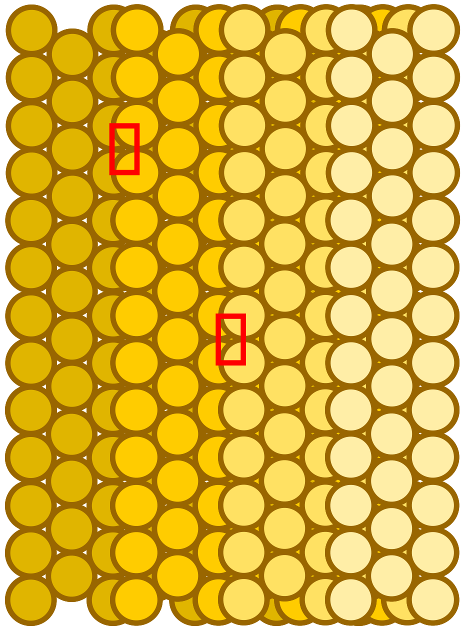

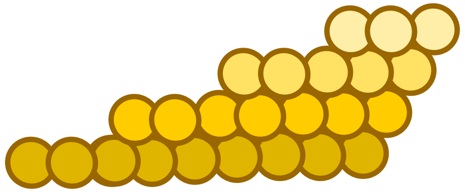

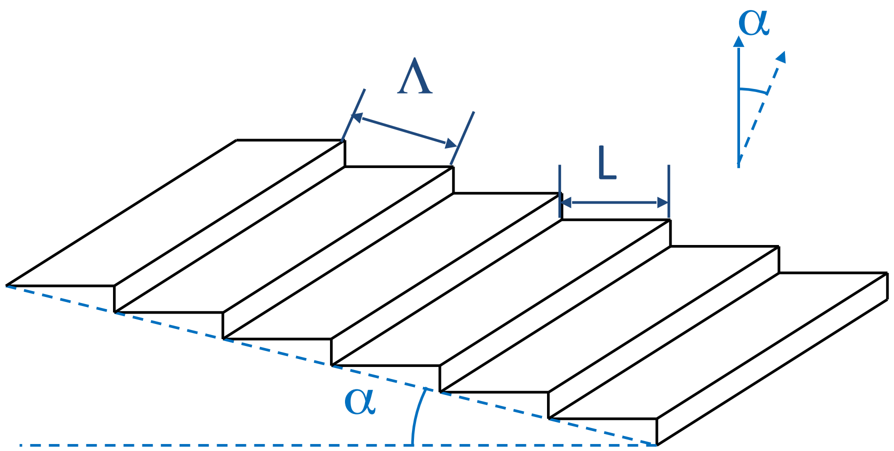

α = 19.41°

Λ = 0.626 nm

1 ML Ag/Cu(211) – GIXD

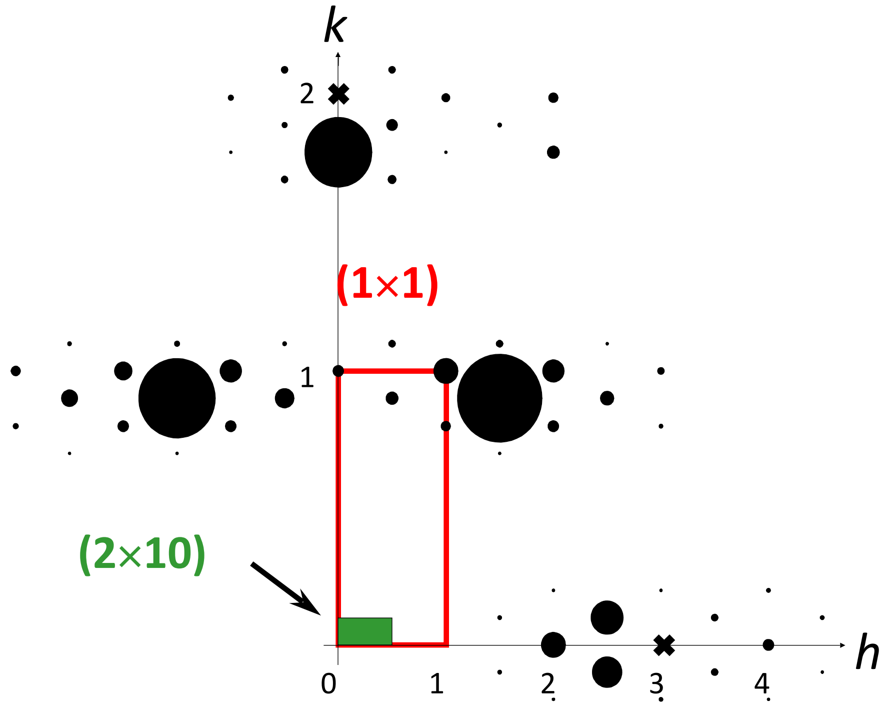

GIXD measurements

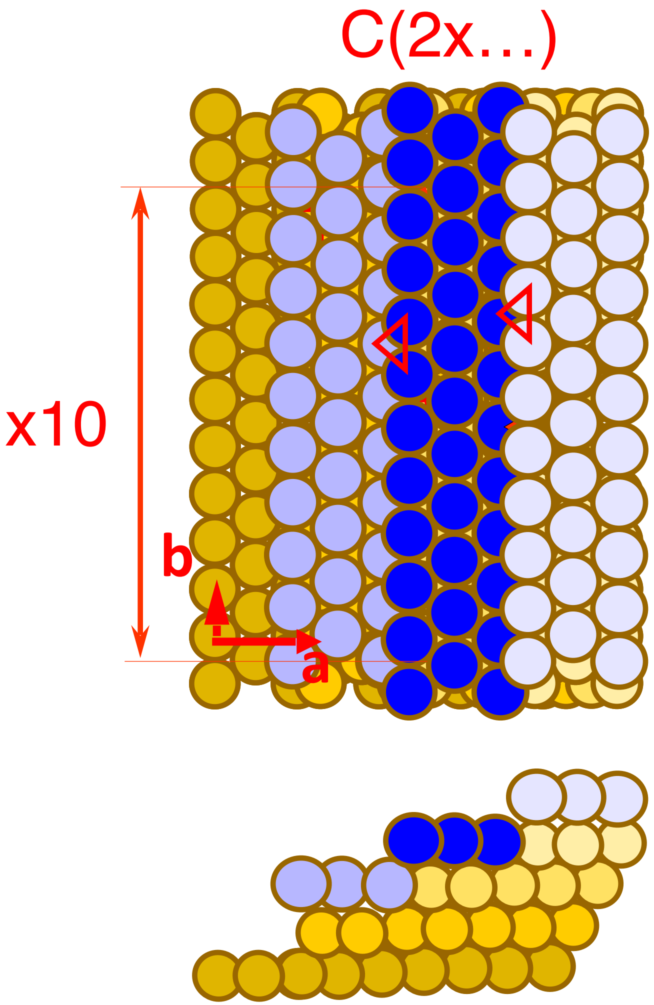

1 ML Ag/Cu(211) – GIXD

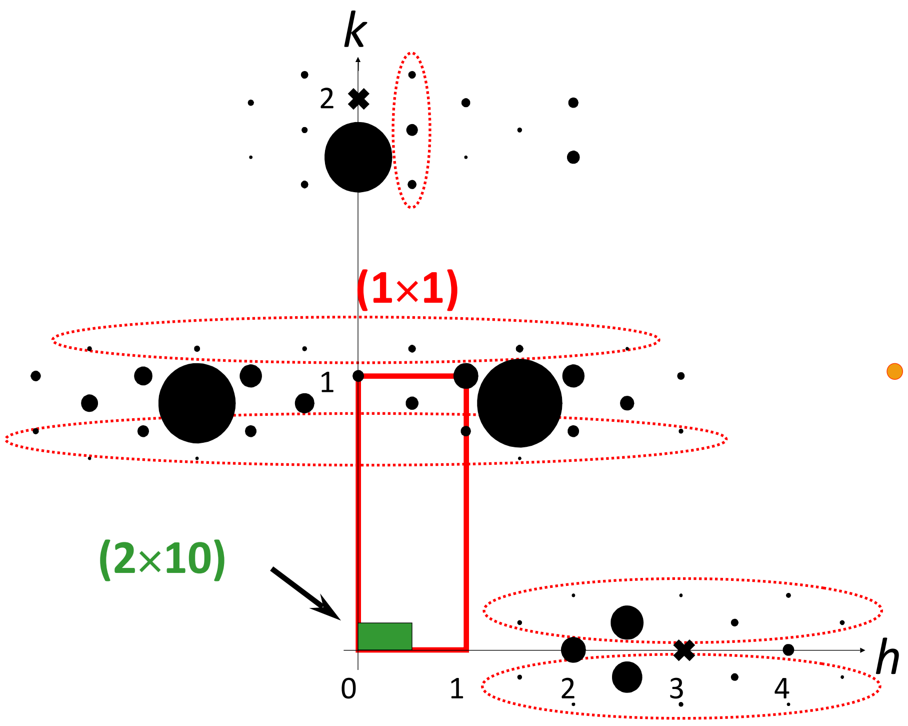

GIXD

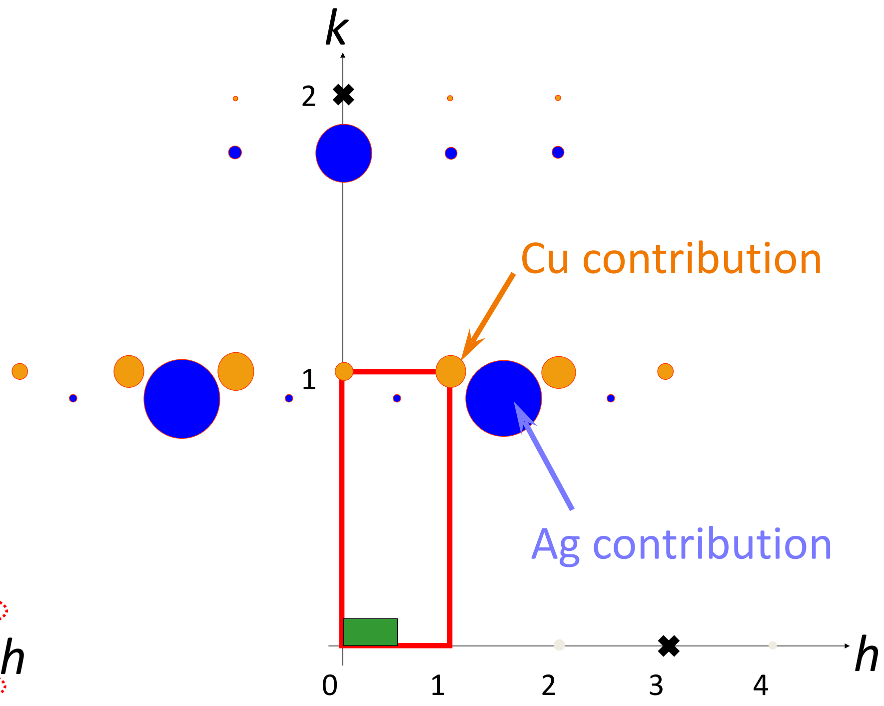

Simulation

The structure is not relaxed !

1 ML Ag/Cu(211) – GIXD and QMD

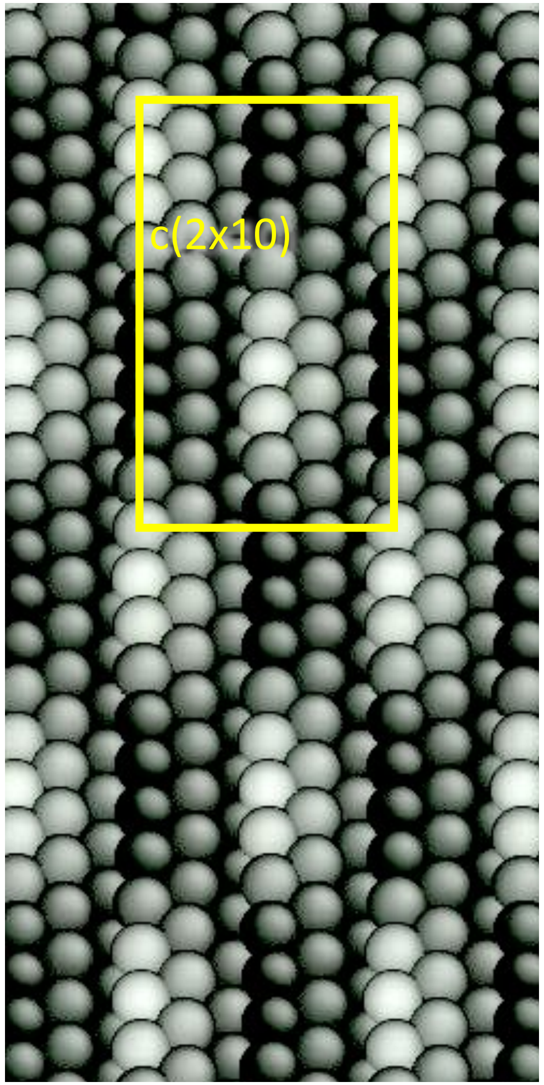

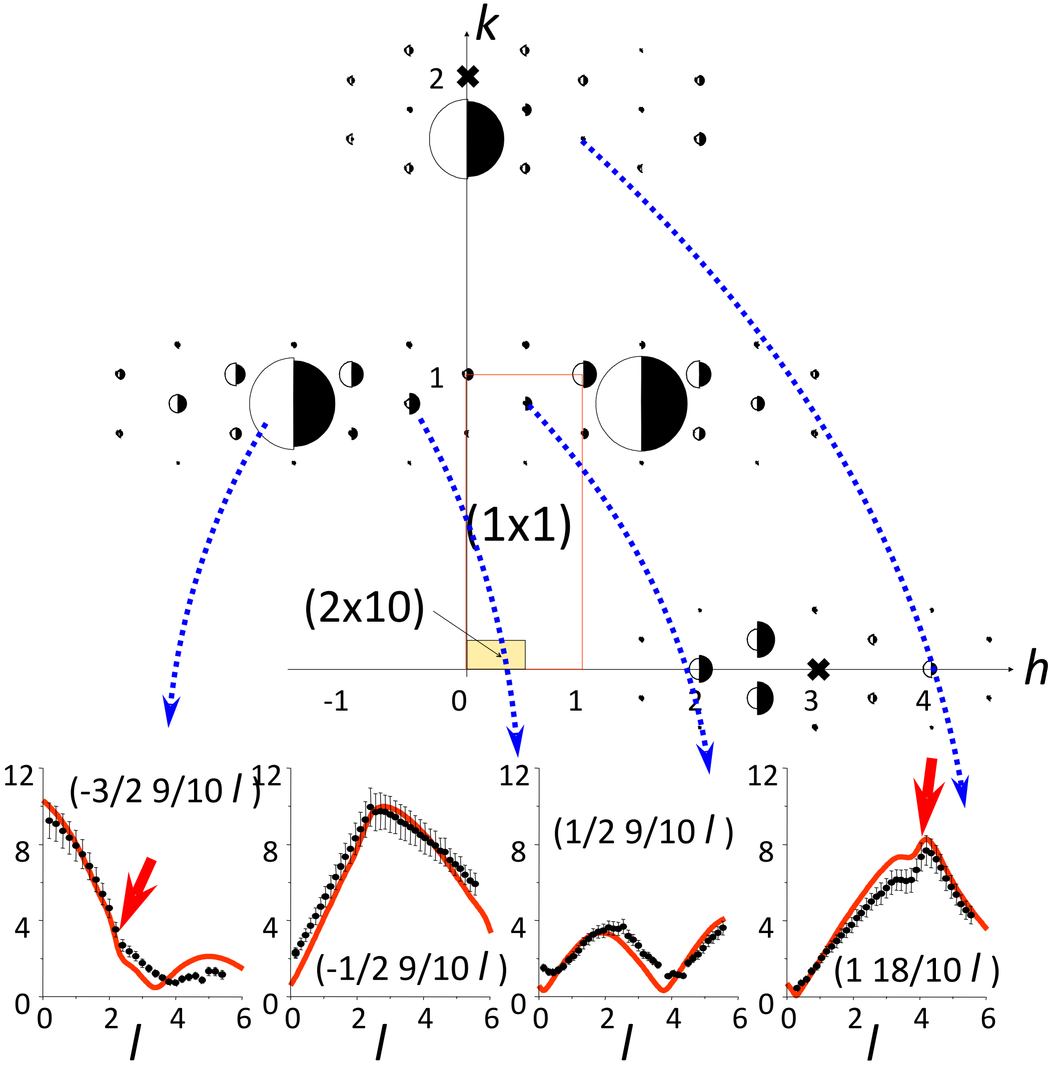

1 ML Ag/Cu(211) – GIXD & STM

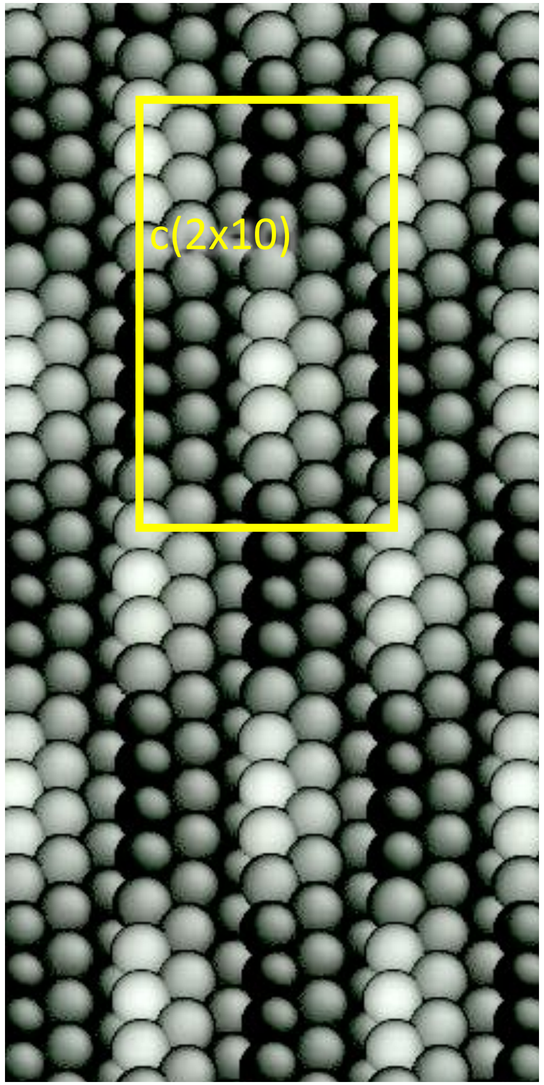

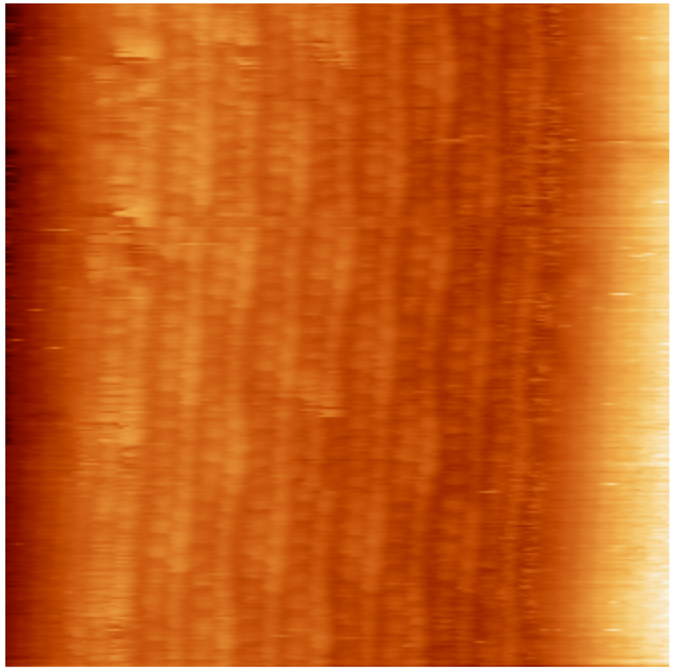

Y. Garreau, A. Coati, A. Zobelli, and J. Creuze
Phys. Rev. Lett. 91, 116101

“Magic” Heteroepitaxy

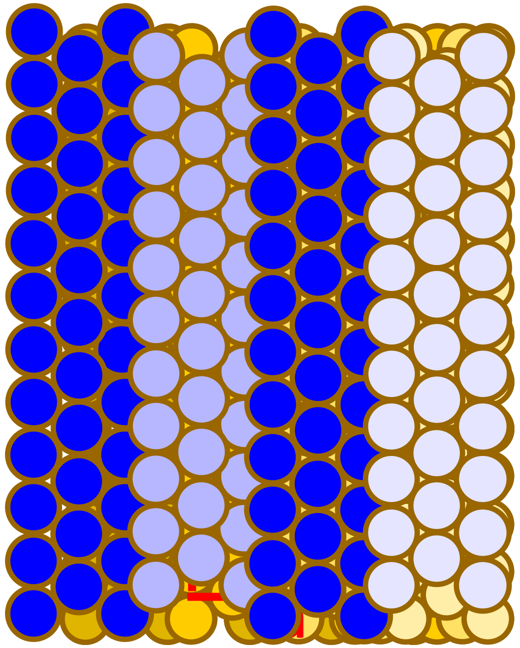

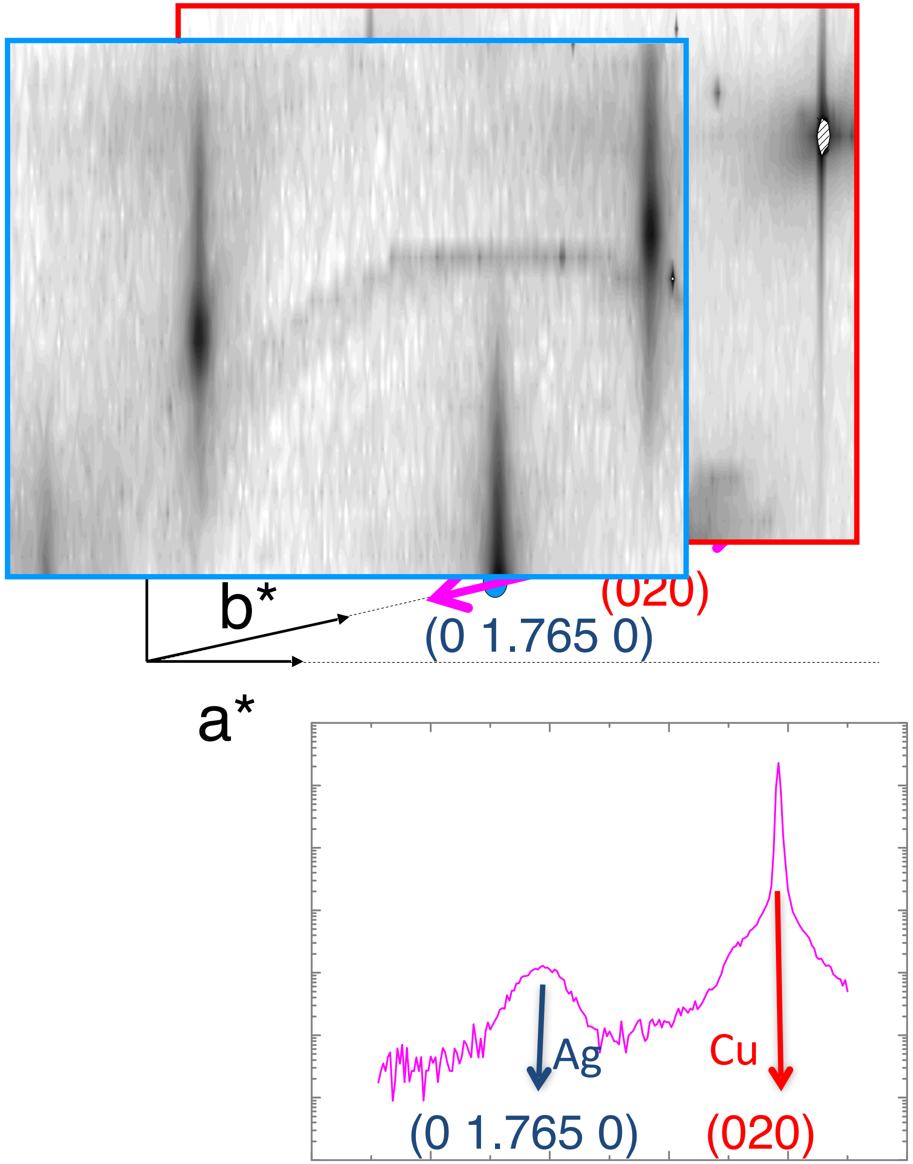

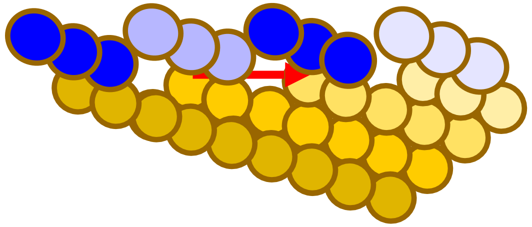

“Magic” Heteroepitaxy

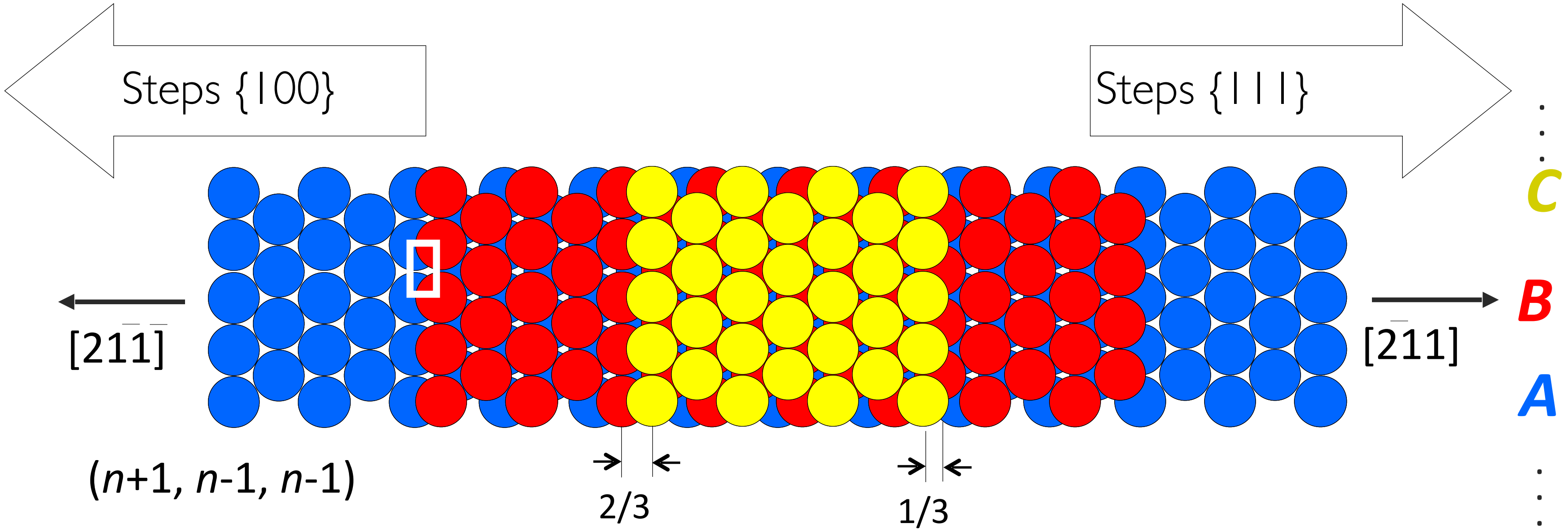

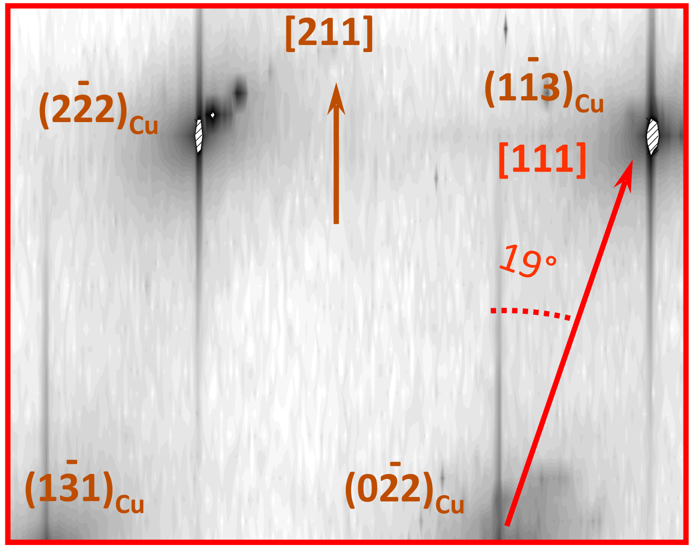

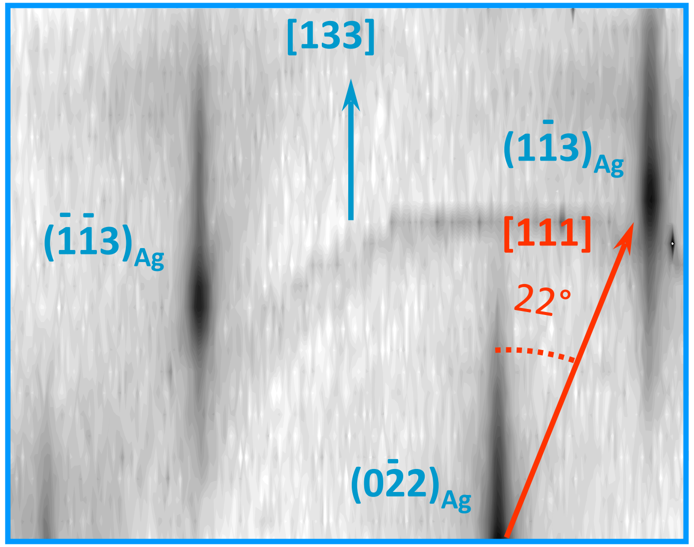

"Magic" Heteroepitaxy

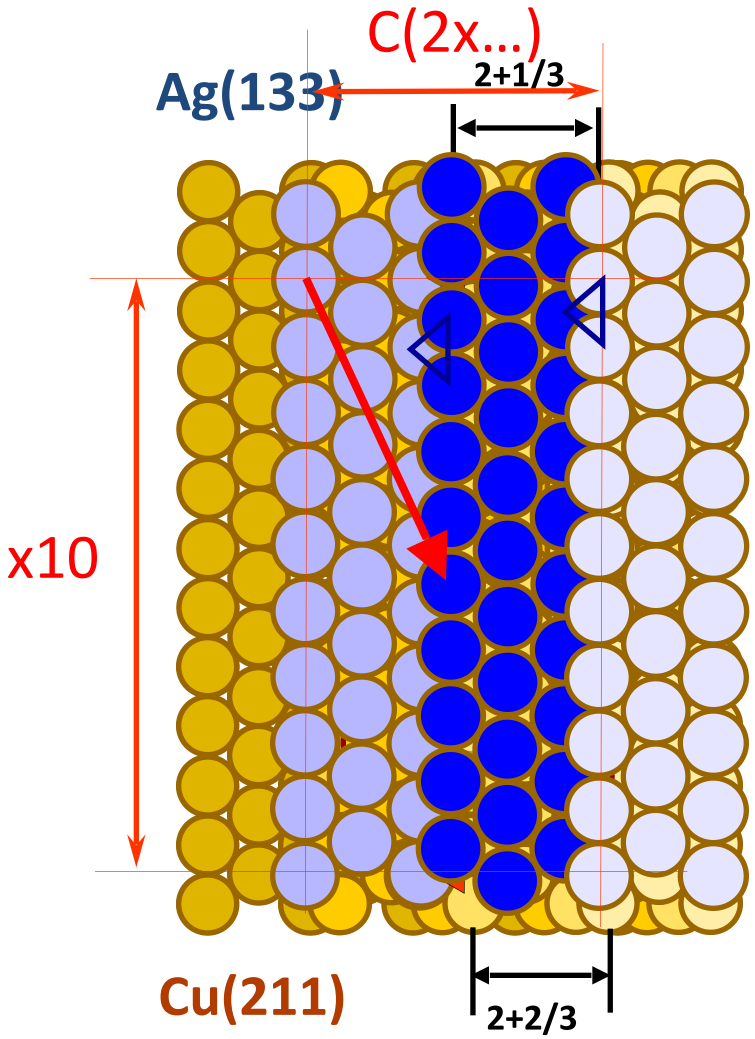

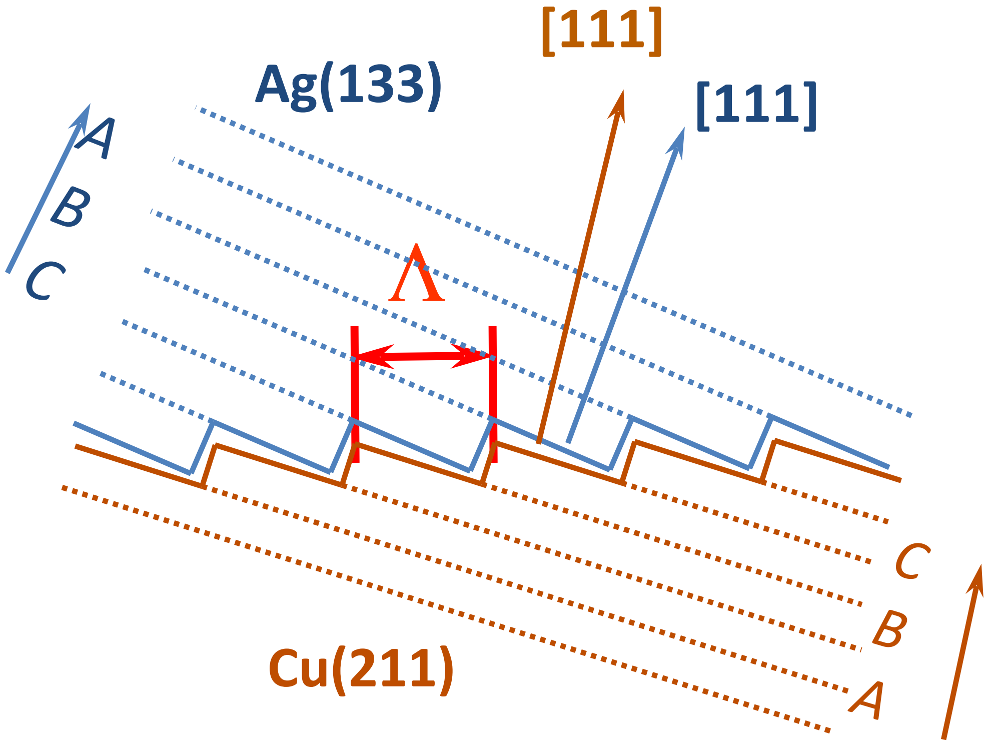

$$\frac{\left(2+\frac{2}{3}\right)\Lambda_{Ag(133)}}{\left(2+\frac{1}{3}\right)\Lambda_{Cu(211)}} = 1.14 \approx \frac{a_{Ag}}{a_{Cu}} = 0.4\%$$

Y. Garreau et al., Phys. Rev. Lett. 91, 116101 (2003)

Vicinal Surfaces (111) fcc

	Angle (°)	Lines	Λ (nm)
Cu(211)	(-)19.5	2+2/3	0.626
Au(322)	(-)11.4	4+2/3	1.17
Ni(1199)	(-) 5.57	9+2/3	2.096

	Angle (°)	Lines	Λ (nm)
Au(233)	10.0	5+1/3	1.33
Ag(133)	22.0	2+1/3	0.629
Ag(799)	6.46	8+1/3	2.095

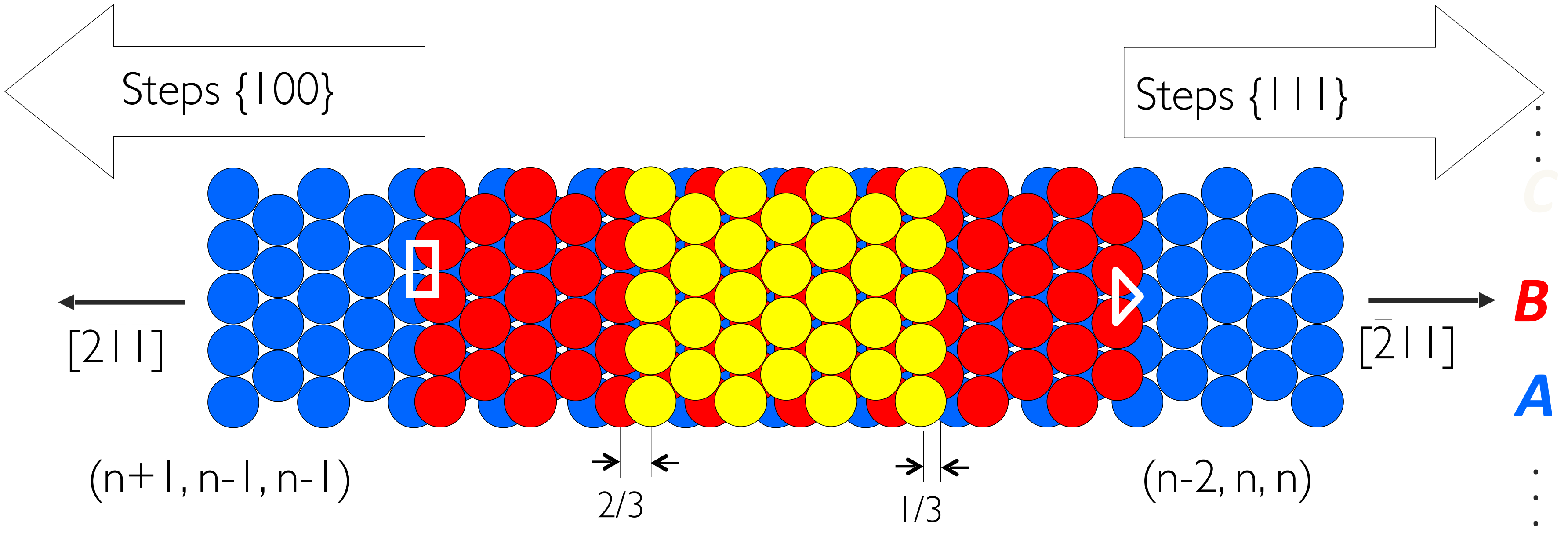

Ni(11 9 9)

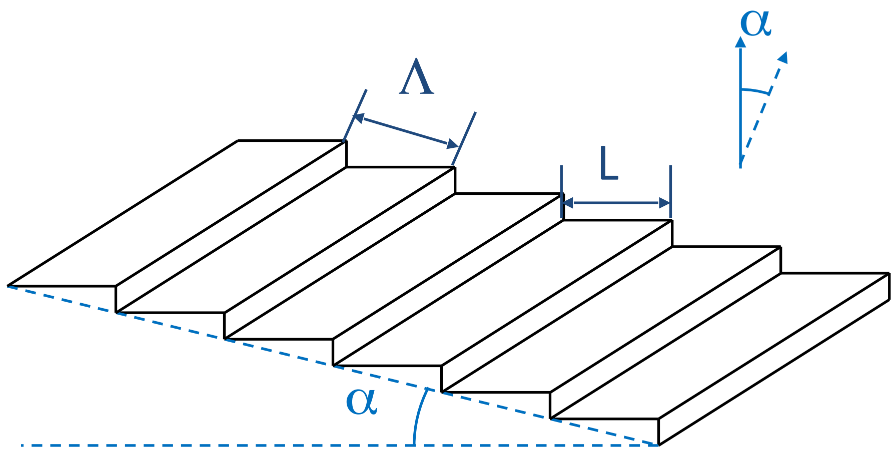

α = 5.57°
L = 2.1 nm

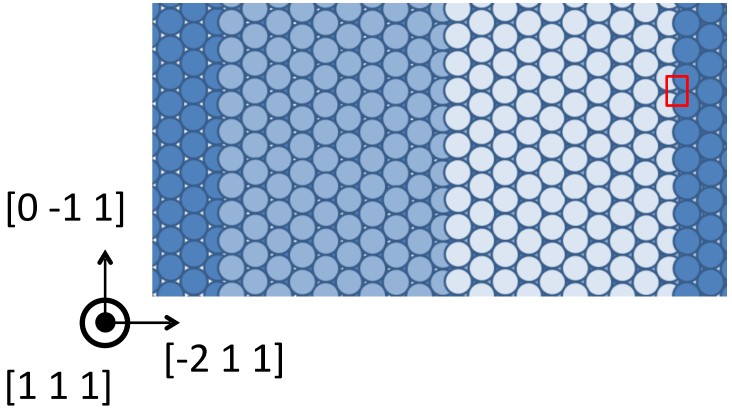

Terrasses : (111)
Steps: (001)

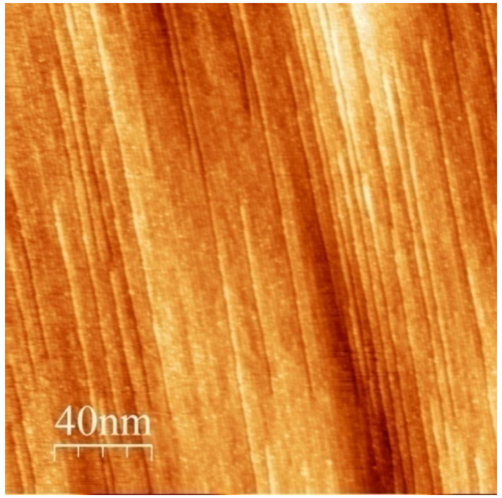

V_S=875mV, I_t=0.22nA

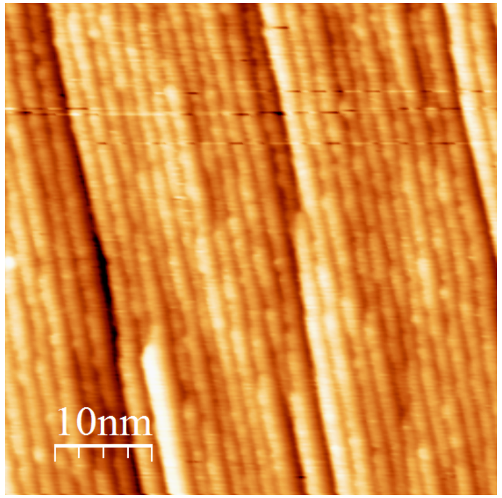

V_S=895mV, I_t=0.11nA

L = 2.09 ± 0.41 nm

Bellec, A., et al., Physical Review B., 96(8): art.n° 085414. (2017)

Ag(4ML) / Ni(11 9 9)

4 ML Ag deposit + annealing @ 190°C

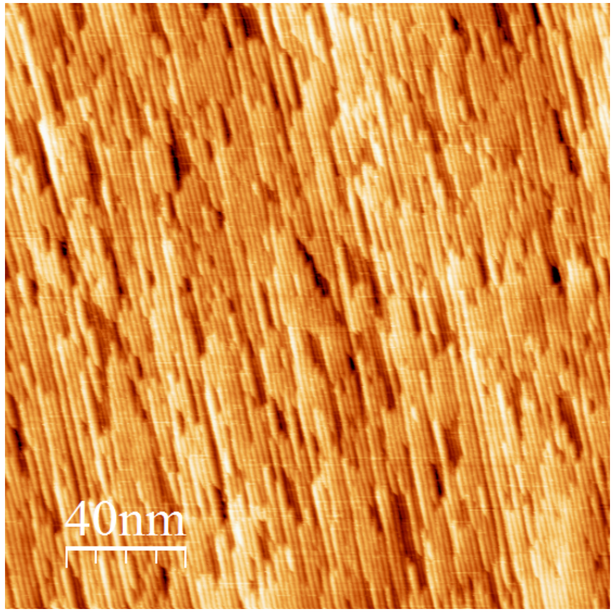

200x200nm² - V_S=0.85V - I_t=0.15nA

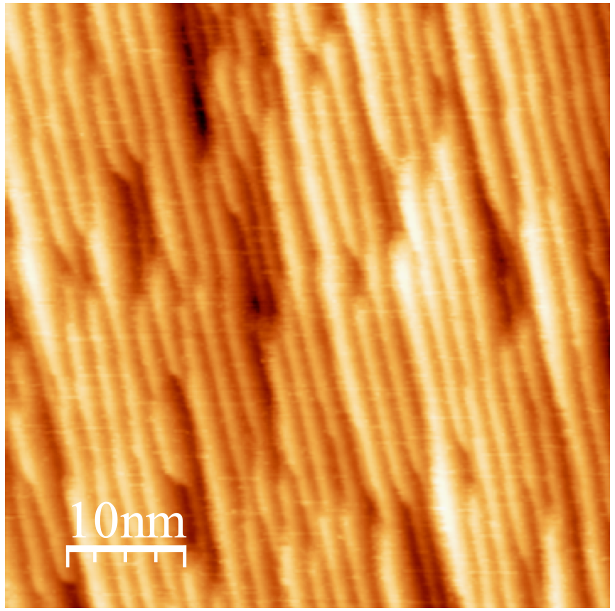

50x50nm² - V_S=0.85V - I_t=0.15nA

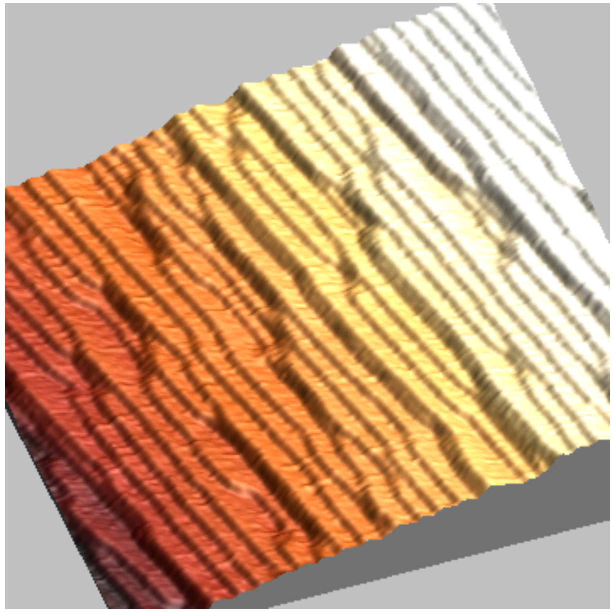

Terrasses width : L =2.1± 0.3 nm

Ni(11 9 9): Vicinal basis

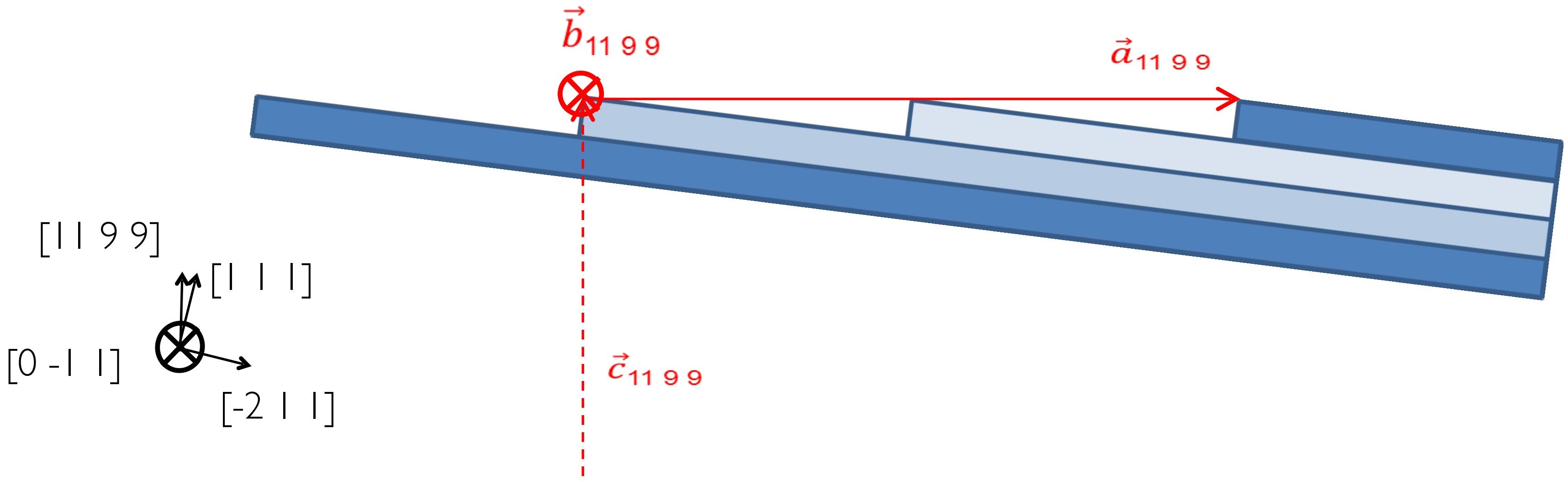

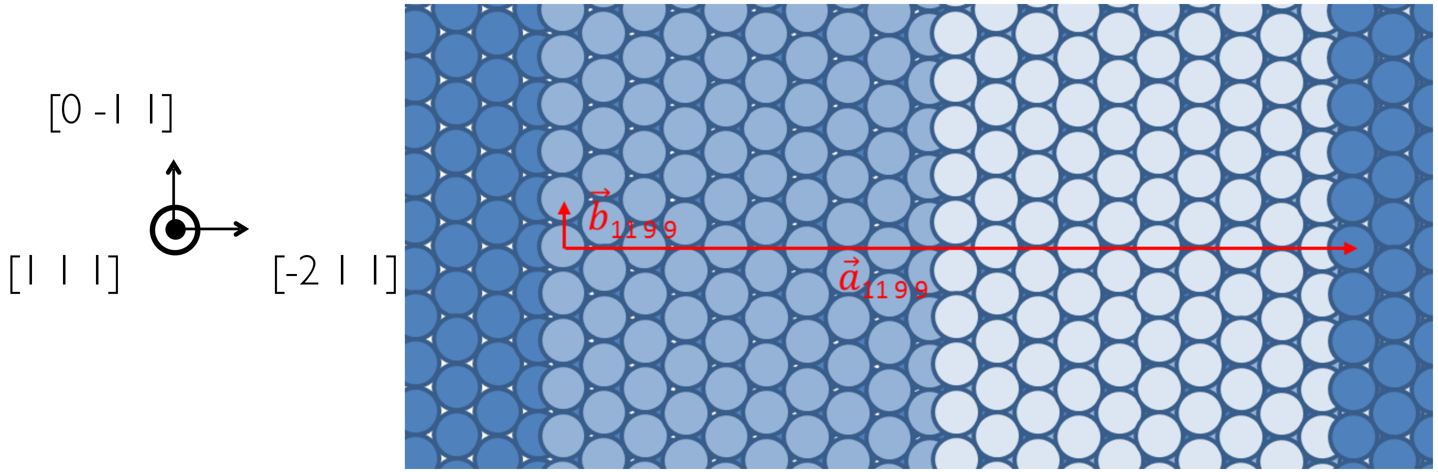

Ag (4ML) / Ni(11 9 9) : Along step edges

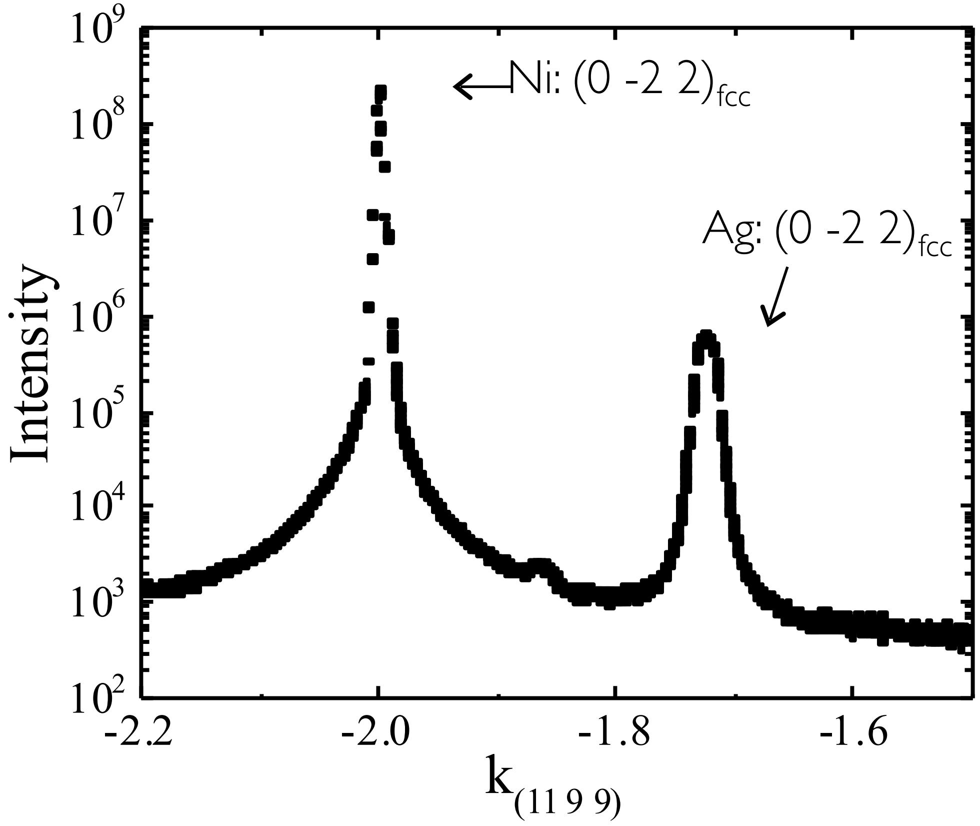

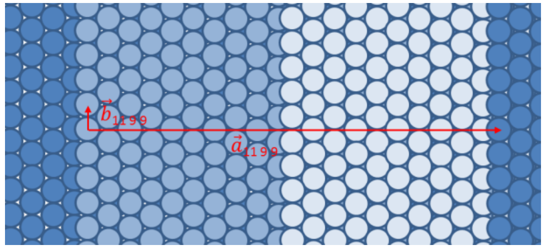

Lattice mismatch:

$$\left| \frac{a_{Ni}^{bulk} - a_{Ag}^{bulk}}{a_{Ni}^{bulk}} \right| = 0{,}159$$

Measure:

$$\left| \frac{a_{Ni}^{//} - a_{Ag}^{//}}{a_{Ni}^{//}} \right| = 0{,}161$$

Ag is relaxed along the step edges

Reciprocal space mapping

Ni map - $k_{11\,9\,9} = -2$

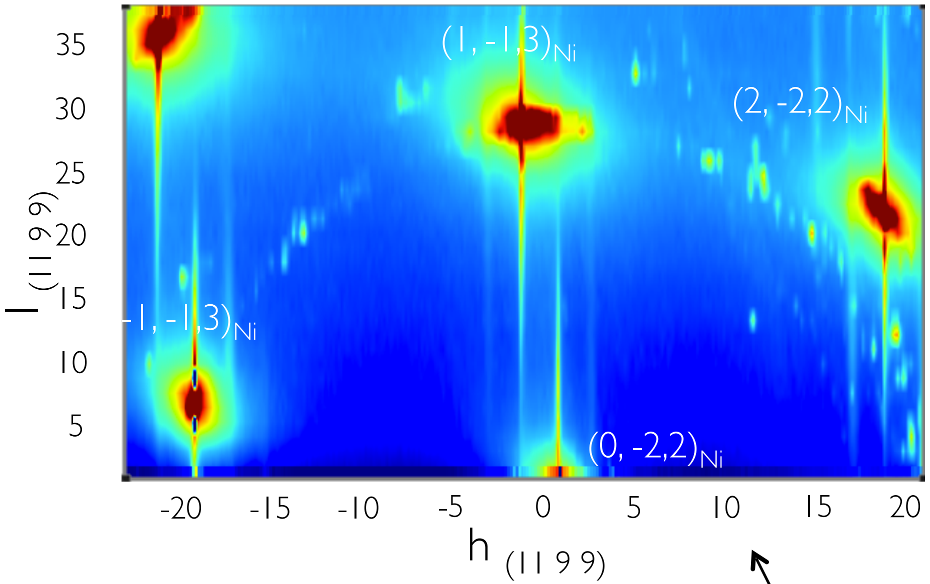

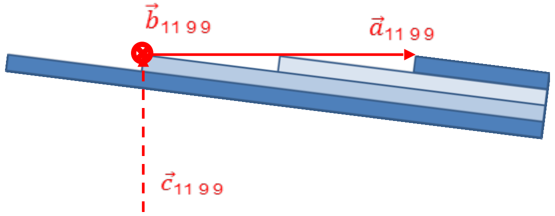

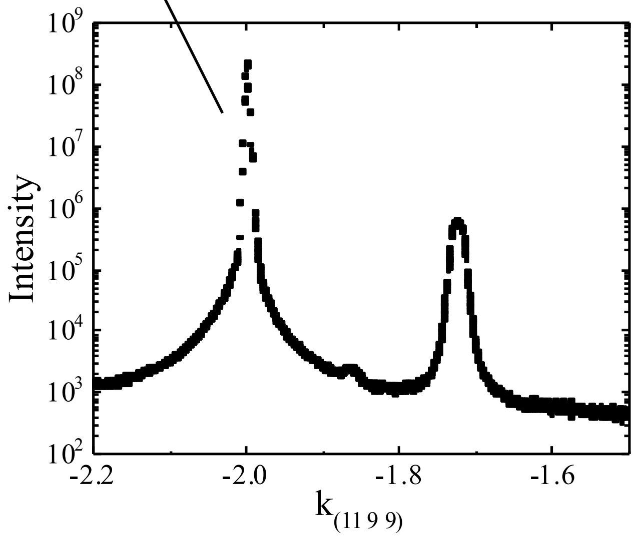

Reciprocal space mapping

Ni map - $k_{11\,9\,9} = -2$

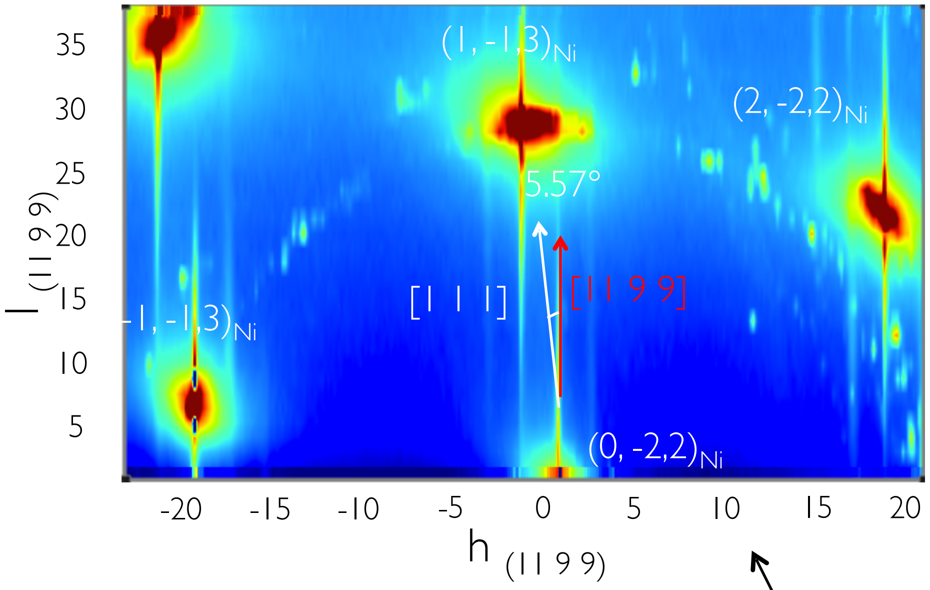

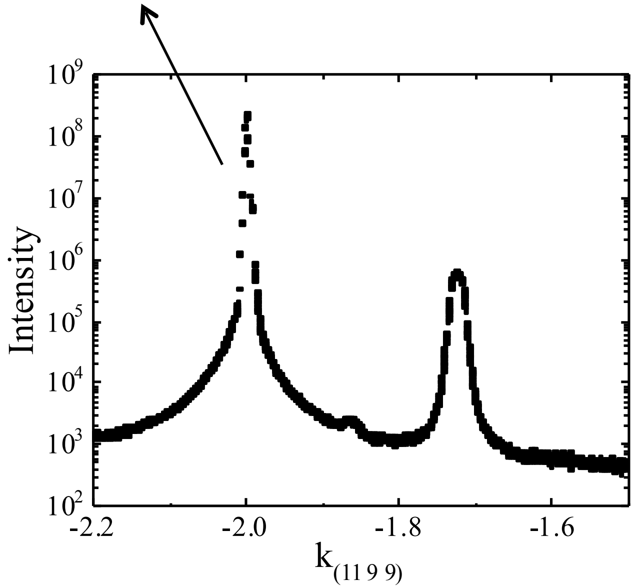

Reciprocal space mapping

Ni map - $k_{11\,9\,9} = -2$

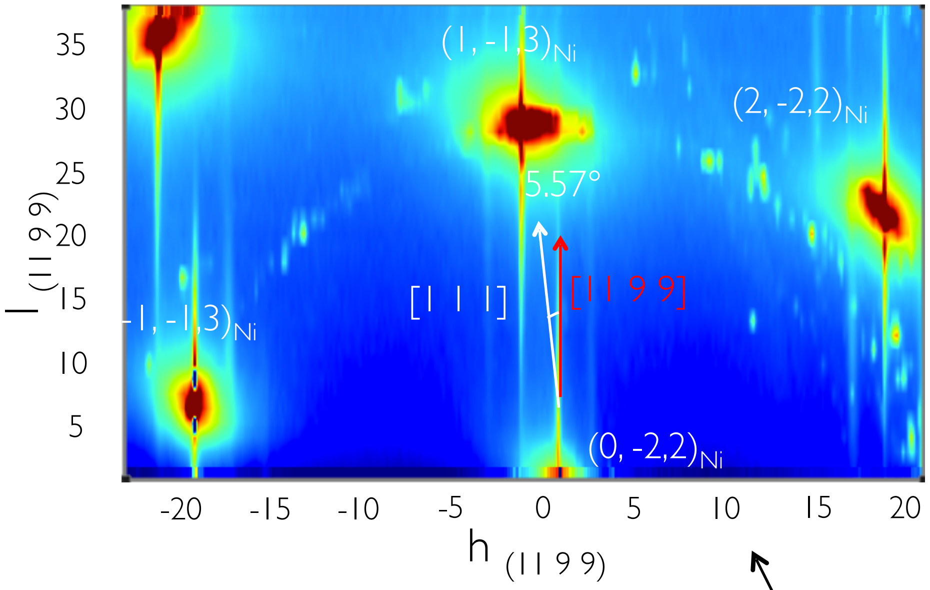

Ag map - $k_{11\,9\,9} = -1.73$

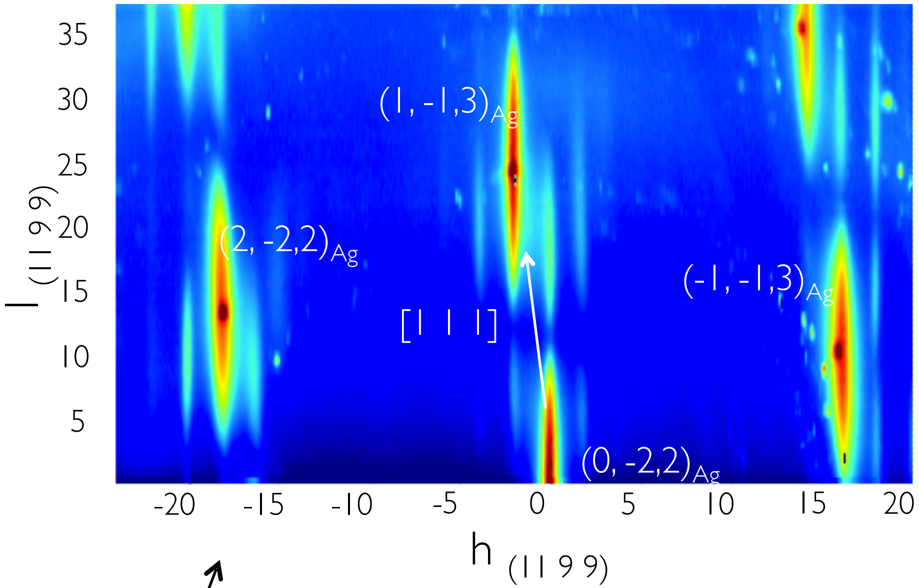

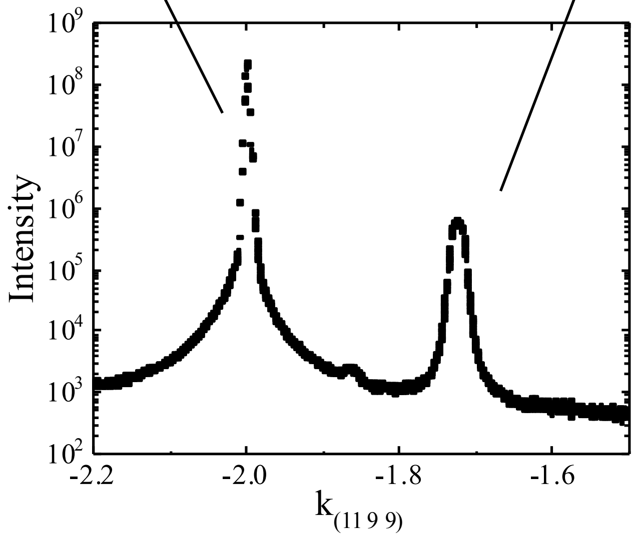

Ag layer presents a fcc structure

Inversion of the stacking between the Ag layer and the Ni substrate

Reciprocal space mapping

Ni map - $k_{11\,9\,9} = -2$

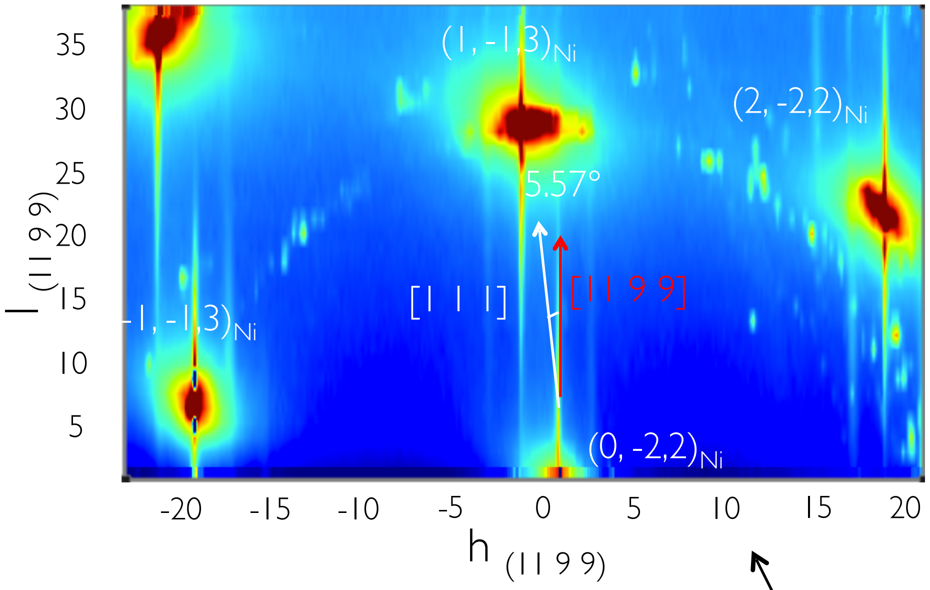

Ag map - $k_{11\,9\,9} = -1.73$

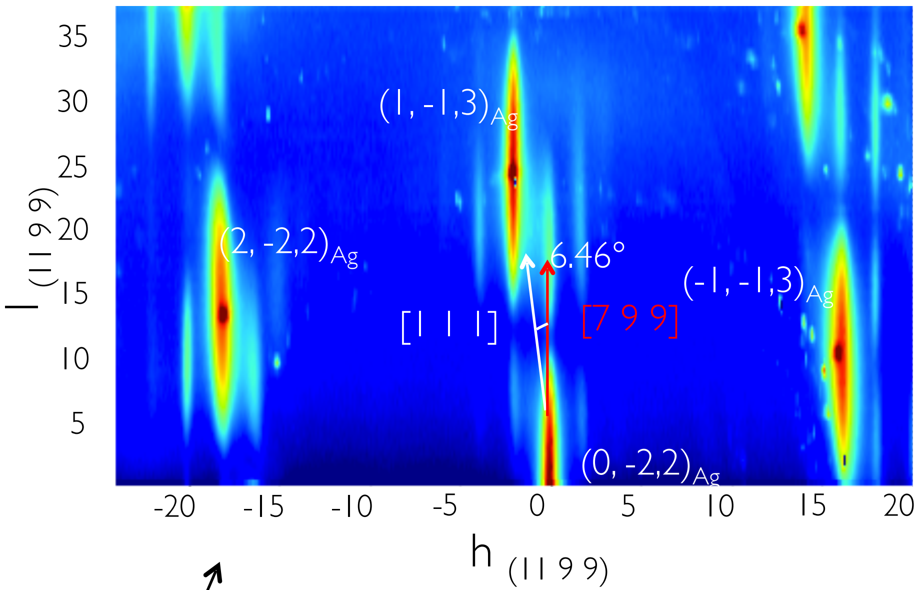

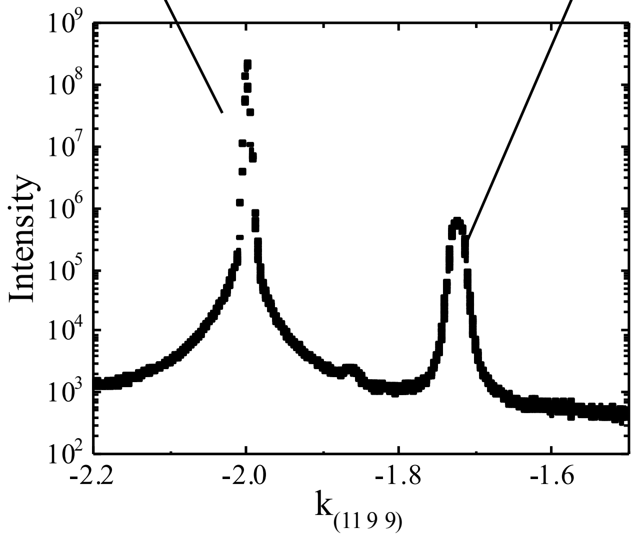

Ag: vicinal surface [7 9 9]

$\Lambda_{Ag(7\,9\,9)} = 20.95$Å

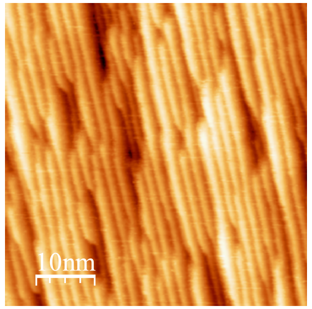

L = 20.7 ± 5.1 Å

“magic” heteroepitaxy

Formation of Ag homogeneous thin film

Ni (11 9 9): terrasses (111)
steps (001)

Ag (7 9 9): terrasses (111)
steps (111)

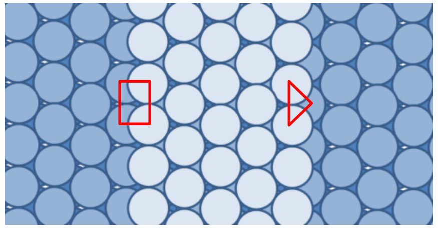

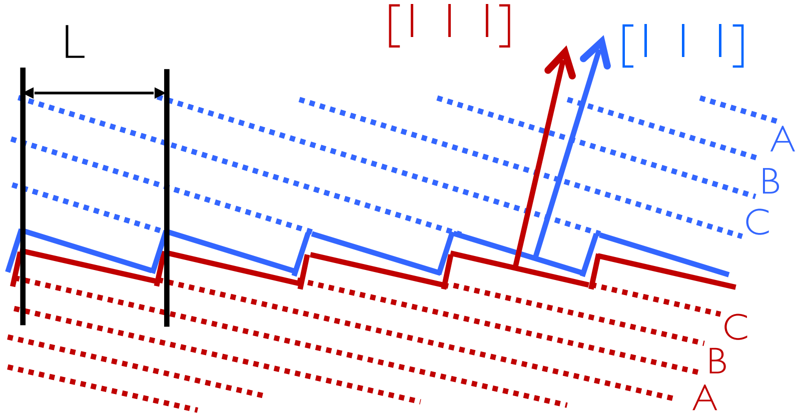

$\Lambda_{Ag(7\,9\,9)} = 20.95Å$

$\Lambda_{Ni(11\,9\,9)} = 20.96Å$

Step period governs the growth of the Ag layer

Ag Islands

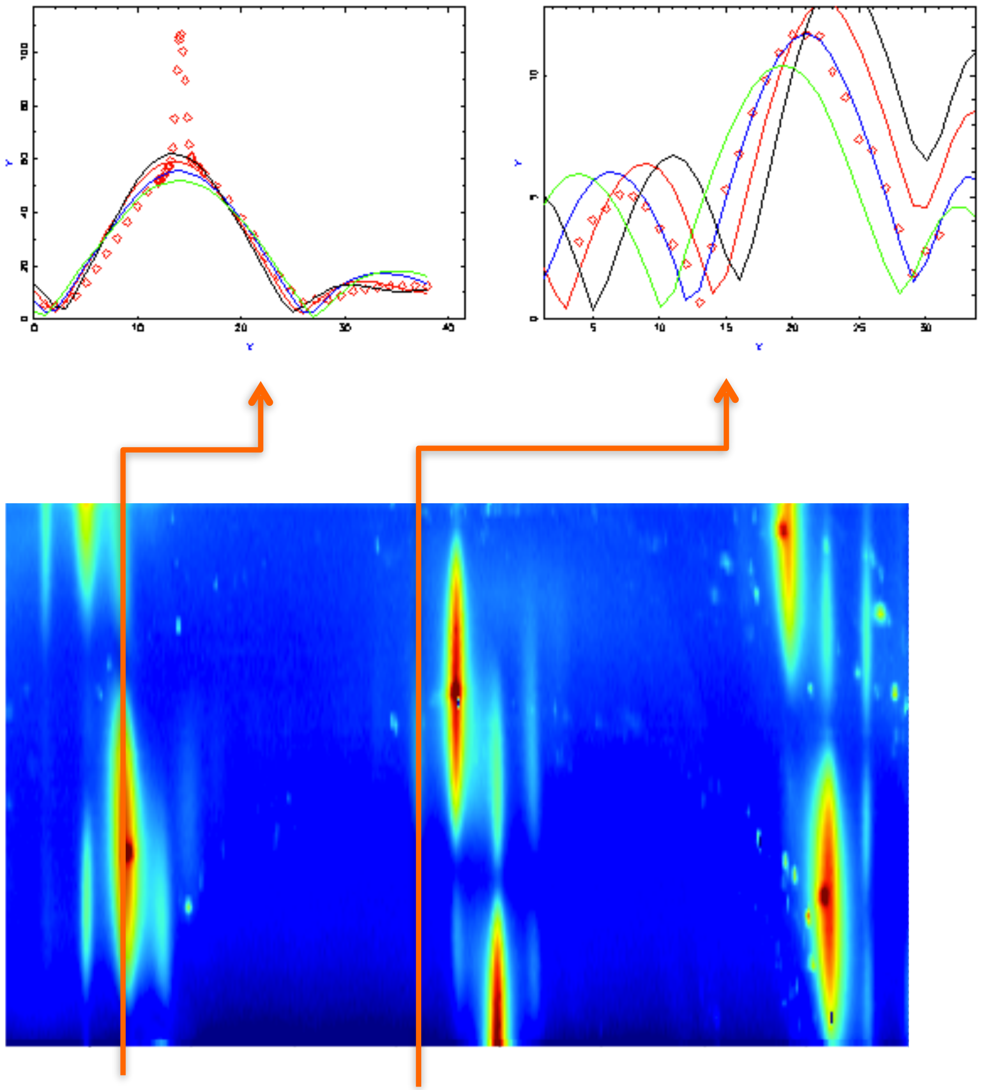

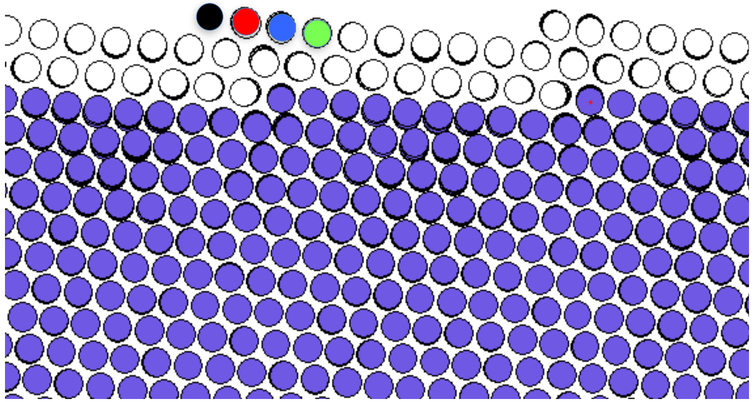

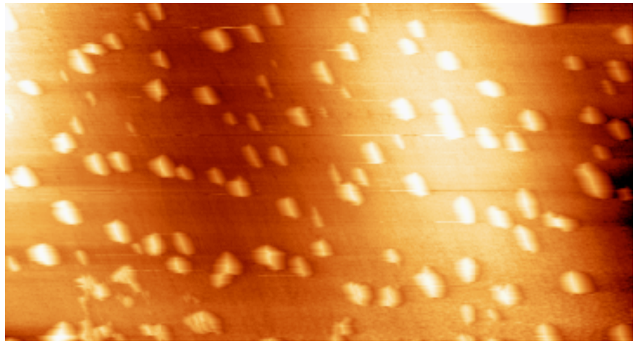

1500 x 750 nm2

Ag Islands

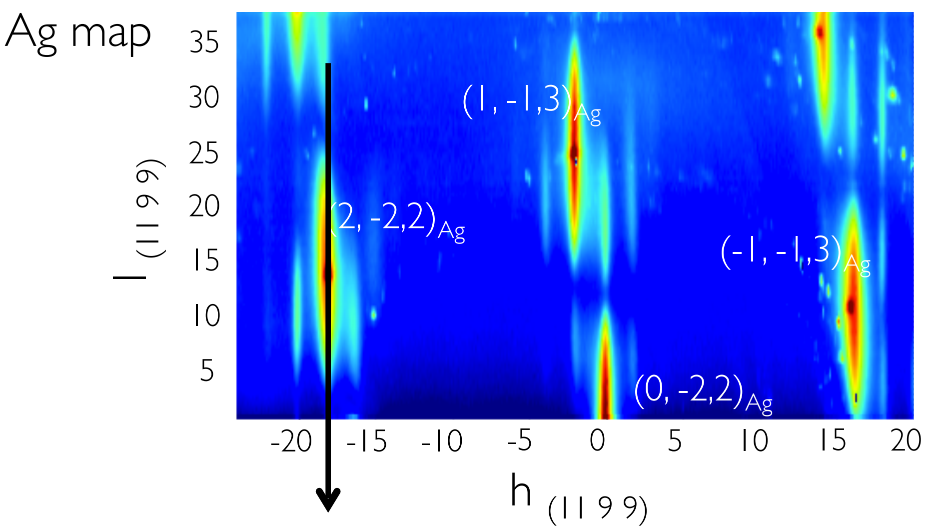

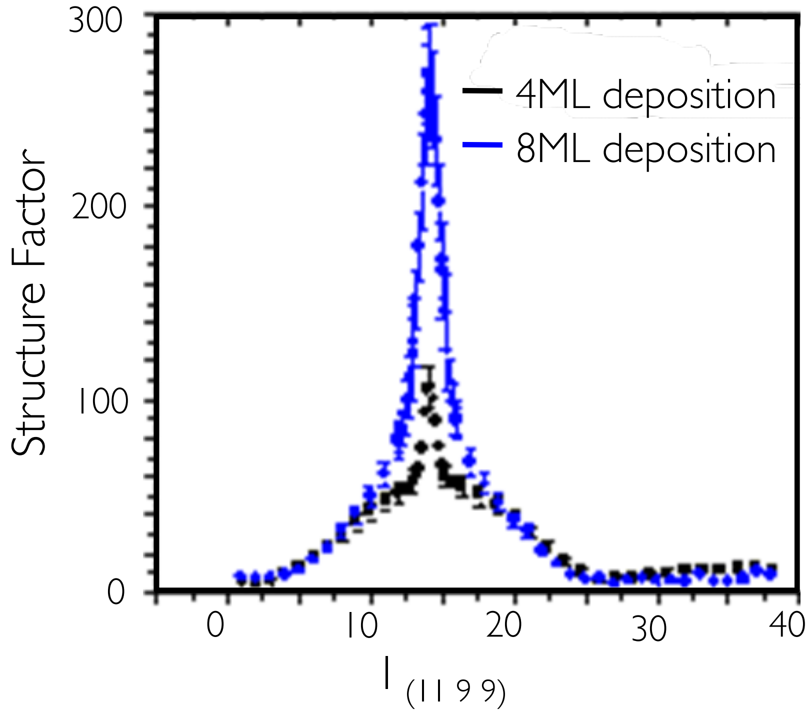

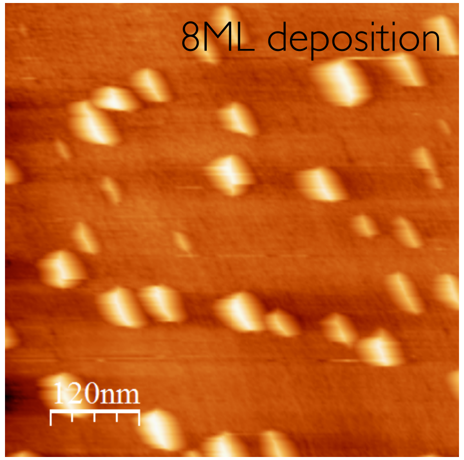

600x600nm², V=2.4V, I=2.5nA

Island formation on a 2ML Ag(7 9 9) layer

Co growth on vicinal Au(111) surface

Y. Girard et al., Phys. Rev. B72, 155434 (2005)

Co growth on vicinal Au(111) surface

hcp (...ABAB...)

Co

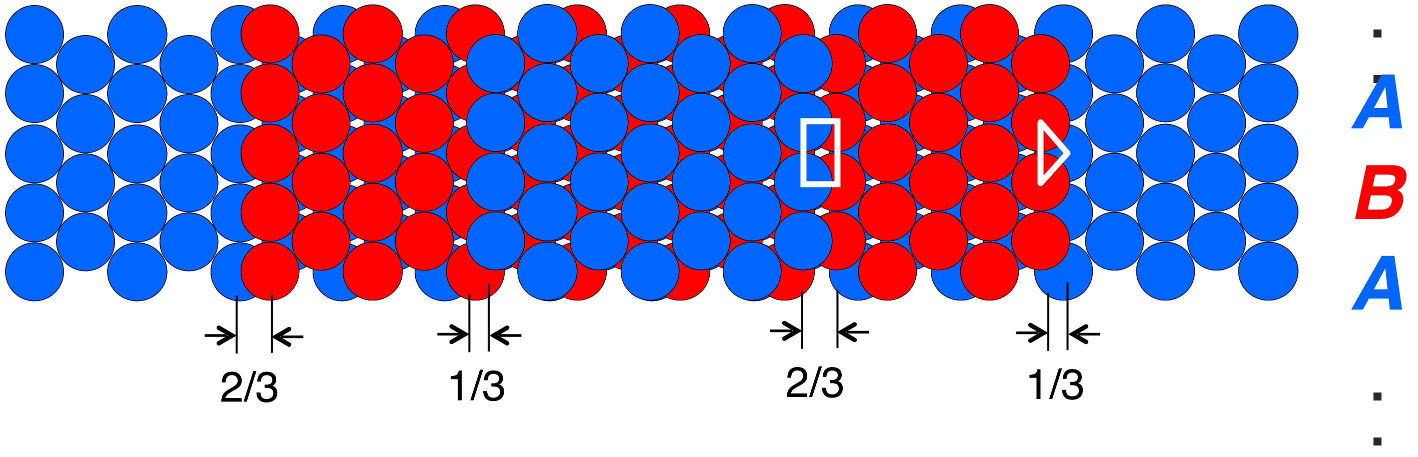

fcc (...ABCABC...)

Au

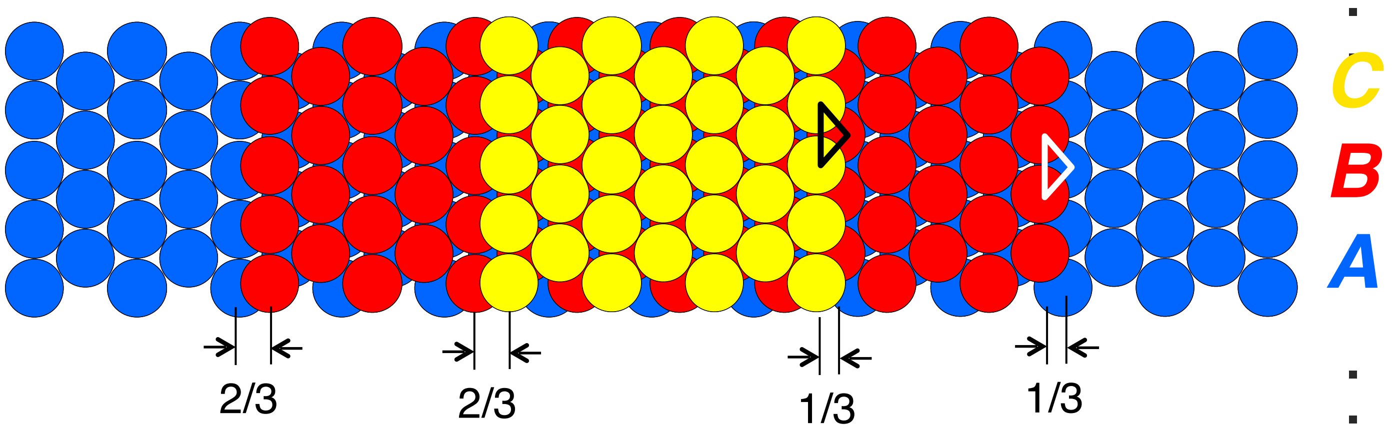

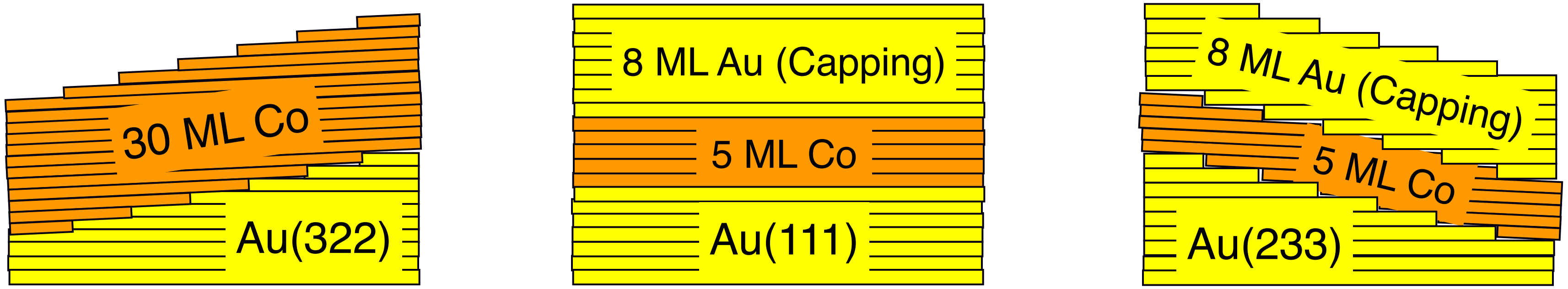

Terraces 1.17 nm
Steps {100}

Terraces 1.33 nm
Steps {111}

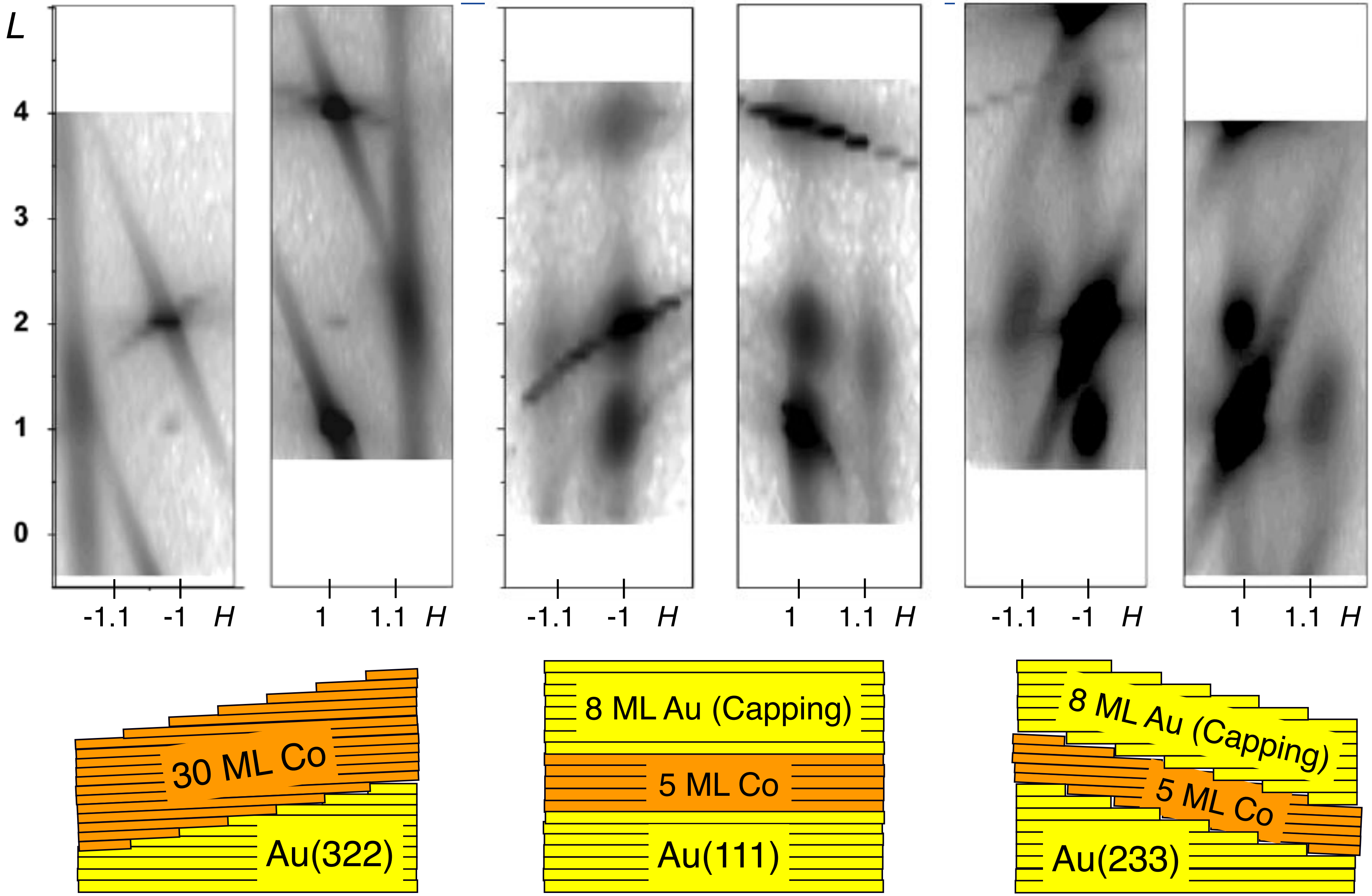

Terraces 1.17 nm
Steps {100}

Terraces 1.33 nm
Steps {111}

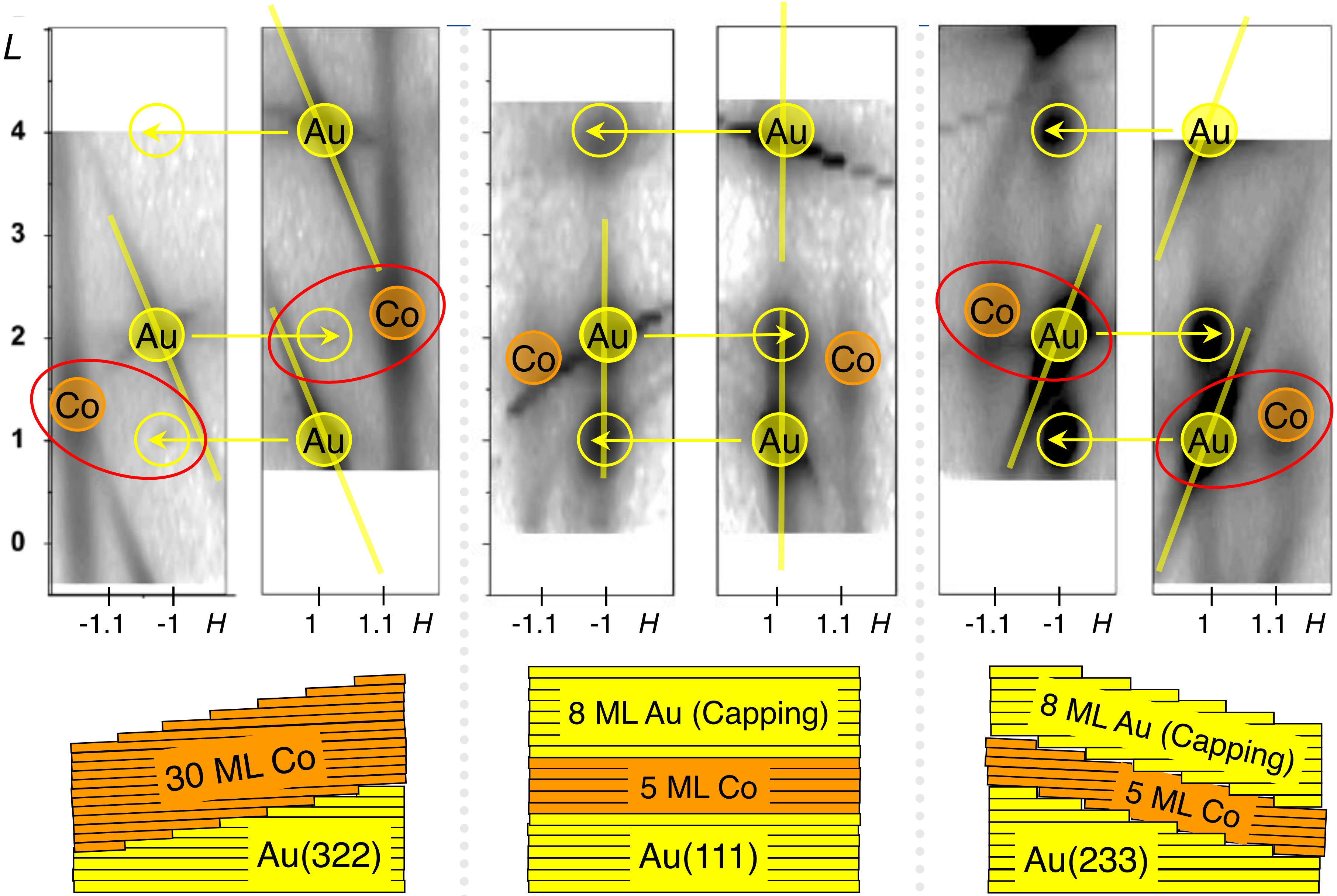

Terraces 1.17 nm
Steps {100}

Terraces 1.33 nm
Steps {111}

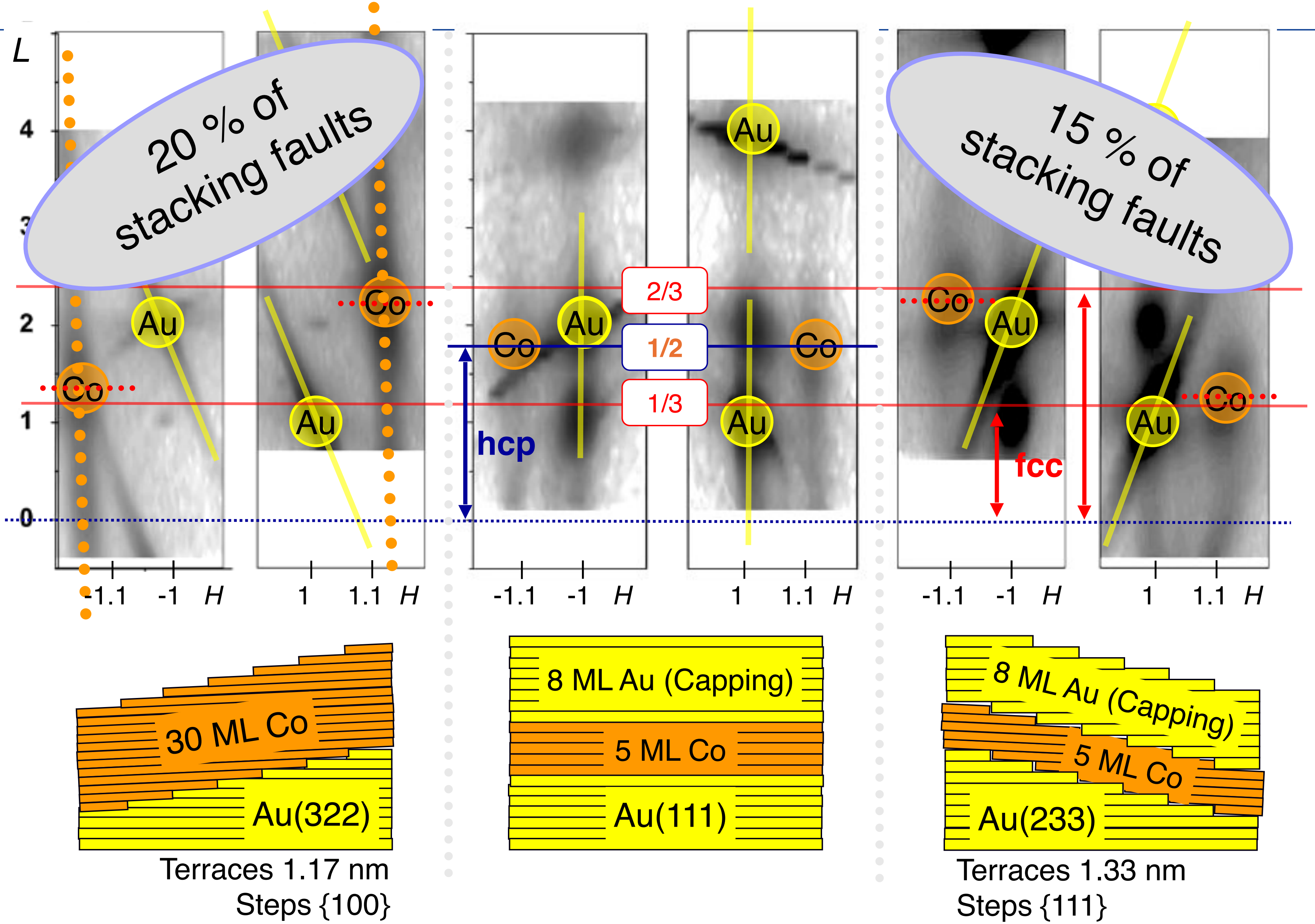

L
4
3
2
1
0
20 % of stacking faults
15 % of stacking faults
Au
Co
2/3
1/2
1/3
hcp
fcc
-1.1
-1
H
1
1.1
30 ML Co
Au(322)
8 ML Au (Capping)
5 ML Co
Au(111)
Au(233)
Terraces 1.17 nm
Steps {100}
Terraces 1.33 nm
Steps {111}

Grazing Incidence Small Angle X-ray Scattering (GISAXS)

- Grazing incidence → surface sensitivity

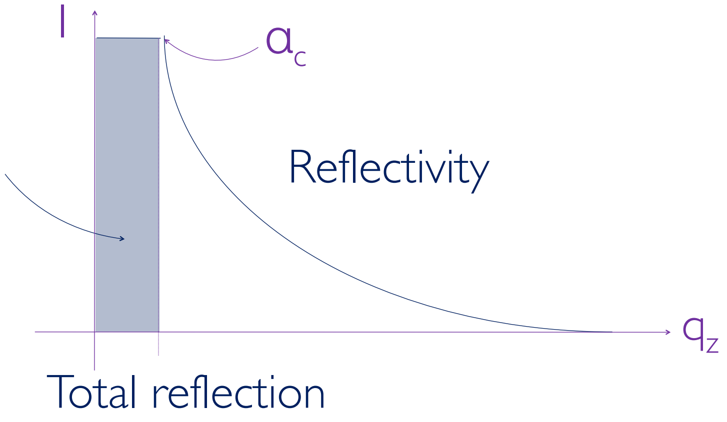

$n = 1 - \delta - i\beta$

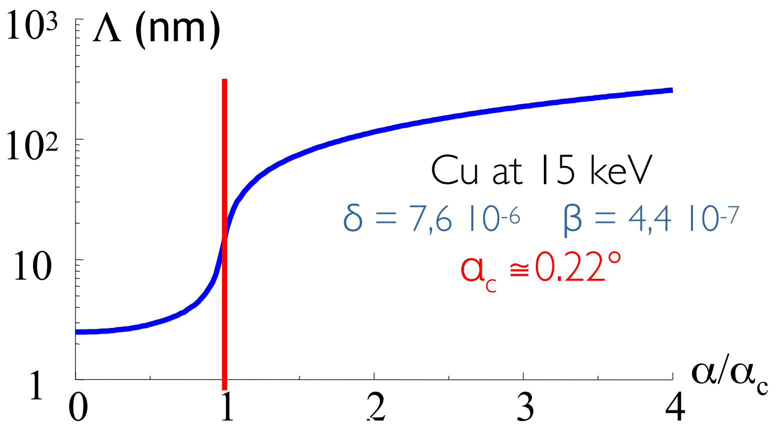

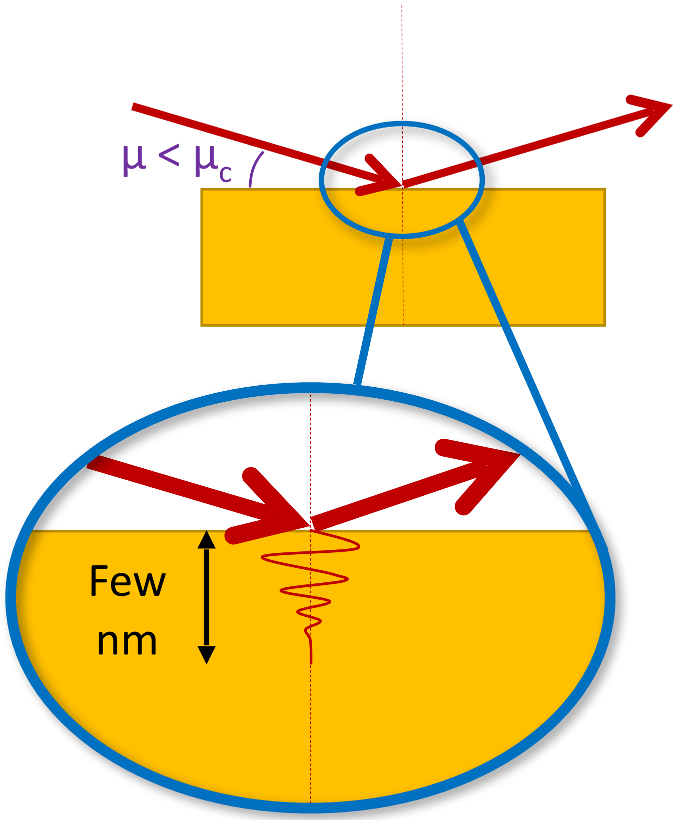

GISAXS - principle

Example : 20 Å Ag/MgO(001) 500K

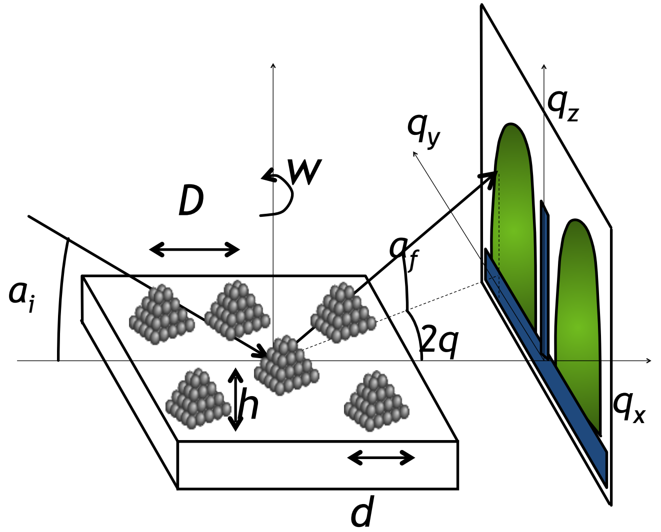

2D image around direct beam:
Fourier transform of objects

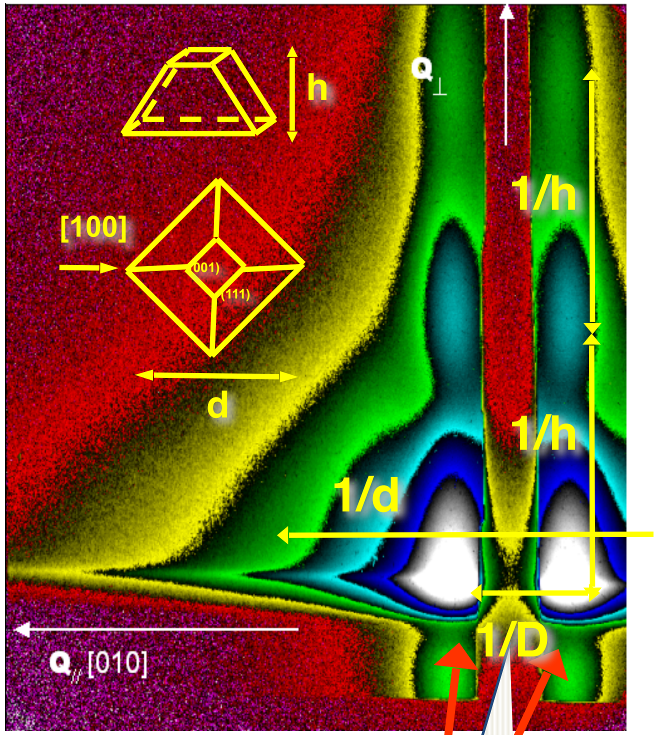

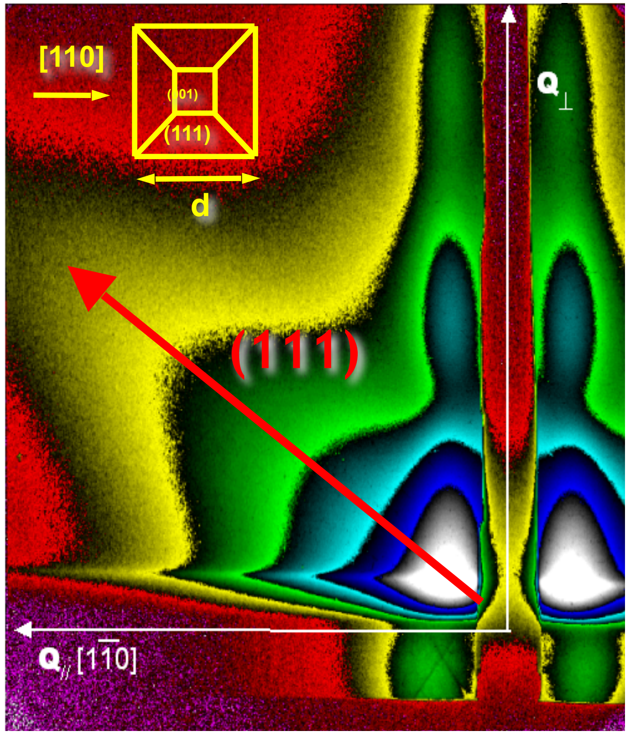

- Shape
- Sizes
- Size distributions
- Particle-particle
pair correlation function

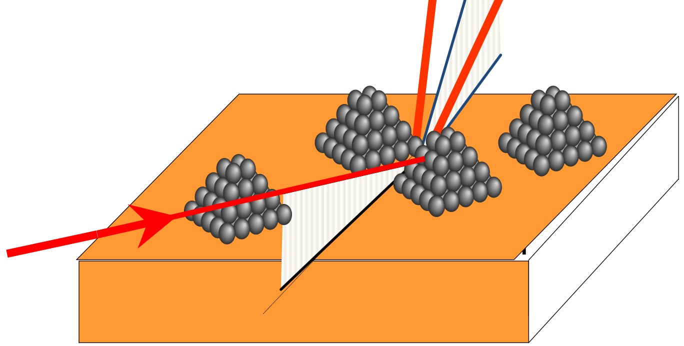

Anisotropic islands:
truncated square pyramids
with (111) facets

G. Renaud et al, Surf. Sc. Rep. 64, 255 (2009)

GISAXS – supported NPs

Pt NPs / C / Si

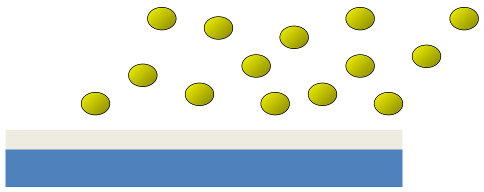

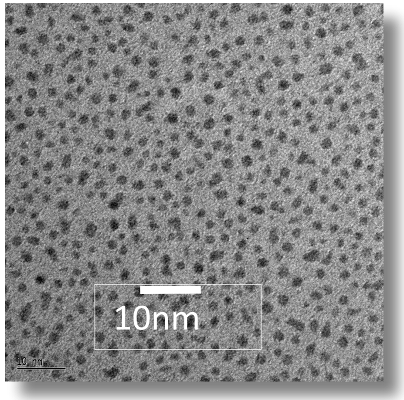

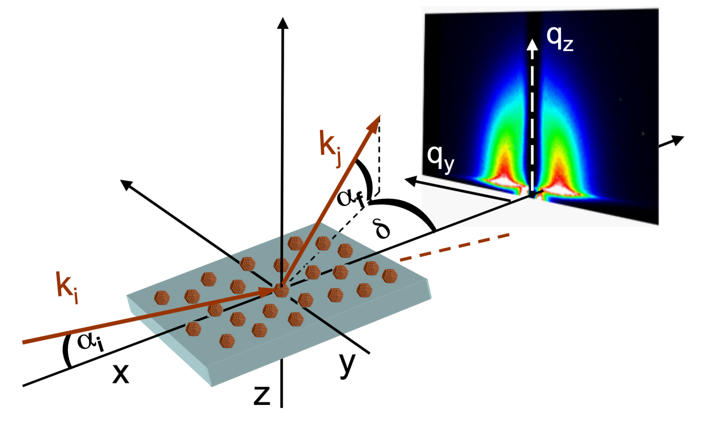

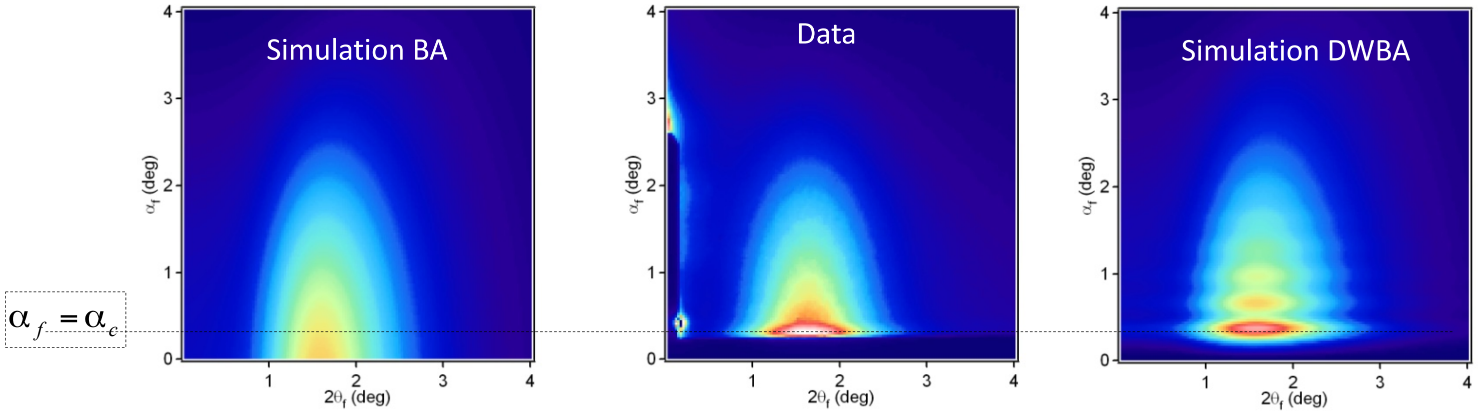

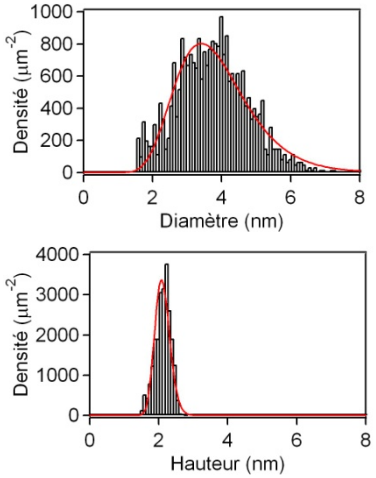

R. Lazzari, Journal of Applied Crystallography 35, 406 (2002) ➡ **IsGisaxs** software

D. Babonneau, J. Appl. Crystallogr. 43, 929 (2010) ➡ **FitGisaxs** software

GISAXS – NPs size distributions

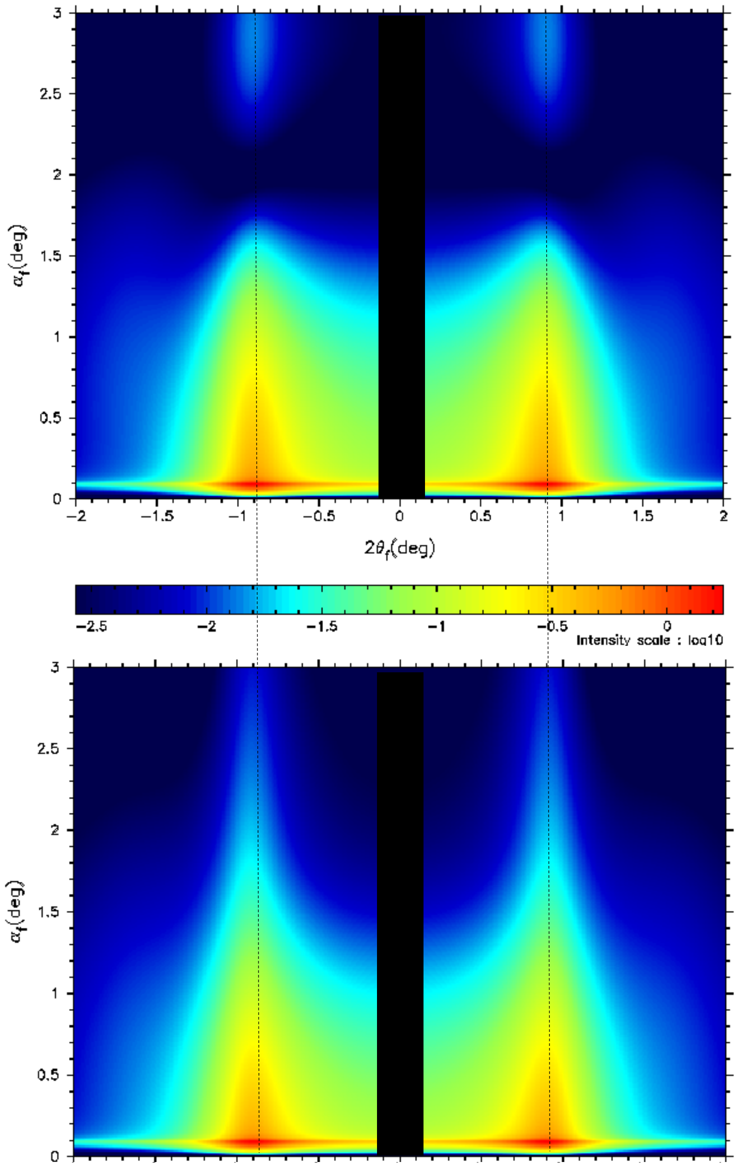

R. Lazzari, J. Applied Cryst. 35, 406 (2002)

Nanoparticle Assembly with same shape

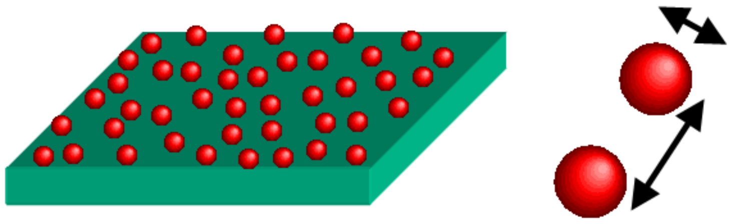

Diameter : 1.5nm
Interparticle Distance : 4nm

Identification of the morphology

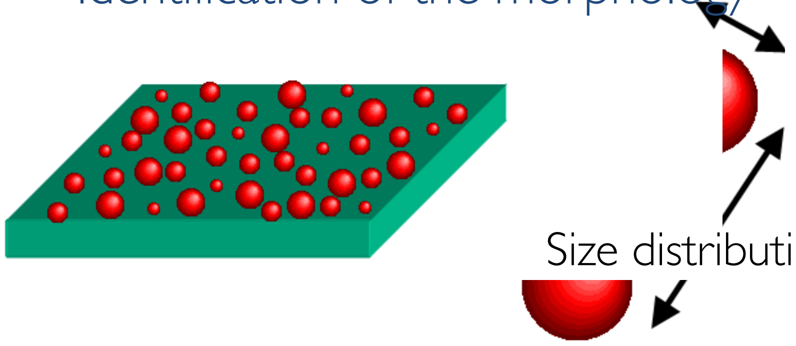

Size distribution

Diameter : 3nm
Interparticle Distance : 8nm

GISAXS

- Morphology on nanometer scale
- Growth monitoring
- Average interparticle distances on the surface
- Not limited to cristalline systems

- Not easy to fit
- Requires rather smooth surfaces

In situ GISAXS during ALD of Pt

Dendooven, J., et al. Nat Commun 8, 1074 (2017)

Setup ALD at SixS

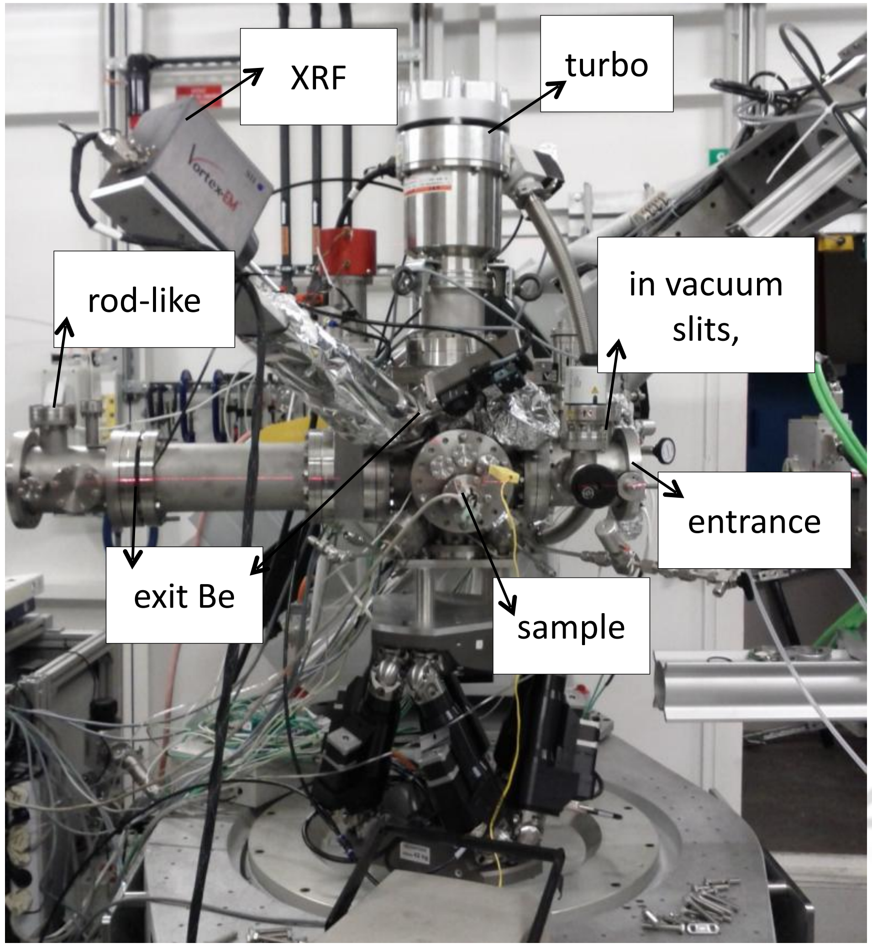

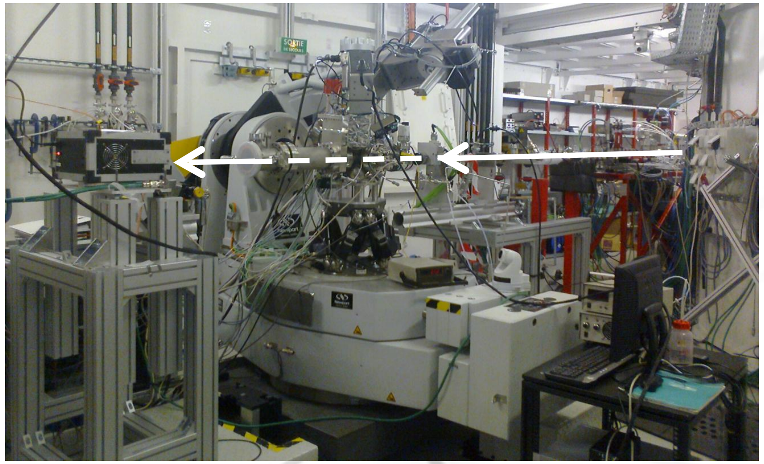

Dendooven et al. Nature Communications 2017

coati@synchrotron-soleil.fr

Pt catalytic NPs by ALD

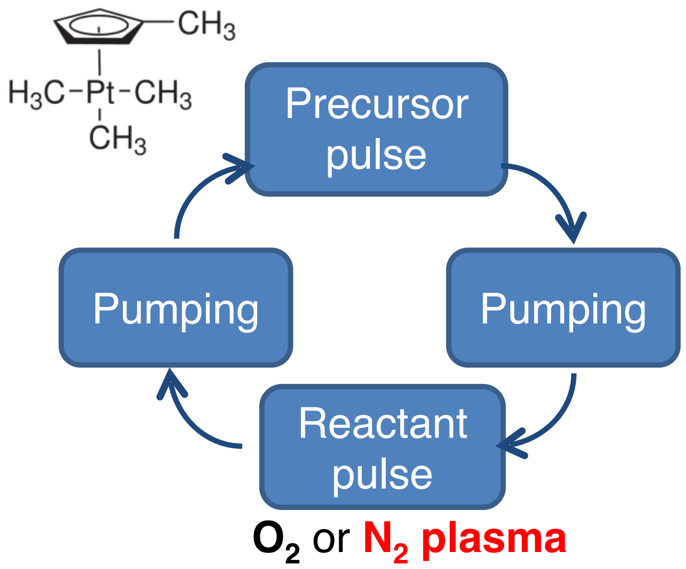

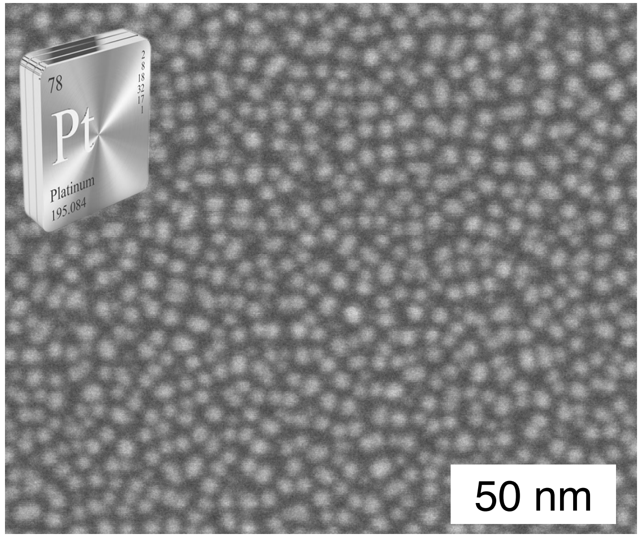

Pt ALD with the $MeCpPtMe_3$ precursor

Key advantages of ALD:

atomic level tuning of

- Pt loading
- Pt nanoparticle size

Usually achieved by changing the number of ALD cycles

This work:
Role of the co-reactant in Pt nanoparticle ALD?
Can this ALD parameter offer additional tuning opportunities?

Dendooven et al. Nature Communications 2017

Pt catalytic NPs by ALD

Goal:
dimensions
control

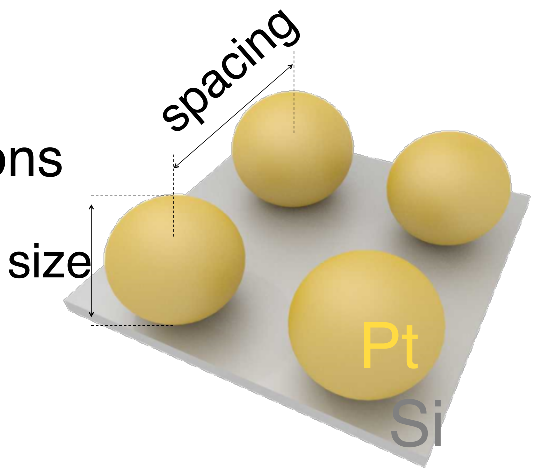

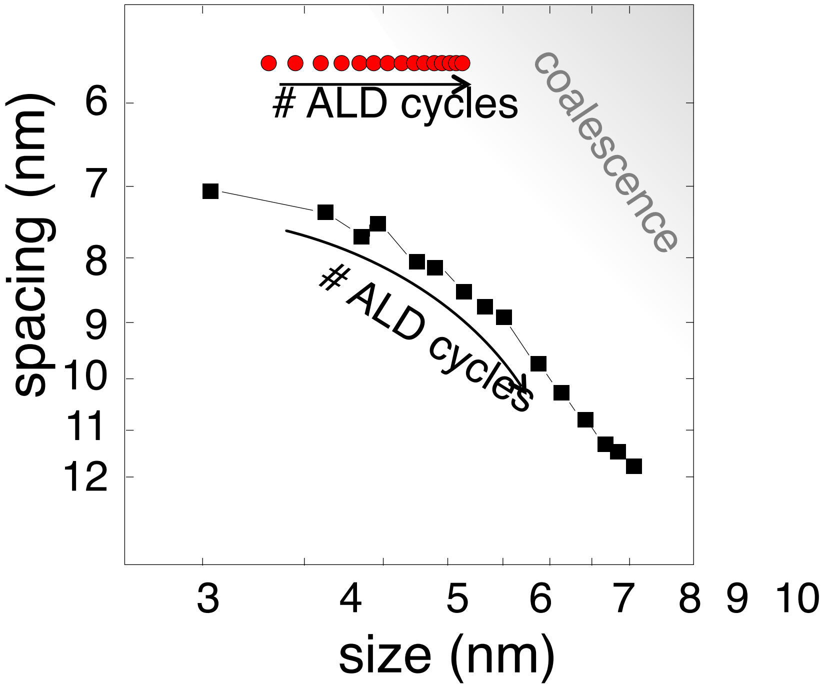

Process A: O_2

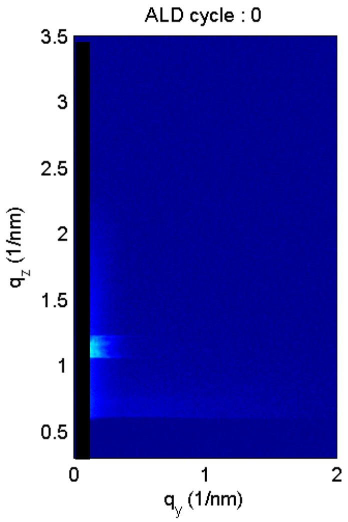

Process B: N_2 plasma

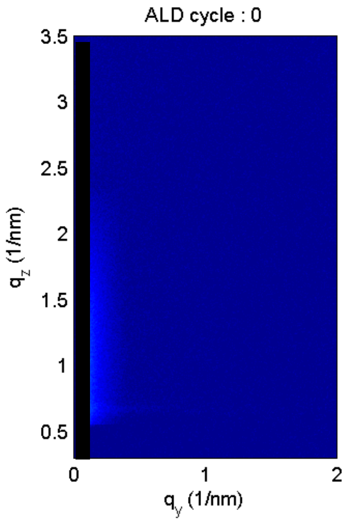

Static vs. **dynamic** particle growth and coalescence

Dendooven et al. Nature Communications 2017

Effect of reactant choice: N2 plasma vs. O2 gas

MeCpPtMe_3 / **N_2 plasma**
Nucleation & vertical growth

MeCpPtMe_3 / **O_2 gas**
Diffusion-driven coalescence & lateral growth

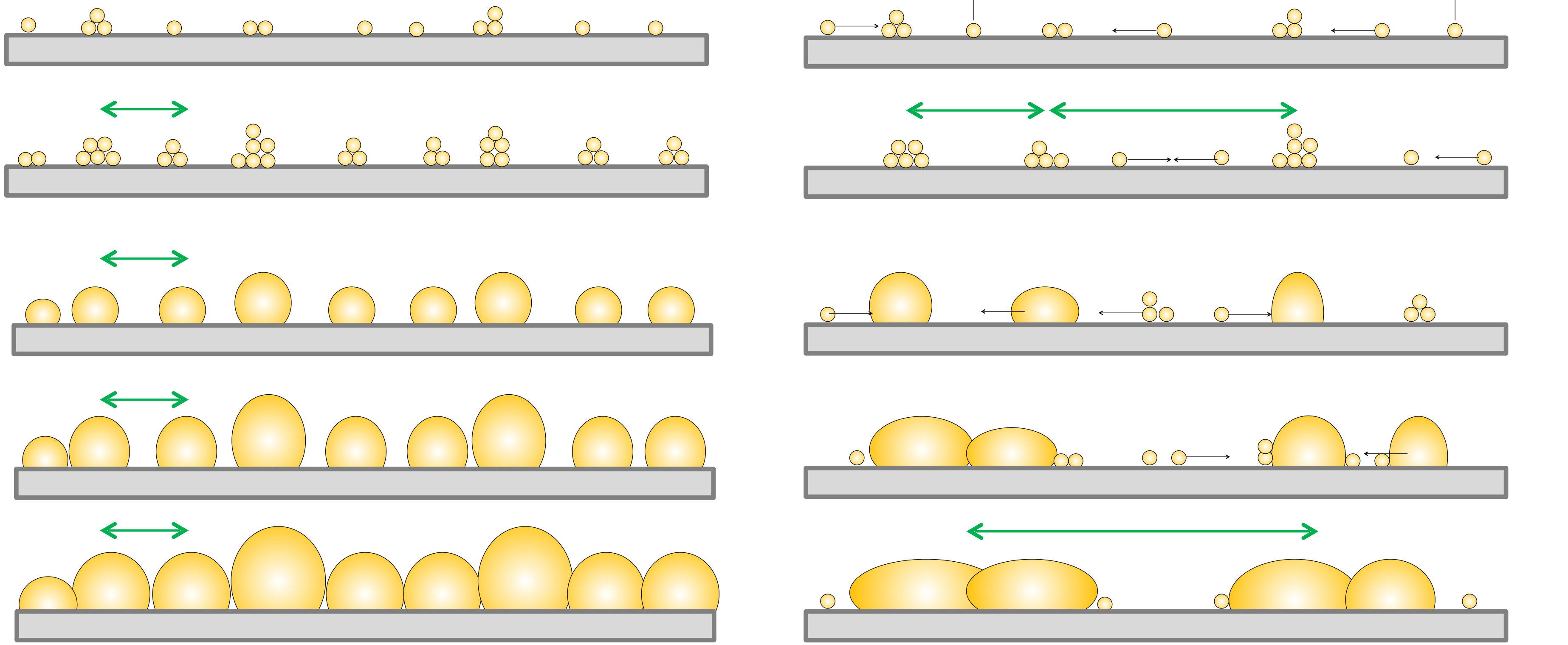

spacing D is constant

spacing D increases:
large clusters grow at the cost of individual atoms and small clusters

Dendooven et al. Nature Communications 2017

Accurate dimensions control in Pt nanoparticle ALD

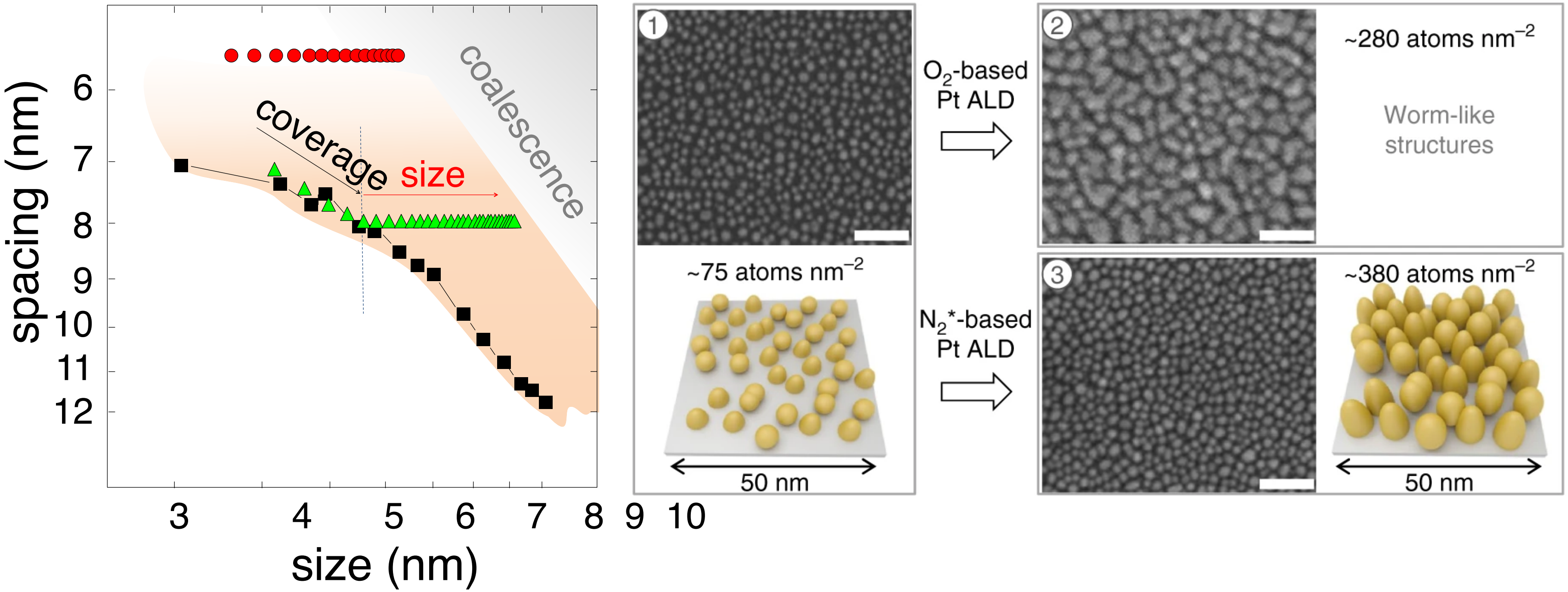

By combining $\mathbf{O_2}$-based and **N_2 plasma**-based Pt ALD, we can <u>independently tune</u> the **spacing** and **size**

Dendooven et al. Nature Communications 2017

In-situ alumina nanoporus

T. Gorisse, L. Dupré, D. Buttard, CEA, Grenoble

In-situ observation of nanoporous alumina formation

electrochemical cell

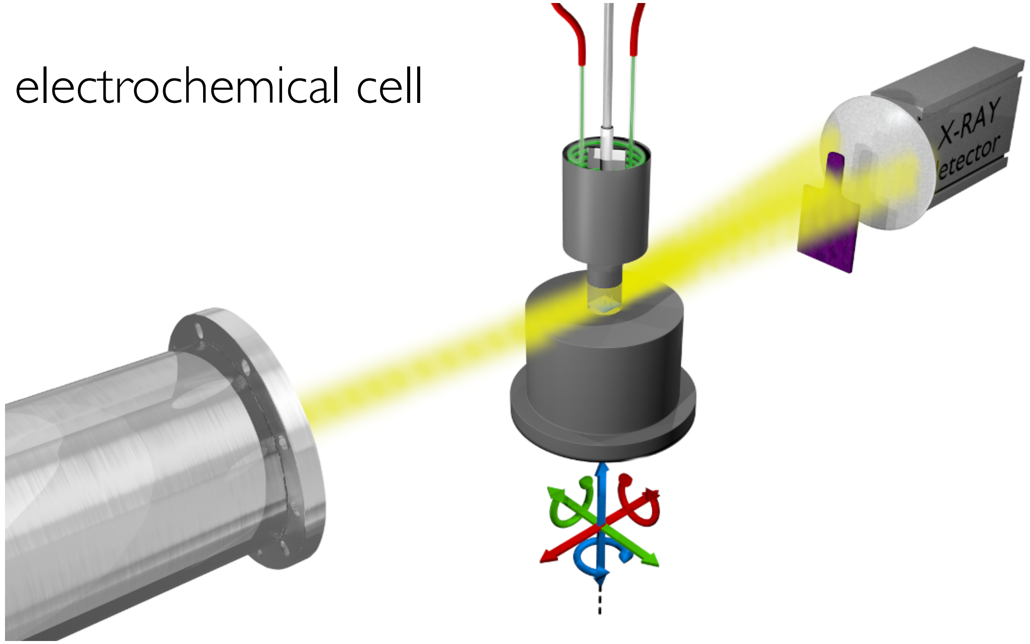

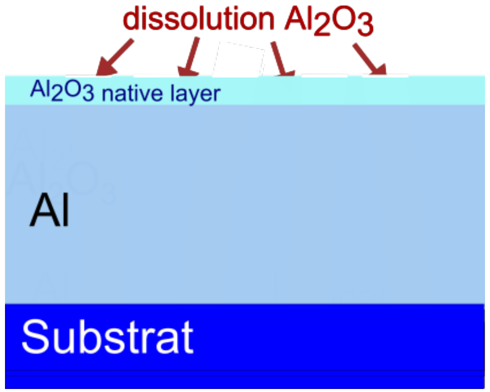

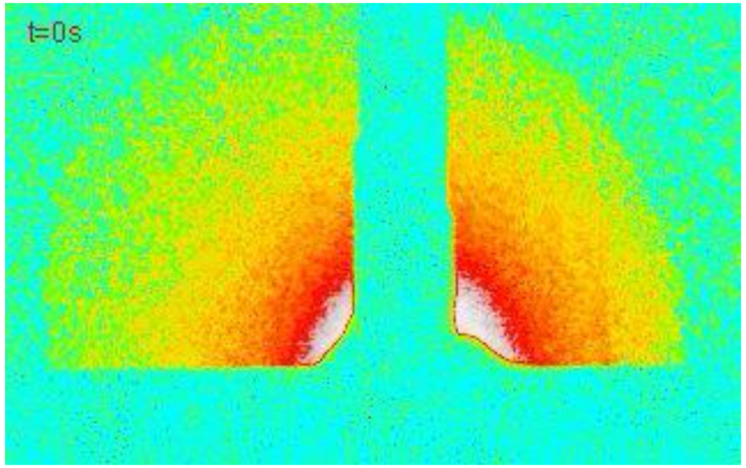

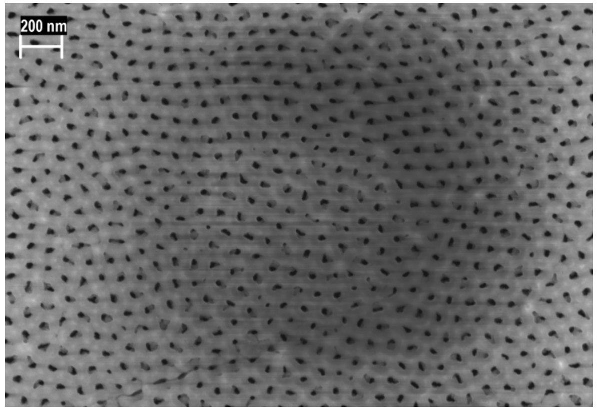

Period 90 nm
Thickness 450 nm

Conclusions, Acknowledgments, References

Surface x-ray Scattering Techniques

- Reliable quantitative analysis
- Statistical information
- Beyond the surface (buried interfaces…)
- *In-situ* and *operando* measurements In very different kinds of environments, and under very different conditions (real advantage of X-rays over other surface probes, e.g. electrons)
  - surface reactivity (catalytic reactions, annealings ...)
  - growth (during MBE, (MO)CVD, LPE)
  - use of gaseous, liquid or solid surfactants, at High p, T …
- Atomic structure, composition and morphology
- Shape, roughness, film thickness, surfaces morphologies
- Any kind of substrates (e.g. insulating)
- Depth sensitivity from 20 Å up to several mm

Other X-ray techniques to investigate surfaces and interfaces

- Surface X-ray absorption spectroscopy (SEXAFS …)
  - Local atomic structure
  - Electronic structure information
- Surface X-ray standing waves (S-XSW)
  - Location of adsorbates on surfaces / epilayer relaxation
- X-ray Photoelectron Spectroscopy (XPS, UPS …)
  - Electronic structure / bonding
- X-ray photoelectron diffraction (XPD)
  - Surface electronic + atomic structure

Acknowledgments

- Synchrotron SOLEIL, SixS beamline team: A. Vlad, A. Resta, Y. Garreau, B. Voisin, C. Fourmental, M. Sauvage-Simkin
- MPQ lab, Université Paris Cité: A. Bellec, C. Fourmental, V. Repain
- Gent University: J. Dendooven, R. K. Ramachandran, E. Solano, M. Kurttepeli, L. Geerts, G. Heremans, J. Rongé, M. Minjauw, C. Detavernier
- CEA Grenoble: D. Buttard, T. Gorisse, L. Dupré
- Institut P’, Poitier, France: D. Babonneau
- ICMN Orléans: P. Andreazza, C. Andreazza-Vignolle, A. Lemoine

References

- Surface diffraction
  - R. Feidenhans'l, Surface structure determination by X-ray diffraction, Surf. Sci. Reports 10 (1989) 105-188
  - I.K. Robinson and D.J. Tweet, Surface X-ray diffraction, Rep. Prog. Phys. 55 (1992) 599-651
  - H. Dosch, Critical Phenomena at Surfaces and Interfaces, Springer 1992

- The « ROD » code
  - E. Vlieg, J. Appl. Cryst, 33, 401 (2000) interactive webpage ANA-ROD
  - http://www.esrf.fr/computing/scientific/joint_projects/ANA-ROD/index.html

- GISAXS
  - G. Renaud et al., Probing surface and interface morphology with grazing incidencesmall angle x-ray scattering, Surf. Sci. Rep. 64 (2009) 255-380.

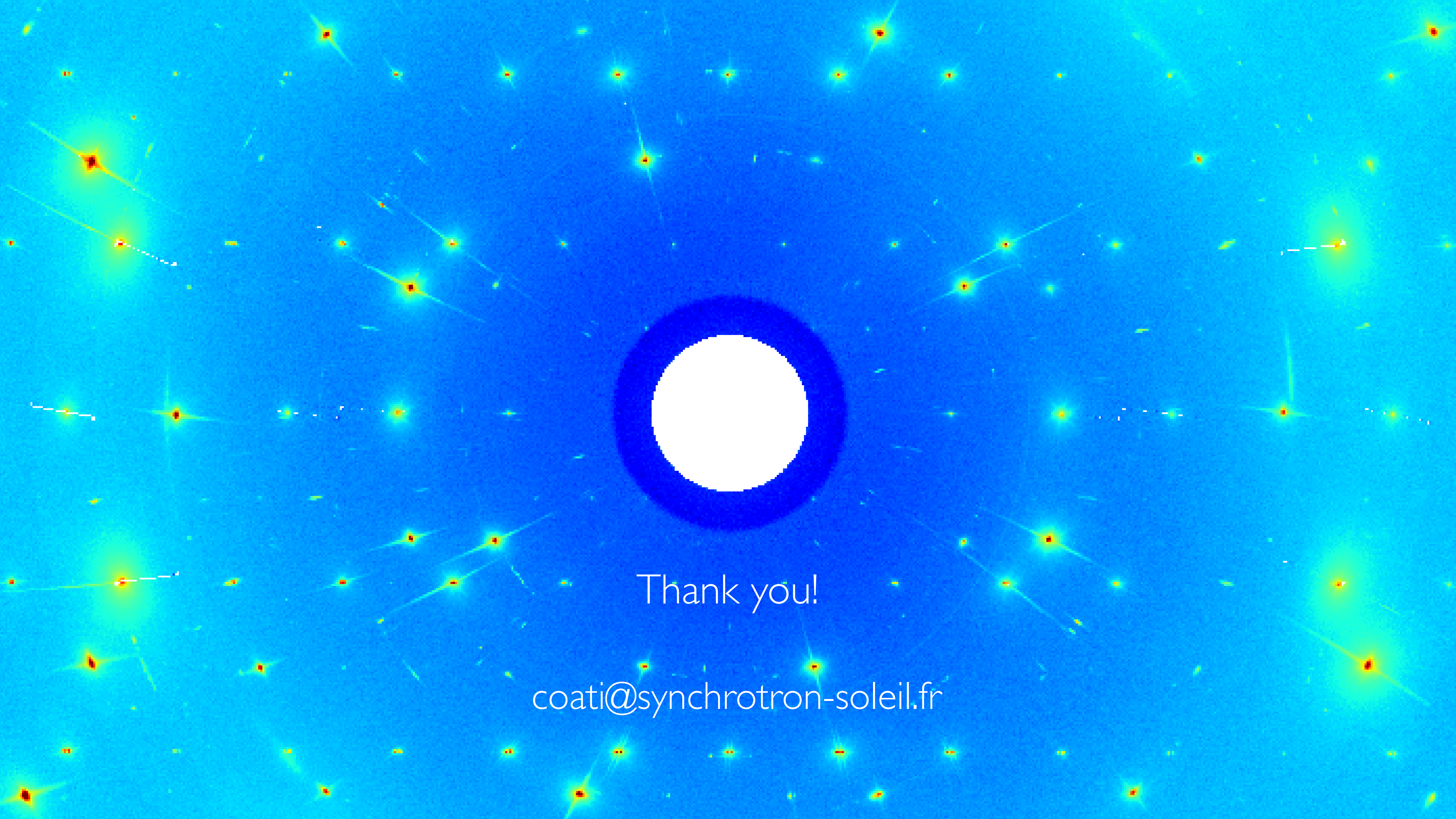

Thank you!

coati@synchrotron-soleil.fr